Contents lists available at ScienceDirect

Dyes and Pigments

journal homepage: www.elsevier.com

Ferrocene: An unrivaled electroactive building block for the design of push-pull dyes with near-infrared and infrared absorptions

Damien Brunel *, Guillaume Noirbent , Frédéric Dumur **

Aix Marseille Univ, CNRS, ICR UMR 7273, F-13397, Marseille, France

ARTICLE INFO

Keywords:
Ferrocene
Push-pull
Dye
Oxidation
Reduction
Iron
Donor
Acceptor

ABSTRACT

Ferrocene is an exceptional building block for the development of dyes with reversible redox properties. Dyes absorbing int the near infrared and infrared region are actively researched due to their potential applications ranging from telecommunication to defence systems. In this review, an overview of the different NIR and infrared dyes reported to date is presented. Parallel to the photophysical characteristics, the synthetic pathways giving access to these structures is presented.

1. Introduction

Since its discovery in 1951 [1–5], ferrocene has driven a great deal of interest due to its remarkable electrochemical properties (see Fig. 1). This metallocene made of an iron (II) cation sandwiched between two parallel cyclopentadienyl rings is characterized by a reversible single-electron oxidation process that made this compound a reference in electrochemistry [6]. This sandwich structure is also a strong electron donor and its combination with various electron acceptors allowed the design of numerous push-pull structures [7]. Ferrocene is photochemically and thermally stable, what constitutes appealing features for numerous applications [8]. Resulting from the infinite of possible combinations, its remarkable photochemical, electrochemical and thermal stability, the scope of applicability of ferrocene has been greatly enlarged, and over the years, applications going from Organic Electronics i.e. solar cells [9–11], light-emitting diodes [12], transistors [13], to non-linear optical (NLO) applications [14], molecular recognition [15], corrosion inhibition [16], ion sensing [17], photoinitiation of polymerization [18] or cancer research have been developed [19]. Parallel to the emergence of new applications, chemistry of ferrocene has greatly progressed in 70 years and this chemistry is now a mature field with regards to the number of publications reporting to the chemical modification of ferrocene. In this context, the design of new push-pull chromophores comprising ferrocene as electron donor has greatly benefited from advances in ferrocene chemistry.

Typically, push-pull compounds are composed of an electron donor connected to an electron acceptor by mean of a conjugated or a non-conjugated spacer. If numerous dyes have been designed on the basis of purely organic molecules [20,21], push-pull compounds comprising metal complexes as electron donors are more scarce and this rarity can be assigned to the cost and toxicity issues raised by the use of transition metals [22]. At present, visible light chromophores based on ferrocene are well-documented in the literature. Conversely, availability of ferrocene-based dyes with absorption bands extending until the near-infrared (NIR) and the far-infrared region is more limited. Besides, the development of dyes absorbing in this specific part of the absorption spectrum is of crucial importance as these compounds can find applications in research fields ranging from anti-counterfeiting inks, laser printing, acidochromic dyes or optical data storage [23]. Parallel to dyes naturally absorbing in the NIR and infrared region, modification of the oxidation state of one of the two partners of the push-pull structure constitutes an effective way to create new transitions that are not observed for the neutral form. In this field, ferrocene constitutes a candidate of choice by its facile oxidation and the reversibility of the oxi-

* Corresponding author.
** Corresponding author.
Email addresses: damien.brunel@univ-amu.fr (D. Brunel); frederic.dumur@univ-amu.fr (F. Dumur)

https://doi.org/10.1016/j.dyepig.2019.107611
Received 27 March 2019; Received in revised form 21 May 2019; Accepted 1 June 2019
Available online xxx
0143-7208/

Fig. 1. Chemical structure of ferrocene.

dation process. As a result of this, an efficient regeneration of the neutral form can be ensured, and it thus offers unique opportunities to create and suppress "on demand" absorption bands such as charge transfer (CT) or intervalence charge transfer (IVCT) bands at low energy by simply modifying the oxidation state of the metal center [24]. From this point of view, ferrocene is an unrivalled building block for the design of push-pull structures.

In this review, an overview of the different chromophores designed with ferrocene and exhibiting an absorption in the near and infrared region will be presented. Even if absorption bands can be created in the NIR and infrared region upon modification of the oxidation state of ferrocene, only dyes already exhibiting optical transitions in the NIR region under the neutral form will be discussed. The different applications involving these compounds will also be presented.

2. Near-infrared and infrared absorbing dyes based on ferrocene

2.1. Ferrocene with thiazole acceptors

Heterocyclic structures such as thiazoles, benzothiazoles and benzothiadiazoles are strong electron acceptors extensively studied in the literature for non-linear optical applications and organic photovoltaics [25–33]. When these acceptors are connected to electron donors by mean of a triple bond, their electron-withdrawing ability can be greatly improved by a [2 + 2] cycloaddition-*retro*-cyclization with tetracyanoethylene (TCNE). Using this strategy, **T1** and **T2** could be converted to **T3** and **T4** in 82 and 70% yield. As a consequence of this, **T3** and **T4** displayed a red-shifted absorption compared to that of the parent structures **T1** and **T2** (see Fig. 2) [34]. Thanks to the conversion of the ethynyl spacer in **T1** and **T2** into the 1,1,4,4-tetracyanobuta-1,3-diene (TCBD) structure, an improvement of the thermal stability was also obtained, the decomposition temperature increasing from 200 °C for **T1** and **T2** to 300 °C for **T3** and **T4**.

Examination of the photophysical properties of **T1-T4** revealed these chromophores to exhibit two main absorption bands, one of these bands being detected between 300 and 350 nm corresponding to π-π* transitions and a red-shifted one centered at ca. 400–650 nm corresponding to the intramolecular charge-transfer (ICT) band of the chromophores. Precisely, ICT bands of **T3** and **T4** were determined as extending until 900 nm as a long tail and broadness of the ICT bands detected between 450 nm and 900 nm made these dyes panchromatic chromophores covering almost the whole visible range, completed by a contribution of their absorption spectra in the NIR region. As expected, the electron-withdrawing ability in **T3** and **T4** was greatly improved by the presence of the TCBD acceptor and a red-shift of the ICT bands by more than 150 nm were evidenced (See Table 1). Parallel to this, elongation of the π-conjugation in **T3** and **T4** gave a 2-fold enhancement of the molar extinction coefficients compared to **T1** and **T2**. By electrochemistry, the strong interaction of the ferrocene donor with the acceptor in **T3** and **T4** could be easily evidenced by the oxidation potential of ferrocene, increased of ca. 300 mV compared to that of ferrocene in **T1** and **T2**.

2.2. Ferrocene with BODIPY

BODIPYs (which stands for 4,4-difluoro-4-bora-3a,4a-diaza-*s*-indacene) are highly emissive structures widely studied in the literature for applications ranging from organic photovoltaics (OPVs) [35–37], optoelectronic devices [38–41], NLO applications [42–44], bioimaging and ion sensing [45–49], fluorescence spectroscopy [50–52] and phototherapy [53,54]. These compounds are also characterized by large Stokes shift, making BODIPYs appealing candidates for bioimaging. Indeed, BOPIDYs are biocompatible compounds and can be excited at wavelengths enabling to image living cells without inducing damages to the biological tissues [55]. With regards to their absorptions, BODIPYs only exhibit extremely narrow absorption bands at ca 500 nm. By introducing electron donors connected to the pyrroles of BODIPYs, additional transitions can be observed in the NIR region, resulting from the push-pull effect and expending the absorption spectra. Using this strategy, the Highest Occupied Molecular Orbital (HOMO) level is therefore centered onto the peripheral donors whereas the Lowest Unoccupied Molecular Orbital (LUMO) level is localized on the BODIPY motif. Due to the predominance of this repartition i.e. the HOMO level located onto the ferrocene moiety and the LUMO on the BODIPY core, unique opportunities to create metal-to-ligand (MLCT) transitions at low energy and of variable intensity are thus offered. Indeed, depending on the strength of the electron donor (i.e. the ferrocene unit), an admixture of the MLCT band together with BODIPY-centered π-π* transitions can be obtained, modulating the intensity of the NIR band [56]. To achieve the peripheral substitution of BODIPY, the most straightforward strategy consists in the functionalization of the methyl groups of the pyrrole moieties by mean of a Knoevenagel reaction. In this field, one of the first report mentioning the design of NIR-absorbing BODIPYs with ferrocene was reported in 2009 with **BDP-1** [57]. As specificity, the functionalization of pyrroles at the α-position was difficult and the reaction yield was extremely low, only reaching 15% for **BDP-1**, despites the large excess of ferrocene introduced (see Fig. 3). While comparing **BDP-1** with its parent BODIPY, three main absorption bands could be detected, one centered in the 300–350 nm region and assigned to $d_z^2 \rightarrow d_{xy}$ and $d_{x\text{-}y}{}^{22} \rightarrow d_{xz}$ transitions of ferrocene. A second band at 550 nm and shifted by about 50 nm with regards to the parent BODIPY was also detected. This transition corresponds to the $S_0 \rightarrow S_1$ of BODIPY and the red-shift of this band is consistent with an extension of the π-conjugation. Finally, an additional band only observed for **BDP-1** and detected between 600 and 850 nm was assigned to the ICT band. Interestingly, if BODIPYs are highly emissive compounds, a complete quenching of luminescence was observed for **BDP-1** resulting from a

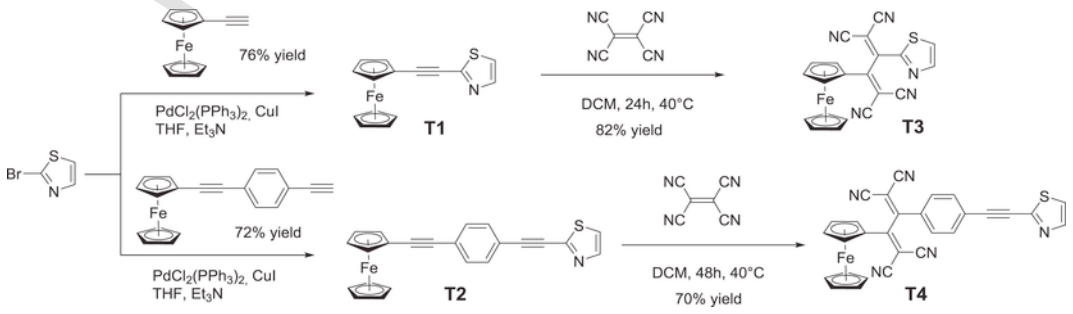

Fig. 2. Synthetic pathways to T1-T4.

Table 1
Photophysical characteristics of **T1-T4**.

	λ_{abs1} (nm)[a]	λ_{abs2} (nm)[a]	ε_1 (M^{-1} cm^{-1})[a]	ε_2 (M^{-1} cm^{-1})[a]	E_{ox} (V)/E_{red}(V)[b]	T_d (°C)[c]	Ref
T1	311	452	30600	2050	0.59	212	33
T2	333	456	39800	Sh	0.53	231	33
T3	350	600	48600	4374	0.84, −0.44, −0.75	336	33
T4	359	630	49800	3984	0.85, −0.48, −0.80	443	33

[a] Measured in DCM, C = 5×10^{-5} M.
[b] Recorded in DCM ([$TBAPF_6$] = 0.1 M, scan rate: 100 mV/s, potentials determined vs. SCE electrode.
[c] Decomposition temperatures determined at a heating rate of 10 °C/min under nitrogen atmosphere for 5% weight loss.

charge transfer between the ferrocene units and the BODIPY core. Electrochemical measurements also revealed the mutual influence existing between the two ferrocene units in **BDP-1**. By reducing the scan rate, the single two-electron oxidation wave could be split into two one-electron oxidation waves, demonstrating the oxidation of the first ferrocene unit to influence the oxidation of the second one. Electron-pulling effect of BODIPY was confirmed by the anodic shift of the oxidation potentials of the two ferrocene units (0.5 V instead of 0.3 V for ferrocene in DCM).

Considering that the two ferrocene units are electronically connected by mean of the BOPIDY core, electrochromic experiments were carried out. By cycling between 0.7 V (oxidation) and 0 V (reduction) (vs Ag wire), a colour change alternating between blue and red could be observed. Notably, upon oxidation, a decrease of the peak at 700 nm accompanied by the appearance of a new peak at 600 nm was detected by spectro-electrochemistry, assigned to the formation of the oxidized state **BDP-1**$^{2+}$. Initial absorption spectrum could be restored upon reduction at 0 V. No fatigue of the system upon cycling was evidenced, and it can be confidently assigned to the remarkable electrochemical stability of ferrocene. Finally, authors also demonstrated the possibility for **BDP-1** to be chemically oxidized to the dication state upon addition of Cu^{2+}, furnishing the same modifications of the absorption spectra than that observed upon electro-oxidation.

The same year, a parallel study was developed by another group on the same compound i.e. **BDP-1** and a comparison could be established with the mono-substituted **BDP-2** [58]. The synthetic approach was slightly different from the former one since **BDP-2** and **BDP-1** were obtained during the same reaction, the mono and the disubstituted BOPIDYs being separated by column chromatography. It has to be noticed that compared to the former approach, the overall yield is improved, since **BDP-1** was obtained in 27% yield and **BDP-2** in 22% yield whereas ferrocene was only introduced in a 1:1 ratio with respect to BOPIDY (see Fig. 4). In the previous synthesis of **BDP-1**, an excess as large as 10 equivalents was used.

As main difference from the former study, the absorption spectra of **BDP-2** and **BDP-1** were examined until 1100 nm (and not 800 nm) so that new conclusions could be established about their photophysical properties. Thus, upon oxidation of **BDP-1**, the presence of a charge

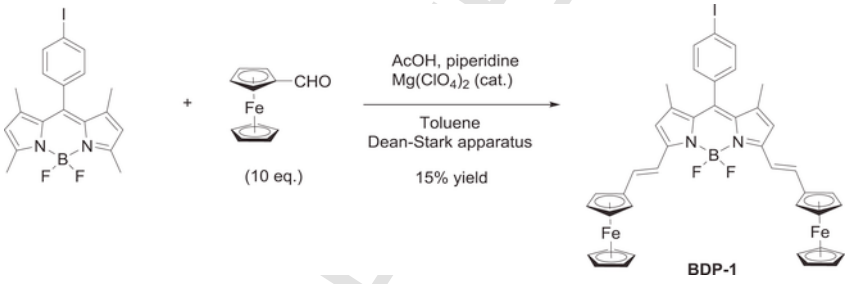

Fig. 3. Synthetic route to **BDP-1**.

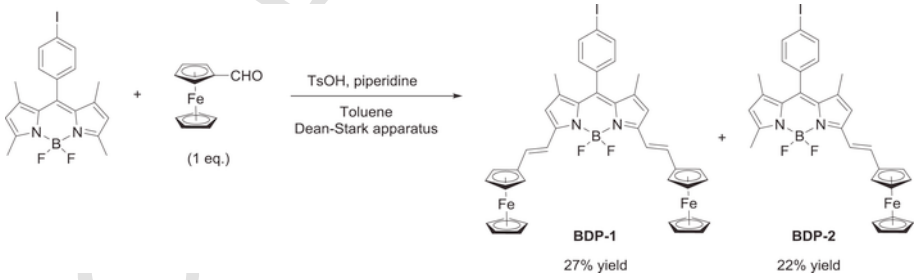

Fig. 4. Synthetic route to **BDP-1** and **BDP-2**.

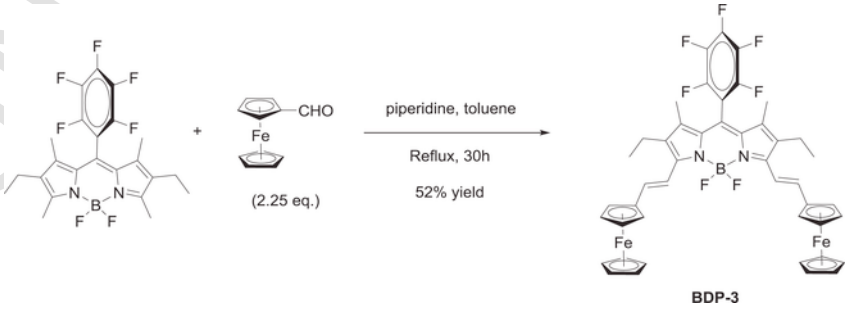

Fig. 5. Synthetic route to **BDP-3**.

Table 2
Photophysical characteristics of **BDP-1**, **BDP-2** and **BDP-3**.

Compound	λ_{abs1} (nm)[a]	λ_{abs2} (nm)[a]	E_{ox} (V)/E_{red}(V)	Ref
BDP-1	550	710	1.07, 0.49, 0.42, −1.06, −1.97[b]	57
BDP-2	540	601	1.04, 0.44, −1.13[b]	57
BDP-3	590	739	0.75, 0.13, 0.05, −1.32[c]	58

[a] Measured in DCM.
[b] Recorded in DCM, [$TBAPF_6$] = 0.1 M, potentials determined vs. SCE electrode.
[c] Recorded in DCM, [$TBAPF_6$] = 0.1 M, potentials determined vs. Ag^+/Ag reference.

transfer band located at 860 nm could be detected. Appearance of new bands upon oxidation are consistent with a redistribution of the electronic density. Indeed, a complete modification of the location of the HOMO and the LUMO levels occurs since the initial D-A-D system is converted to a A-D-A triad by oxidation of the two ferrocene units. In this situation, the metal center reachs its maximum oxidation degree i.e. +III, making the oxidized form of ferrocene a strong electron acceptor. Upon cycling between oxidation and reduction, presence of several sets of isobestic points were detected on the absorption spectrum of **BDP-1**, characterizing the formation of a half-oxidized species **BDP-1**$^+$. Interestingly, this intermediate that constitutes a D-A-A triad exhibits a strong intramolecular charge transfer between the neutral and the oxidized form of ferrocene so that an absorption band at low energy and extending between 900 and 1100 nm could be detected on the absorption spectrum. This major redistribution of the HOMO/LUMO energy levels between **BDP-1**, **BDP-1**$^+$ and **BDP-1**$^{2+}$ also supports the change observed for the solution colour, varying between blue and red as a function of the oxidation state of ferrocene. To tune the electrochromic properties of the ferrocene-BODIPY conjugates, several groups examined the impact of the substitution pattern at the *meso*-position of BODIPY. Choice of the *meso*-substituent of BOPIBY can potentially affect the electrochromic properties of the donor-acceptor-donor triad, what was evidenced by use of the strong electron accepting pentafluorophenyl substituent (see Fig. 5) [59]. In this case, the synthetic conditions were optimized and simplified compared to the previous ones since **BDP-3** could be obtained in 52% yield by refluxing the two reagents in toluene without Dean & Stark apparatus and in the presence of a catalytic amount of piperidine.

As observed for the previous BODIPYs, **BDP-3** exhibited the usual absorption bands located at 350, 430, 590 and 739 nm. The first peaks at 350 and 430 nm were assigned to transitions centered on the ferrocene unit (π- π * and metal-centered d–d transitions) as well as to a $S_0 \rightarrow S_2$ transition of BODIPY. The bands at 590 and 739 nm correspond to the $S_0 \rightarrow S_1$ transition of BODIPY and the ICT between the ferrocenyl donors and the BODIPY acceptor. The ICT band is extremely broad, this transition extending from ca. 600 nm until 960 nm. Compared to **BDP-1**, a clear influence of the substituent attached at the *meso* posi-

Table 3
Photophysical characteristics of **BDP-5- BDP-7**, **BDP-9, BDP-10 and BDP-11**.

	λ_{abs1} (nm)[a]	λ_{abs2} (nm)[a]	λ_{abs3} (nm)[a]	ε_1 (M^{-1} cm^{-1})[a]	ε_2 (M^{-1} cm^{-1})[a]	ε_3 (M^{-1} cm^{-1})[a]	E_{ox} (V)/E_{red}(V)	Ref
BDP-5	369	554	671	18000	54000	18000	0.56, 0.08, −1.19[b]	56
BDP-6	358	575	750	17000	18000	16000	1.29, 0.17, 0.02, −1.21[c]	56
BDP-7	363	650	750	29000	31000	40000	0.72, 0.31, 0.06, −1.16[b]	56
BDP-9	366	613	715	12000	48000	22000	0.98, 0.10, −1.04[c]	56
BDP-10	398	581		10400	92000		0.11, −1.07[b]	60
BDP-11	313	651		18400	106000		0.09, 0.02, −0.90[b]	60

[a] Measured in DCM.
[b] Recorded in DCM with $TBAClO_4$ as the support electrolyte, potentials determined vs. ferrocene/ferrocenium couple.
[c] Recorded in DCM with $TBA(C_6F_5)_4$ as the support electrolyte, potentials determined vs. ferrocene/ferrocenium couple.

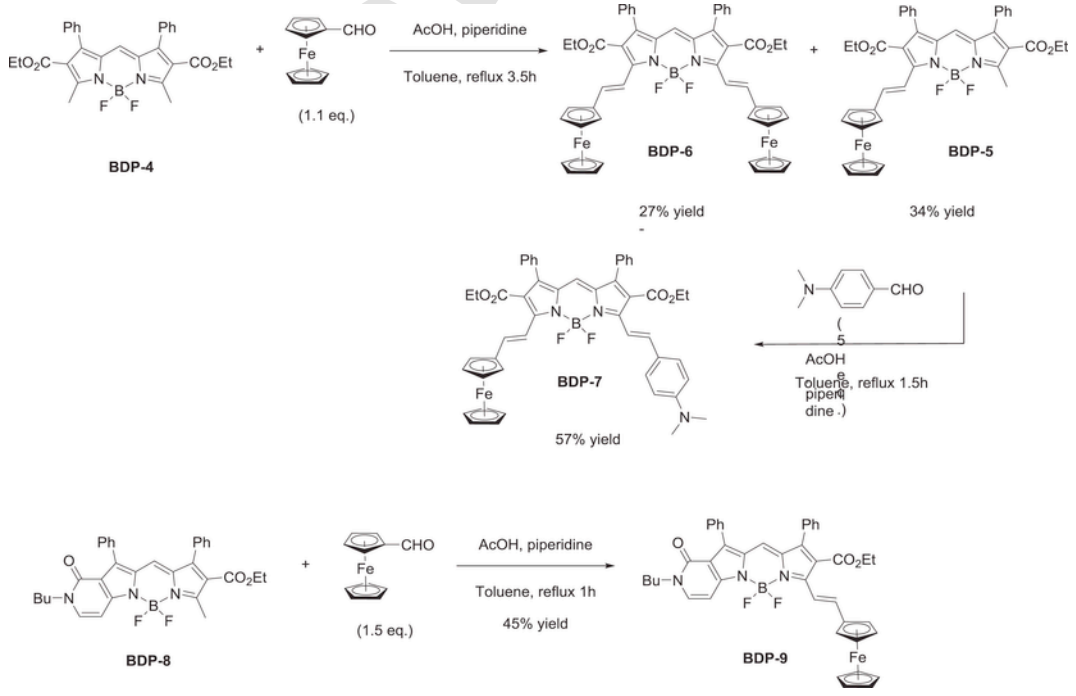

Fig. 6. Synthetic routes to **BDP-5- BDP-7**, **BDP-9.**

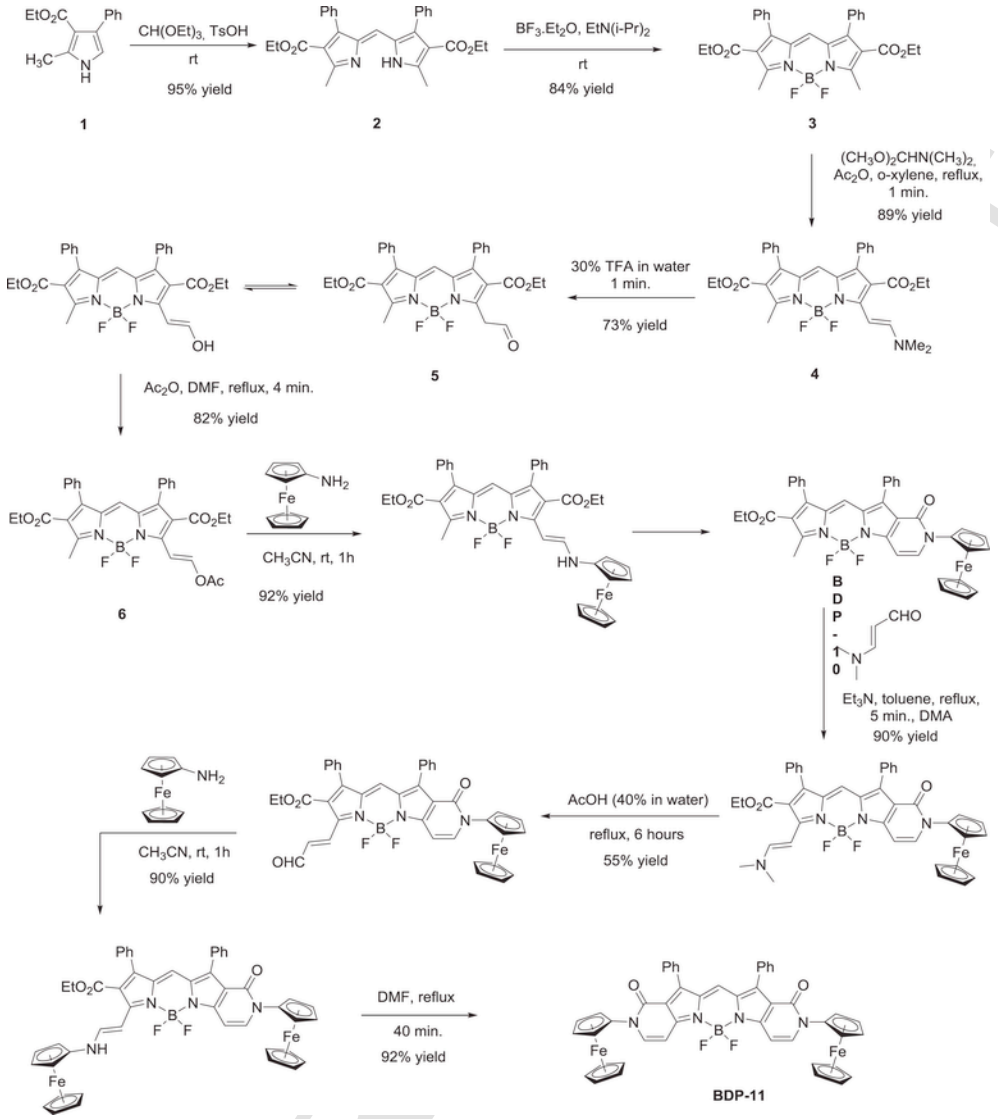

Fig. 7. Synthetic routes to **BDP-10** and **BDP-11.**

tion of BODIPY was evidenced, all peaks being red-shift by ca. 40 nm for **BDP-3** compared to those of **BDP-1** with an onset for the ICT band of **BDP-3** occurring at 950 nm contrarily to 850 nm for **BDP-1** (see Table 2). However, this impact remains limited due to the steric hindrance existing between the methyl groups of pyrroles and the aromatic substituent at the *meso*-position, enforcing this latter to adopt an almost orthogonal orientation, relative to the plane of the pyrroles. Besides, an electronic communication of the *meso*-substituent with the rest of the BOPIDY exists and could be demonstrated by electrochemistry. Indeed, reduction of the BOPIDY core of **BDP-3** occurred at a less negative potential than that observed for **BDP-1** due to the electron-withdrawing ability of the pentafluorophenyl group (see Table 3).

In the specific case of **BDP-3**, the absorption spectra of the anionic, cationic and dicationic states of **BDP-3** could be acquired separately by spectroelectrochemistry. Upon reduction or oxidation of **BDP-3**, intensity of the ICT band of **BDP-3** decreased, consistent with the disappearance of the charge transfer interaction between BOPIDY and the ferrocene unit. Upon re-oxidation of the anion or the reduction of the cation of **BDP-3**, presence of isobestic points confirmed the stability of the anion and the cation by the reversibility of the electrochemical process. As interesting feature, the new band detected at 870 nm in the absorption spectrum of the **BDP-3** cation is consistent with the formation of a donor-acceptor-acceptor triad with elongation of the π-conjugation between the donor and the acceptor. Parallel to the electrochemical oxidation of **BDP-3**, the possibility to chemically oxidized the two ferrocene units was examined and $FeCl_3$ was used as the oxidant. In this work, authors also demonstrated the possibility to restore the fluorescence of BOPIDY by cancelling the electron-donating ability of the ferrocene units. By switching between the neutral and the dication states, the fluorescence could be restored or suppressed. In all the above-mentioned examples, an aromatic ring was introduced at the *meso*-position of BODIPYs, simply due to the easiness of synthesis.

Synthesis of BODIPYs without substituents at the *meso*-position is more challenging than those comprising an aromatic ring. However, considering that the *meso*-substituent does not drastically impact the photophysical properties of BODIPYs by the lack of electronic communication between the BODIPy core and the *meso*-substituent due to the orthogonality of the aromatic substituent, a series of BODIPYs **BDP-4- BDP-9** without substituents at the *meso*-position was designed and synthesized (see Fig. 6) [56]. From a synthetic point of view, **BDP-5** and **BDP-6** were obtained during the same reaction, by opposing the BOPIDY **BDP-4** to 1.1 equivalent of ferrocenecarboxaldehyde. The monosubstituted BODIPY **BDP-5** could be obtained in 34% yield whereas the disubstituted one **BDP-6** was isolated in 27% yield. Fi-

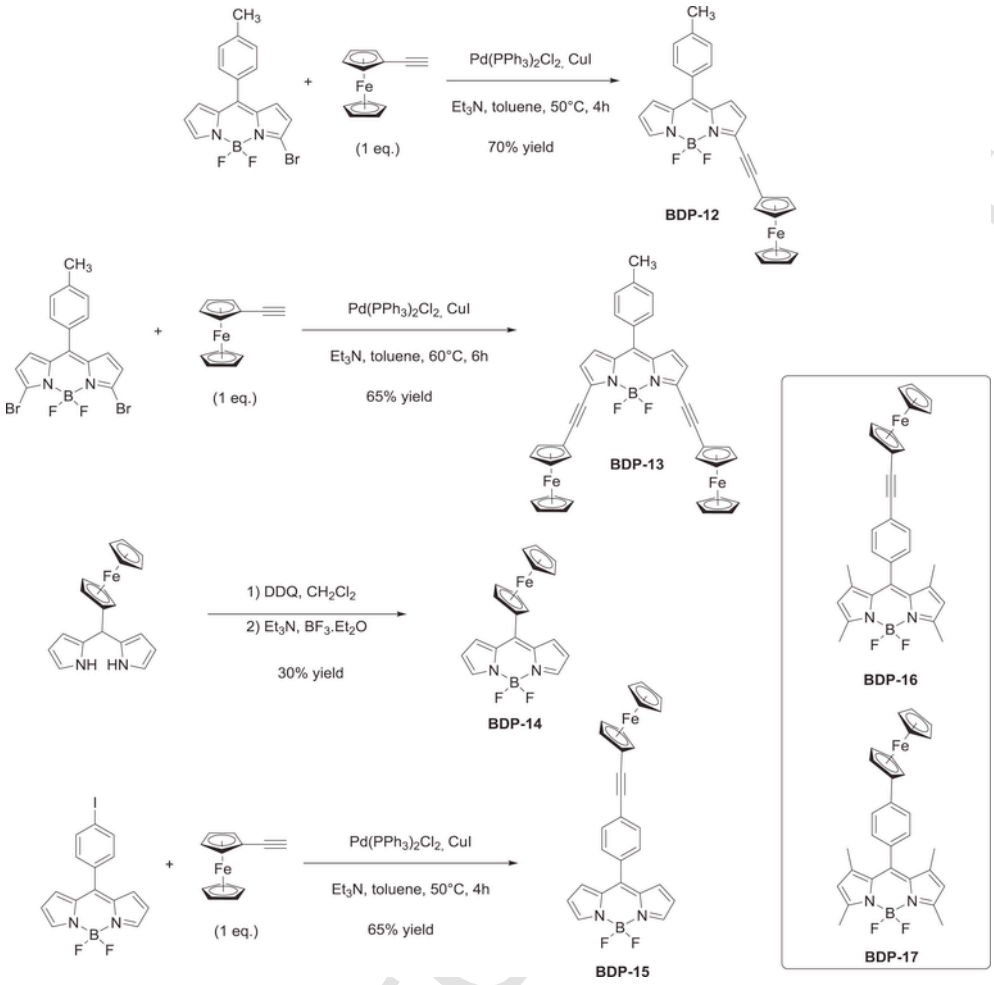

Fig. 8. Synthetic routes to **BDP-12- BDP-15**.

Table 4
Photophysical characteristics of **BDP-12- BDP-34.**

	λ_{abs1} (nm)[a]	λ_{abs2} (nm)[a]	ε_1 ($mol^{-1}.cm^{-1}$)[a]	ε_2($mol^{-1}.cm^{-1}$)[a]	E_{ox} (V)/E_{red}(V)	Ref
BDP-12	531	613	46770	15500	1.57, 0.64, −0.74[b]	62
BDP-13	558	680	26300	20420	1.36, 0.64, −0.70[b]	62
BDP-14	509	656	75850	5250	1.56, 0.74, −0.80[b]	62
BDP-15	505	–	44668	–	0.62, −0.71[b]	62
BDP-16	498	–	–	–	1.16, 0.52, −1.24[c]	63
BDP-17	498	–	–	–	1.13, 0.41, −1.33[c]	63
BDP-18	513	–	32300	–	–	64
BDP-19	523	–	32400	–	–	64
BDP-20	543	–	35900	–	–	64
BDP-21	544	–	35700	–	–	64
BDP-22	538	–	74622	–	1.03, 0.25, −1.01, −1.28[c]	65
BDP-23	544	–	108769	–	1.09, 0.08, −0.95, −1.34[c]	65
BDP-24	546	–	88977	–	1.11, 0.07, −0.93, −1.32[c]	65
BDP-25	551	–	103285	–	1.12, 0.11, −0.94, −1.34[c]	65
BDP-26	512	–	46000	–	1.17, 0.10, −1.12, −1.41[c]	66
BDP-27	567	–	34000	–	1.28, 0.52, −0.35, −0.71-1.32, −1.80[c]	66
BDP-28	561	–	49000	–	1.21, 0.48, −0.79, −0.88, −1.16, −1.29[c]	66
BDP-29	521	–	45000	–	1.34, 1.10, 0.40, −0.73, −1.42, −2.03, −2.23[c]	66
BDP-31	530	610	6310	–	0.70, −0.75	67
BDP-32	554	646	25120	–	0.65, −0.62	67
BDP-33	561	668	19950	–	0.66, −0.57	67
BDP-34	570	690	19950	–	0.65, −0.54	67

[a] Measured in toluene.
[b] Recorded in DCM with $TBAClO_4$ as the support electrolyte at a scan rate of 50 mV/s, potentials determined vs. SCE.
[c] Recorded in DCM with $TBAPF_6$ as the support electrolyte at a scan rate of 100 mV/s, potentials determined vs. SCE.

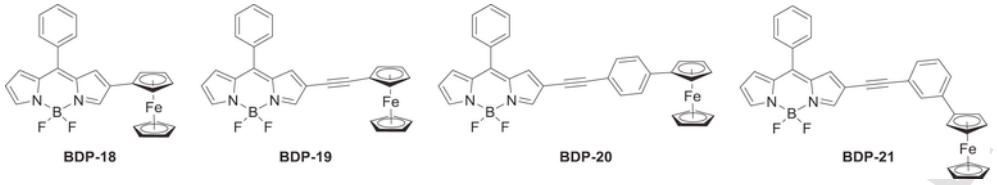

Fig. 9. Chemical structures of BODIPYs **BDP-18- BDP-21**.

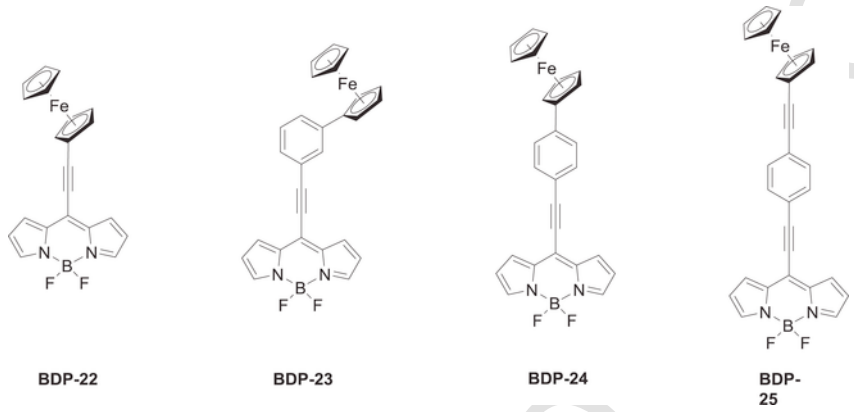

Fig. 10. Chemical structures of BODIPYs **BDP-22- BDP-25**.

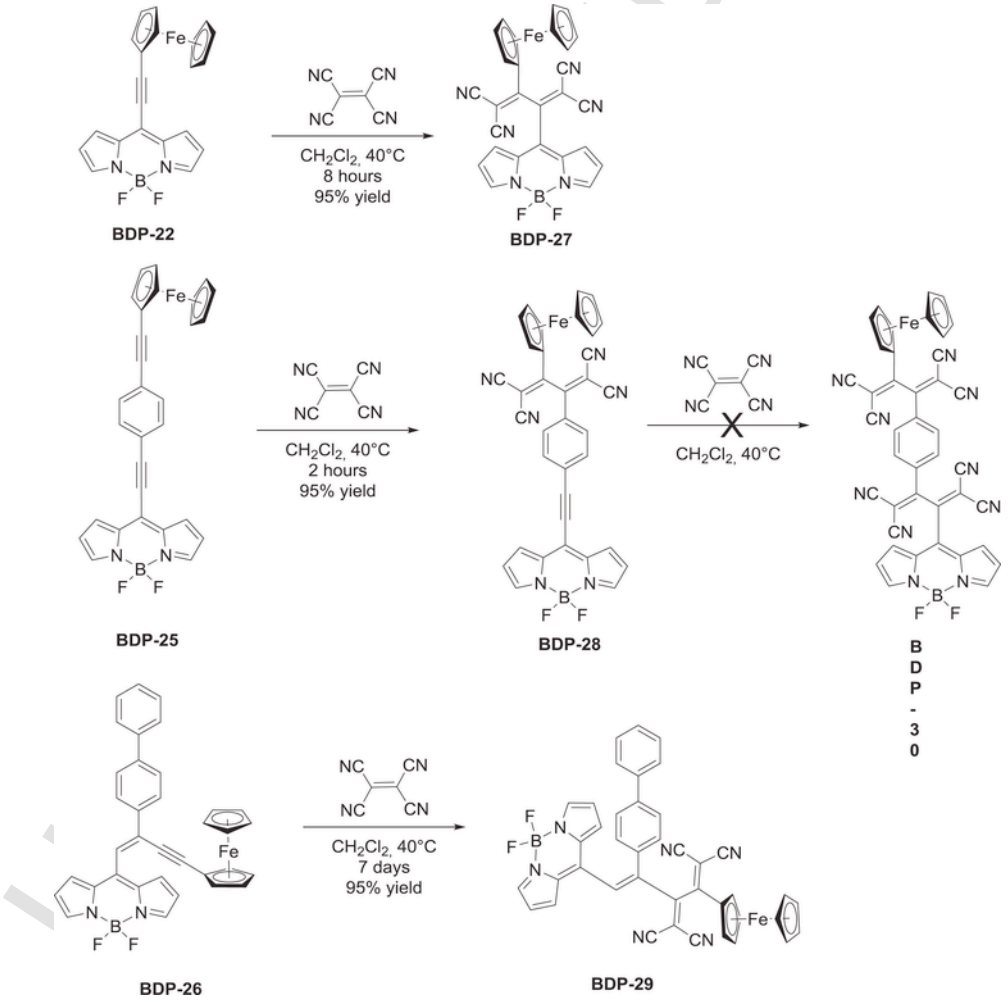

Fig. 11. Chemical structures of BODIPYs resulting from the [2 + 2] cycloaddition-*retro*-cyclization with TCNE.

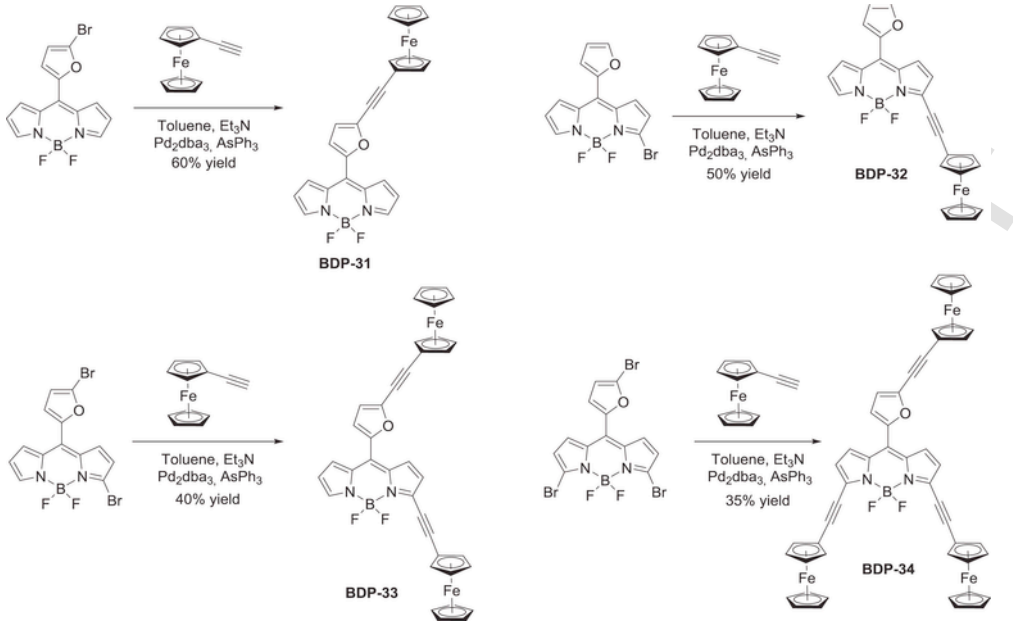

Fig. 12. Synthetic routes to BODIPYs **BDP-31- BDP-34**.

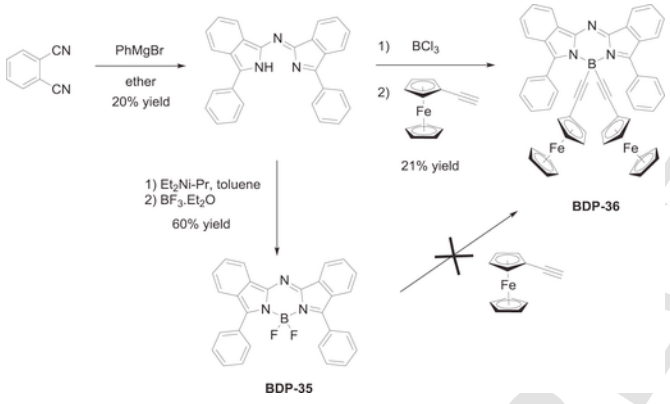

Fig. 13. Synthetic route to **BDP-35** and **BDP-36**.

nally, reaction of **BDP-5** with an excess of 4-dimethylaminobenzalhyde furnished **BDP-7** in 57% yield (see Fig. 6). Due to the specific substitution of **BDP-8**, only one position can react during the Knoevenagel reaction so that only 1.5 equivalent of ferrocenecarboxaldehyde was required to produce **BDP-9** in 45% yield.

Interestingly, for **BDP-6** and **BDP-7**, panchromatic absorption spectra were found with an absorption extending from 350 until 950 nm. i.e. the infrared region. While comparing the absorption spectra of the symmetrically substituted **BDP-6** with the asymmetrically substituted **BDP-7**, all peaks were found to be at almost the same positions excepted for the near absorption band that was split into two peaks at 650 and 750 nm for **BDP-7** due to the double contribution of ferrocene and the electron-donating dimethylaminobenzene. In the case of **BDP-6**, a unique peak was found at 750 nm, consistent with a symmetrical substitution of BODIPY. Compared to the previously discussed ferrocene-BODIPY conjugates for which differences could be found for their redox potentials, depending of their respective substitutions (see Tables 1 and 2), in the case of **BDP-5- BDP-7** and **BDP-9**, similar electrochemical data were determined. Noticeably, for **BDP-6** which is symmetrically substituted, the two ferrocene groups could be oxidized separately with an interval of 150 mV by reducing the scan rate, what is greater than that observed for the previous ferrocene-BODIPY combinations. By spectro-electrochemistry, oxidation of **BDP-5- BDP-7**,

Table 5
Photophysical characteristics of **aza-BODIPY.**

	λ_{abs1} (nm)[a]	λ_{abs2} (nm)[a]	ε_1 (M^{-1} cm^{-1})[a]	ε_2 (M^{-1} cm^{-1})[a]	E_{ox} (V)/E_{red}(V)	Ref
BDP-35	715	–	87000	–	1.076, 0.558, −1.062, −1.837[b]	68
BDP-36	706	–	80000	–	0.537, 0.157, 0.072, −1.190, −1.909[b]	68
BDP-39	602	–	65000	–	1.02, 0.12, −1.18, −1.51[c]	72
BDP-40	602	–	66000	–	1.03, 0.13, −1.56, −2.18[c]	72
BDP-41	651	–	67000	–	1.09, 0.13, −0.80, −1.47, −2.02[c]	71
BDP-42	653	–	70000	–	1.06, 0.14, −1.51, −2.07[c]	71
BDP-43	623	850	16500	14000	0.45, −0.01, −1.15[b]	69
BDP-44	599	837	15000	25000	0.71, 0.35, 0.09, −0.07, −1.31[d]	72
BDP-45	628	856	49700	43800	0.62, −0.53, −1.29[e]	74
BDP-46	680	824	50000	43400	0.59, −0.55, −1.35[e]	74

[a] Measured in DCM.
[b] Recorded in DCM with TBAF as the support electrolyte, potentials determined vs. ferrocene/ferrocenium couple.
[c] Recorded in DCM with $TBAPF_6$ as the support electrolyte, potentials determined vs. ferrocene/ferrocenium couple.
[d] Recorded in DCM with TBAB as the support electrolyte, potentials determined vs. ferrocene/ferrocenium couple.
[e] Recorded in DCM with TBAP as the support electrolyte, potentials determined vs. ferrocene/ferrocenium couple.

BDP-9 resulted in a decrease of the ICT band, accompanied by the appearance of new bands in the NIR region, at 754 nm for **BDP-5** and 842 nm for **BDP-9** together with a broad band at ca. 1200 nm for the two systems. Similarly, oxidation of the asymmetrically substituted **BDP-7** resulted in a decrease of the ICT band, combined with the appearance of two new bands at 1000 and 1500 nm respectively. Comparison of the absorption spectra of **BDP-7**$^+$ with those of the monosubstituted **BDP-6**$^+$ and **BDP-9**$^+$ revealed similar changes so that the

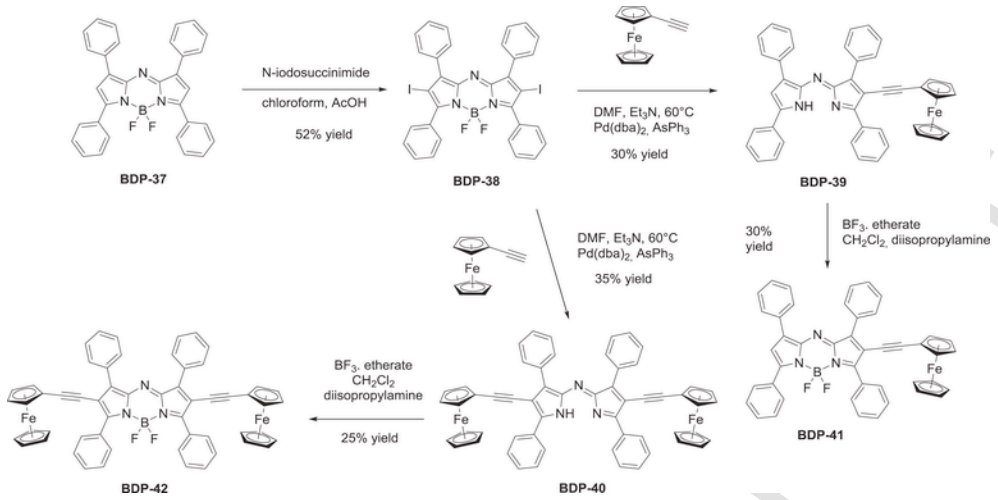

Fig. 14. Synthetic route to **BDP-41** and **BDP-42**.

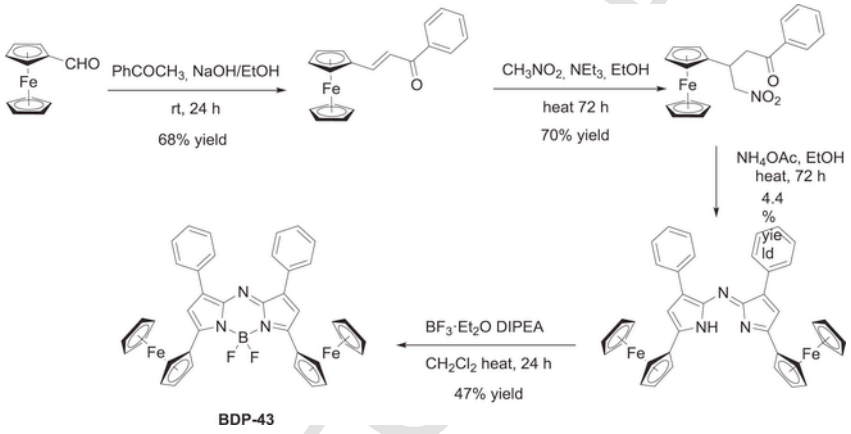

Fig. 15. Synthetic route to **BDP-43**.

first oxidation process was determined as occurring on the ferrocene side. These conclusions were confirmed by the reversibility of the oxidation process, consistent with an electrochemical process centered on the ferrocene moiety, irrespective of the conjugates. Here again, possibility to oxidize **BDP-5- BDP-7** and **BDP-9** with a chemical agent was examined and $Fe(ClO_4)_3$ was selected as the oxidant. However, for **BDP-7**, an oxidation sequence inverted compared to that observed during the electrochemical process was found. By chemically oxidizing **BDP-7** with $Fe(ClO_4)_3$, the oxidation of the dimethylaminophenyl group preceded that of ferrocene. No clear explanation could be provided to support this unexpected result. Finally, the usual conclusions could be once again deduced from the examination of the photoluminescence properties of these conjugates, with a partial recovery of the luminescence properties subsequent to the oxidation of ferrocene.

As other strategy of interest to generate ferrocene-based NIR dyes is the direct linkage of ferrocene to the pyrrole moieties. This strategy is recent since the first example was reported in 2017.

To examine this unprecedented combination, ferrocene was connected to the pyrrole groups of 2-pyridone-appended BODIPYs and it proves to be an effective strategy to lower the MLCT state and red-shift the NIR absorption band [60]. From a synthetic point of view, the synthesis of **BDP-10** and **BDP-11** is quite complicated and requires 11 steps for **BDP-11** and 7 steps for **BDP-10** respectively. The key step for the synthesis of **BDP-10** and **BDP-11** is 3-(2-acetoxyethen-1-yl)-5-methyl-1,7-diphenyl-2,6-dicarbethoxy-4,4-difluoro-4-bora-3a,4a,-diaza-*s*-indacene **6** which is not commercially available and can only be obtained in five steps starting from the benchmark ethyl 2-methyl-4-phenyl-1*H*-pyrrole-3-carboxylate **1** by following the procedure depicted in Fig. 7 [61]. Briefly, **BDP-10** is obtained first by condensing aminoferrocene to **6**, furnishing the intermediate imine that is subsequently cyclized to form the monosubstituted BOPIDY **BDP-10**. By converting **BDP-10** to enamine and by subsequent hydrolysis, an aldehyde could be introduced and by repeating the condensation of aminoferrocene and the intramolecular cyclization steps, **BDP-11** could be obtained in low yields, this latter being obtained after four additional steps.

By analysing the optical properties, a red-shift of the π-π* transition of BOPIDY from 552 nm for **3**–581 nm for **BDP-10** and 651 nm for **BDP-11** were respectively determined in dichloromethane. Contrarily to **BDP-9**, no intense MLCT bands were detected for **BDP-10** and **BDP-11** in the NIR region. Authors assigned the low intensity of the MLCT bands to their broadness resulting from their overlap with other π–π* transitions. However, an absorption extending until 750 nm and 850 nm could be still detected in the UV–visible absorption spectra of **BDP-10** and **BDP-11**. By spectroelectrochemistry, the lack of electronic coupling between the two ferrocenes in **BDP-11** was demonstrated by the appearance upon oxidation of the ferrocene units of an intense absorption band peaking at 675 nm; close to the absorption band detected at 607 nm for the monosubstituted **BDP-10**. In fact, this work highlighted the inefficiency of this approach and confirmed the results obtained by electrochemistry, the two ferrocenes units being oxidized at almost the same potentials. If the electronic communication would have existed by mean of a π-conjugated system, a significant difference

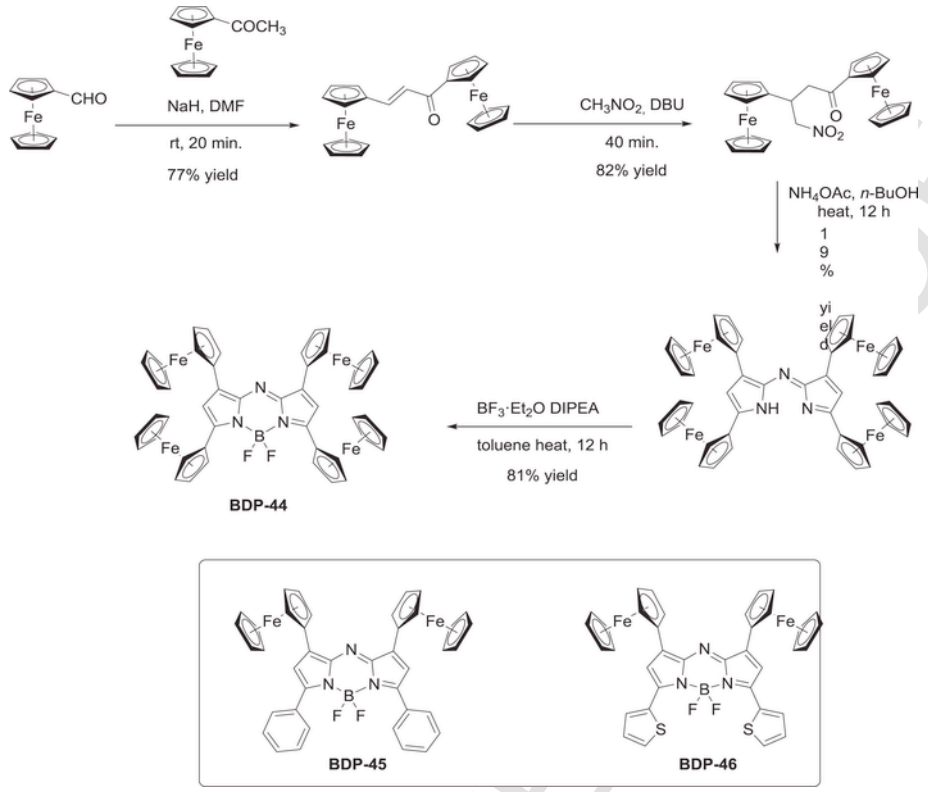

Fig. 16. Synthetic route to **BDP-44** and chemical structures of **BDP-45** and **BDP-46**.

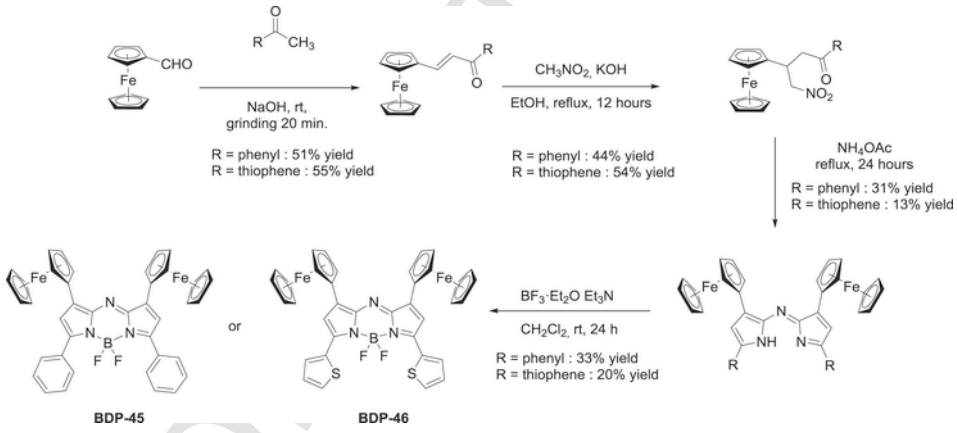

Fig. 17. Synthetic route to **BDP-45** and **BDP-46**.

between the two oxidation waves should have been observed, oxidation of the first ferrocene affecting the oxidation of the second one. Finally, the complete quenching of luminescence detected for **BDP-10** and **BDP-11** reflects the efficient electron-transfer occurring between the ferrocene units and the photoexcited BODIPY, by mean of through-space interactions. By transient absorption spectroscopy, recovery of the ground state by back electron transfer from BODIPY to the oxidized ferrocene was determined to occur in 14.6 ± 1.1 ps and 134.9 ± 4.3 ps for **BDP-10** and **BDP-11** respectively. The faster excited state decay in **BDP-10** was assigned to the high energy level of the HOMO orbital and its more localized character, contrarily to **BDP-11** where the HOMO level is delocalized onto the two ferrocene units.

The vinyl group was not the only spacer to be studied in the literature for the design of ferrocene-BODIPY conjugates and ethynyl spacer was examined as a possible alternative. The first examples of donor-acceptor structures comprising ethynyl spacers were reported in 2010 [62]. The synthetic routes to push-pull **BDP-12- BDP-15** are depicted in Fig. 8. All of them were obtained by a Sonogashira cross-coupling reaction of the benchmark ethynylferrocene with the corresponding BODIPY (with reaction yields ranging from 65 to 70%), excepted **BDP-14** that was synthesized in two steps starting directly from ferrocene-carboxaldehyde. However, if the spacer is different, no major difference could be found between the photophysical properties of the ferrocene-BODIPY conjugates **BDP-12** and **BDP-13** based on an ethynyl spacer and **BDP-2** and **BDP-1** based on a vinylic spacer. Indeed, the two main absorption peaks were found to be at almost the same positions, around 540 nm and 600 nm for **BDP-12** and **BDP-2**, 550 nm and 700 nm for **BDP-13** and **BDP-1** respectively (See Tables 2 and 4). As anticipated, formation of the ferrocene-BODIPY conjugates **BDP-12-BDP-14**resulted in the appearance of an ICT band at low energy in the absorption spectra. For **BDP-12-BDP-14**, a broad ICT band extending between 550 nm and 800 nm could be found for the three chro-

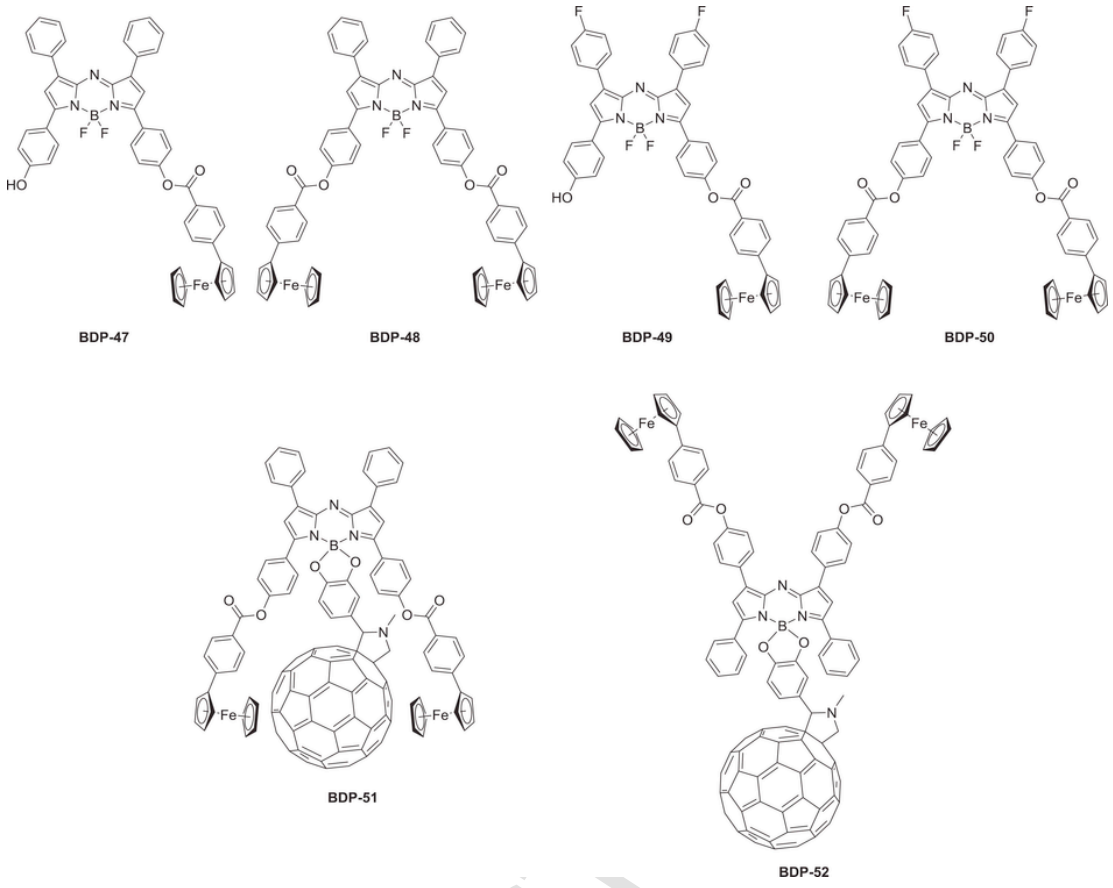

Fig. 18. Ferrocene-BODIPYs conjugates based on ester linkages.

mophores. An almost complete quenching of luminescence was found for **BDP-12-BDP-14**, comparable to that reported in the literature. This extinction of luminescence results from a rapid photoinduced electron transfer between the ferrocene unit and BODIPY.

However, a major difference could be found between **BDP-14** and **BDP-15**, namely, the two chromophores bearing a ferrocene unit attached at the *meso*-position. Indeed, if an ICT band could be found for **BDP-14** where the ferrocene is in direct conjugation with the BODIPY moiety, no ICT band was detected in the absorption spectrum of **BDP-15**, demonstrating that the conjugation between the BODIPY core and the ferrocene unit was interrupted by the phenyl spacer, attributable to its orthogonal orientation relative to that of the BODIPY core. The same conclusions were previously established for **BDP-16** of comparable structure or for **BDP-17**, the electronic conjugation being adversely affected by the presence of the phenyl spacer (see chemical structures in Fig. 8) [63]. However, a slight interaction between the ferrocene unit and the BODIPY core could however be demonstrated by electrochemistry, the ferrocene unit being more difficult to oxidize than the free ferrocene. Possibility to design an ON/OFF optical switch with **BDP-12-BDP-14** by modulating the oxidation state of ferrocene was also demonstrated. In the different examples reported above, substitution of pyrrole was examined at the α-position. Other authors examined the possibility to substitute the pyrrole groups at the β-position, and the dyes **BDP-18- BDP-21**were designed in this aim (see Fig. 9) [64]. Several differences on the photophysical properties could be found between the two substitution modes (See Table 4)

First, comparison of **BDP-12** and **BDP-19** that bear the same ethynylferrocene substituent revealed the position of the ICT bands to be almost similar, peaking at 531 nm for **BDP-12** and 523 nm for **BDP-19**. Conversely, major differences could be found concerning the molar extinction coefficients, peaking at 46770 mol^{-1} cm^{-1} for **BDP-12** and 32400 mol^{-1} cm^{-1} for **BDP-19**. By comparing the **BDP-12- BDP-15** and **BDP-18- BDP-21** series and irrespective of the substitution pattern, a clear improvement of the extinction coefficients can be observed for the dyes substituted at the β-position (~45000–76000 for the α-substituted series vs. ~32000–36000 for the β-substituted series).

As abovementioned, position of the ferrocene unit influences the photophysical properties of ferrocene-BODIPY conjugates. The way how the two partners are connected also affect the optical properties, as exemplified with the introduction of an aromatic spacer between the BODIPY core and the ferrocene unit that isolates both partners (for instance **BDP-15)**. In the search for the best linkers that could optimize the electronic communication at the *meso*-position, a series of conjugates differing by the type, the substitution pattern and the size of the spacer separating the ferrocene unit from the BODIPY core was investigated (See Fig. 10) [65]. In this study, the systematic presence of the triple bond directly connected to the BODIPY core greatly improved the communication since an ICT band could be detected for all compounds. As the first manifestation of this, a characteristic electronic transition $S_0 \rightarrow S_2$ transition of BODIPY at ca. 430 nm was red-shifted while elongating the spacer between the donor and the acceptor, demonstrating that an interaction exists between ferrocene and the BODIPY motif. In this study, the solvatochromic properties of the four dyes were also examined, what is rarely studied for ferrocene-BODIPY conjugates. A positive solvatochromism could be detected for **BDP-22- BDP-25**. Among the most interesting findings, authors demonstrated the substitution of BOPIDY at the *meso* position to induce a more efficient electronic delocalization. Indeed, a comparison carried out between **BDP-22**and **BDP-12** (substituted at the α-position of pyrrole) and **BDP-19** (substituted at the β-position of pyrrole) revealed a minor

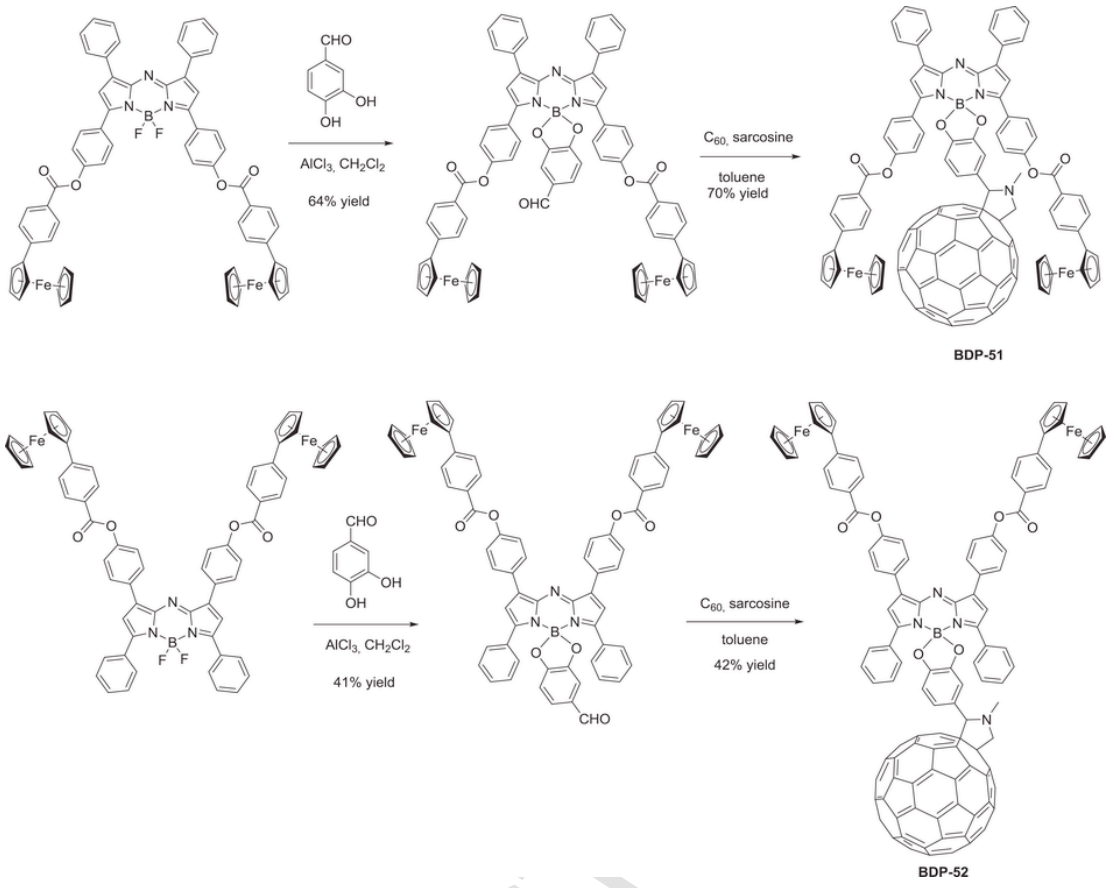

Fig. 19. Ferrocene-BODIPYs conjugates based on ester linkages.

red-shift of the ICT band by about 8 and 15 nm with respect to **BDP-12** and **BDP-19**. Parallel to this, a dramatic increase of the molar extinction coefficient could be observed, the extinction coefficients decreasing from 74622 $mol^{-1} cm^{-1}$ for **BDP-22** to 46770 and 32,400 $mol^{-1} cm^{-1}$ for **BDP-12** and **BDP-19** respectively. In fact, the highest molar extinction coefficients were obtained upon substitution of BODIPYs at the *meso*-position, only if a triple bond is directly connected to the BODIPY core to avoid an internal torsion.

As mentioned in section 2.1, triple bonds can efficiently react with TCNE to form by a [2 + 2] cycloaddition-*retro*-cyclization the electron-withdrawing 1,1,4,4-tetracyanobuta-1,3-diene (TCBD) structure. In this context, **BDP-22** and **BDP-25** were revisited and the corresponding adducts **BDP-27** and **BDP-28** could be obtained by mixing TCNE and the corresponding ferrocene **BDP-22** or **BDP-25** in a 1:1 ratio, at 40 °C for 2 and 8 h respectively [66]. Parallel to this, **BDP-26** could undergo a similar transformation, furnishing after 7 days the targeted **BDP-29** (see Fig. 11).

All compounds **BDP-27**, **BDP-28** and **BDP-29** were obtained in 95% yield, demonstrating the [2 + 2] cycloaddition-*retro*-cyclization to be an efficient reaction, especially for alkyne groups surrounded by electron-rich groups. Due to the steric hindrance existing around the triple bond in **BDP-28** and its electro-deficiency resulting from the simultaneous presence of both the BODIPY and the TCBD unit, **BDP-28** could not be converted to **BDP-30**. Contrarily to what was observed in section 2.1, conversion of the triple bond to TCBD only slightly modified the optical properties of **BDP-27- BDP-29** compared to their parent structures **BDP-22**, **BDP-25** and **BDP-26** respectively. Thus, a redshift of 29, 11 and 9 nm were respectively obtained for the $S_0 \rightarrow S_1$ transitions of BODIPY at ca 550–600 nm with respect to the parent structures **BDP-27- BDP-29**. It can be thus concluded that due to the steric hindrance generated by the TCBD group at the *meso*-position of BODIPY, only a weak electronic communication exists between the peripheral ferrocene and the BODIPY core. Furane is another aromatic spacer that was also investigated as a linker potentially capable to maintain the electronic coupling between ferrocene and BODIPY [67]. In this case, the steric hindrance between the five-membered ring furyl group and pyrroles is drastically reduced compared to what is induced by a six-membered aromatic ring, enabling to reduce the dihedral angle and optimize the electronic conjugation. To investigate this point, four derivatives **BDP-31- BDP-34** were synthesized by Sonogashira cross-coupling reactions of ethynylferrocene with the appropriate BODIPYs, providng the final products with reaction yields ranging from 35 to 60% yield (see Fig. 12).

A significant reduction of the reaction yields by increasing the number of substituents could be evidenced, decreasing from 60% for **BDP-31** to only 35% for the trisubstituted product **BDP-34**. Non classical reaction conditions were employed for the Sonogashira coupling since a combination $AsPh_3/Pd_2dba_3$ was used instead of the standard CuI/$Pd(PPh_3)Cl_2$ mixture. Presence of an electronic coupling between ferrocene and the BODIPY acceptor was evidenced by absorption spectroscopy, the $S_0 \rightarrow S_1$ transition of BODIPY at ca. 500 nm being redshifted to 530–570 nm for **BDP-31- BDP-34**. Parallel to this, presence of ICT bands at low energy for all compounds attests of the electronic conjugation existing within all structures. The most red-shifted ICT band for the series **BDP-31- BDP-34** was determined for **BDP-34** (690 nm) bearing three electron donors. Increase of the molar extinction coefficients with the number of ferrocene units per BODIPY confirmed the contribution of each ferrocene unit to the electronic delocalization and the ability of pyrrole to act as a conjugated spacer.

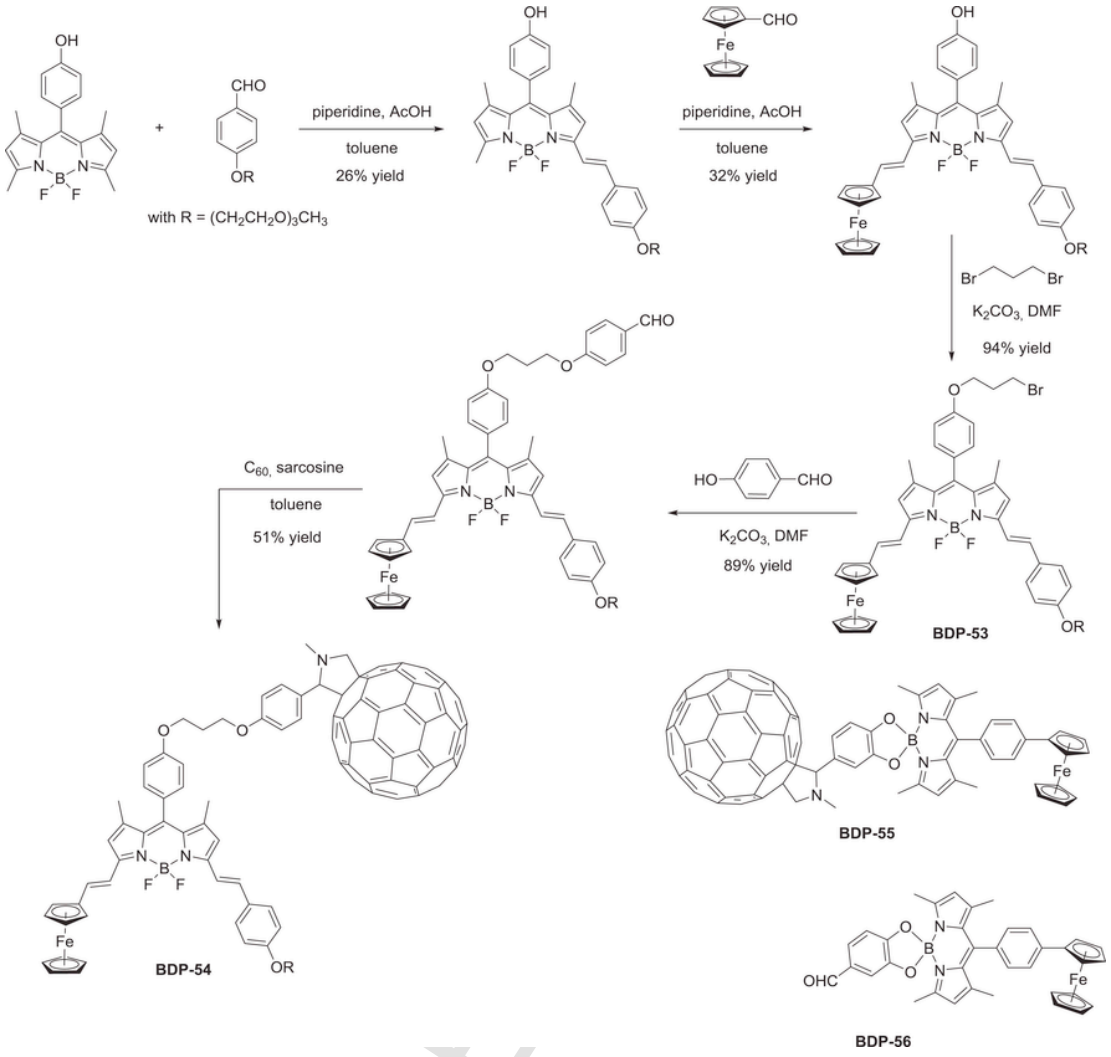

Fig. 20. Ferrocene-BODIPYs conjugates based on a flexible linkage between C_{60} and the conjugate.

Table 6
Photophysical characteristics of **BODIPY-C_{60}**.

	λ_{abs1} (nm)[a]	λ_{abs2}(nm)[a]	E_{ox} (V)/E_{red}(V)	Ref
BDP-47	460	680	0.52, 0.08, –0.84[b]	82
BDP-48	480	660	0.77, 0.07, –0.78[b]	82
BDP-49	460	680	0.55, 0.07, –0.84[b]	82
BDP-50	480	660	0.81, 0.08, –0.76[b]	82
BDP-51	475	650	1.12, 0.44, –0.36, –0.64, –1.04[b]	83
BDP-52	480	645	1.14, 0.49, –0.37, –0.63, 1.02[b]	84
BDP-53	665	–	0.42, –0.57, –0.99[b]	86
BDP-54	665	–	0.50, –0.99[b]	86
BDP-55	505	–	0.05, –1.03, –1.42, –1.61, –2.05[b]	88

[a] Measured in benzonitrile.
[b] Recorded in benzonitrile with $TBAClO_4$ as the support electrolyte, potentials determined vs. ferrocene/ferrocenium couple.

Besides, if ethynyls and pyrroles are two spacers of interest which can greatly contribute to generate push-pull chromophores with a marked intramolecular electronic delocalization, the position of attachment is determinant, and a complete lack of communication was evidenced for BODIPYs functionalized at the boron atom [68]. In this situation, no conjugation could be expected via through-bond couplings but by through-space interactions. Functionalization of the inner positions of BODIPYs is a challenge as the size of the substituent governs its ability to be connected.

In fact, all attempt of double functionalization of the boron atom by ferrocene failed due to its bulkiness and introduction of an ethynyl spacer was required. In this second case, and by use of a chlorine-substituted BODIPY, **BDP-36** could be obtained in 21% yield. Conversely, the fluorine-based aza-BODIPY **BDP-35** did not furnished **BDP-36** (see Fig. 13).

Authors observed **BDP-36** to be only partially stable, the product rapidly degrading in solution. The weak influence of the ferrocene units on the photophysical properties was easily detected, only a slight shift of the absorption maxima being determined between **BDP-35** and **BDP-36**. Thus, absorption maxima peaking at 715 nm for **BDP-35** and 706 nm for **BDP-36** were measured (See Table 5). Conversely, a two-fold decrease of the PLQY of **BDP-36** relative to that of **BDP-35** could be calculated, resulting from a fast electron transfer between the electron-donating ferrocene and the photoexcited aza-BODIPY acceptor. Noticeably, the absorption band was relatively narrow for **BDP-35** and **BDP-36**, ranging from 600 to 750 nm, making this two dyes NIR absorbing dyes. As the most interesting finding of this work, a through-space interaction could be evidenced between the two ferrocene units by electrochemistry, the oxidation waves being separated by 100 mV. This result was unexpected, considering that the two Fe centers are separated from each other by a distance of 9.85 Å, much longer than the distance previously reported in the literature for systems exhibiting a through-space interaction [69]. From a photophysical viewpoint,

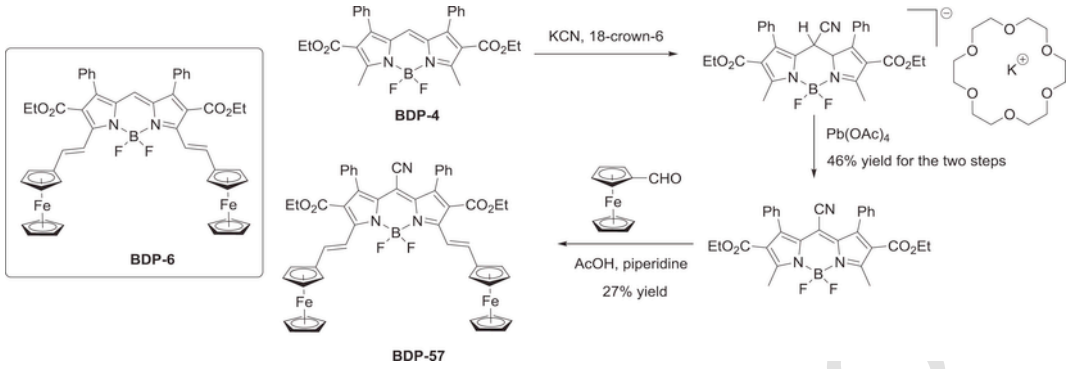

Fig. 21. Synthetic route to BODIPYs **BDP-57**.

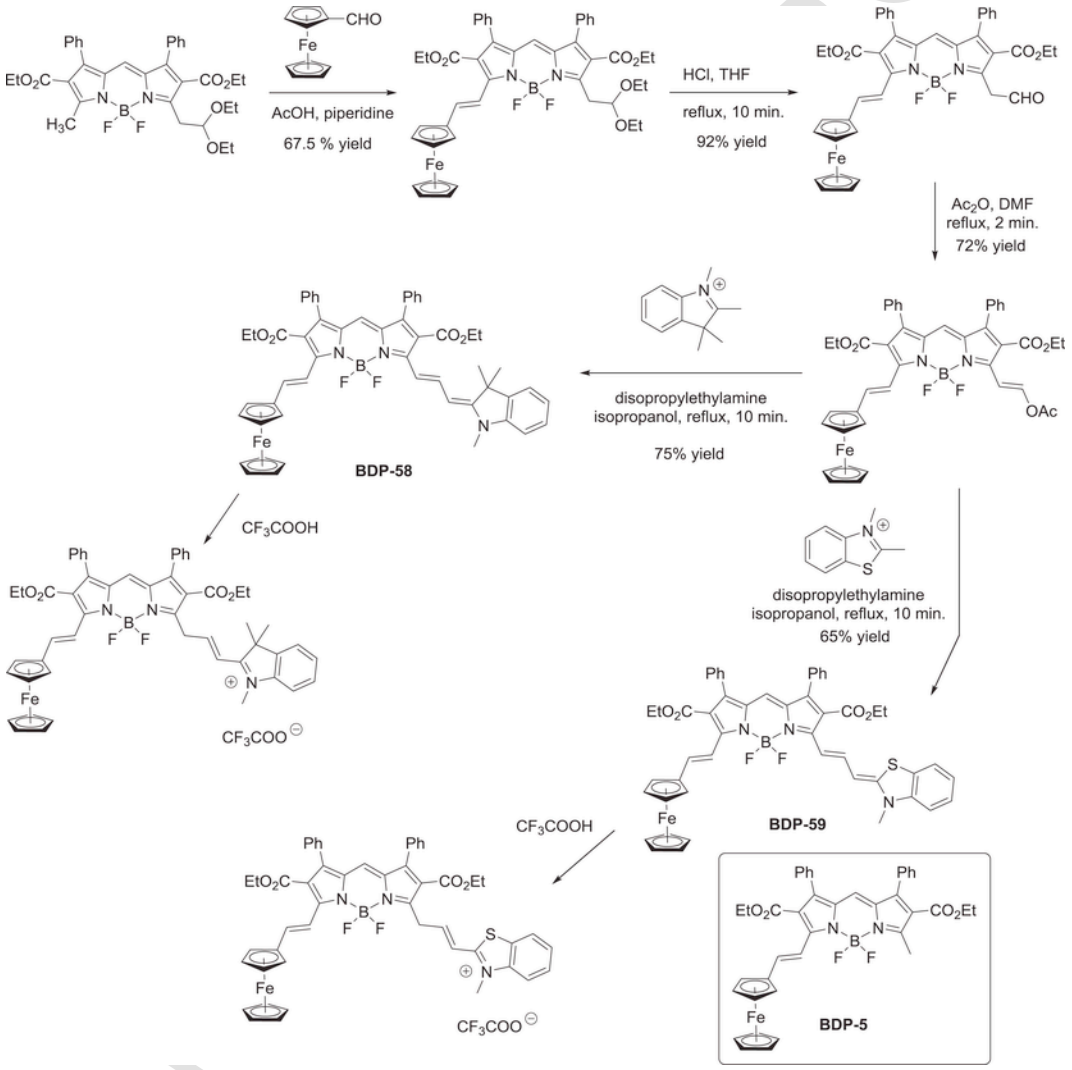

Fig. 22. Synthetic route to BODIPYs **BDP-58** and **BDP-59**.

transient absorption spectroscopy revealed a dramatic elongation of the excited state lifetime, reaching 4.8 μs for **BDP-36** contrarily to 1.9 ns for **BDP-35**. Authors also demonstrated this unexpected elongation of the excited state lifetime to result from complex excited-state dynamics. Upon excitation, the initial excited state resulted in a charge separation state with a reorganization energy of 0.5 eV which is much greater than that reported for similar systems [70]. Following the initial charge separation, a rapid charge recombination occurring in the inverted Markus regime results in the formation of a triplet state located either on the aza-BODIPY or the ferrocene unit. Interestingly, the charge transfer and the charge recombination proved to be extremely fast due to the presence of the triple bonds between the boron atom and the ferrocene units. By mean of this spacer, an efficient spin-orbit coupling could occur, without taking recourse to heavy atoms, opening the way to a variety of applications for these compounds ranging from optoelectronics to photochemistry and photopolymerization. As far as NIR dyes are concerned, the absorbance of **BDP-35** and **BDP-36** in the NIR region was relatively limited, falling around 750 nm. To improve

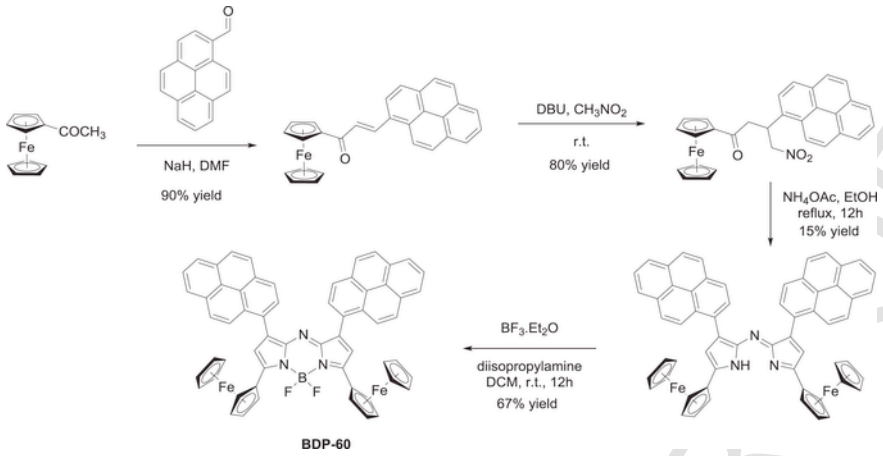

Fig. 23. Synthetic route to aza-BODIPYs **BDP-60**.

Table 7
Photophysical characteristics of **BDP-57, BDP-58, BDP-59, BDP-60 and BDP-62.**

	λ_{abs1} (nm)[a]	λ_{abs2} (nm)[a]	ε_1 (M^{-1} cm^{-1})[a]	ε_2 (M^{-1} cm^{-1})[a]	E_{ox} (V)/E_{red}(V)	Ref
BDP-57	654	926	39000	27500	0.25, 0.05, −0.80, −1.70[b]	95
BDP-58	494	810	18000	68000	0.21, 0.05, −1.23[c]	101
BDP-59	489	818	17500	59000	0.13, −0.13, −1.30[c]	101
BDP-60	638	854	57000	52000	1.1, 0.85, 0.44, 0, −1.16, −1.84[b]	109
BDP-62	564	694	27000	34000	0.90, 0.24, 0.03[d]	110,111

[a] Measured in DCM.
[b] Recorded in DCM with TBAB as the support electrolyte, potentials determined vs. ferrocene/ferrocenium couple.
[c] Recorded in DCM with TBAP as the support electrolyte, potentials determined vs. ferrocene/ferrocenium couple.
[d] Recorded in DCM with TBAF as the support electrolyte, potentials determined vs. ferrocene/ferrocenium couple.

the absorption ability in the NIR region, numerous derivatives differing by the position of the ferrocene-ethynyl group(s) on aza-BODIPY were designed and synthesized. In this field, **BDP-41** and **BDP-42** can be cited as relevant examples, the onset of their absorption spectrum being detected at 1200 nm and 1100 nm respectively [71]. Absorption maxima peaking at 651 and 653 nm were measured in chloroform for **BDP-41** and **BDP-42** respectively. A slight increase of the molar extinction coefficient was observed for the most extended structure i.e. **BDP-42** (70000 $L mol^{-1} cm^{-1}$ vs 67000 $L mol^{-1} cm^{-1}$ for **BDP-41**). Interestingly, the synthesis of **BDP-41** and **BDP-42** was not straightforward since a reduction of **BDP-38** [72] accompanied by the loss of the BF_2 fragment was observed during the Sonogashira cross-coupling reaction. **BDP-39** and **BDP-40** were respectively obtained in 30 and 35% yield after a difficult purification. Loss of the BF_2 fragment was confirmed by ^{19}F NMR analyses. By treating **BDP-39** and **BDP-40** with boron trifluoride etherate in basic conditions, the two aza-BODIPYs **BDP-41** and **BDP-42** were obtained in 30 and 25% yield respectively (see Fig. 14).

The distance between the electron donor and the electron acceptor is another crucial parameter governing the efficiency of the electronic interactions. This point was examined with **BDP-43** (see Fig. 15) [69]. By directly introducing ferrocene onto the BODIPY ligand, absorption of **BDP-43** could be red-shifted by about 150 nm compared to **BDP-36** and the absorption maximum was detected at 850 nm. If the position of the absorption maximum is interesting, **BDP-43** could only be synthesized in low yield, as the cyclization step could only be realized in 4.4% yield. Similar to what was reported for **BDP-36**, aza-BODIPYs are only partially stable in solution and a slow degradation of **BDP-43** was detected upon standing in solution under air. The usual quenching of luminescence by ferrocene, the possibility to restore the luminescence by oxidation of ferrocene and the appearance of new bands in the NIR region upon oxidation were also characterized. While replacing the two aromatic rings of **BDP-43** by ferrocene units, no major change in the absorption properties were found. Indeed, **BDP-44** showed two intense absorption bands at 599 and 837 nm respectively in its absorption spectrum, the band at low energy corresponding to the ICT band of **BDP-44** [73].

These values are consistent with those determined for other structures such as **BDP-45** and **BDP-46** [74]. Thus, the two main absorption bands were detected at 628 and 856 nm for **BDP-45**, 680 and 824 nm for **BDP-46**. From a synthetic point of view, **BDP-44** could be prepared

Table 8
Photophysical characteristics of porphyrin derivatives **P3**, **P4** and **P5**.

	λ_{abs1} (nm)[a]	λ_{abs2} (nm)[a]	λ_{abs3} (nm)[a]	λ_{abs4} (nm)[a]	λ_{abs5} (nm)[a]	ε_1[a]	ε_2[a]	ε_3[a]	ε_4[a]	ε_5[a]	E_{ox} (V)/E_{red}(V)[b]	Ref
P3	423	521	572	604	655	263000	19000	11000	12000	3400	1.18, 1.07, 0.48, −1.20, −1.49	114–118
P3.Cu	420		550	591		246000		21000	15000		1.31, 1.03, 0.48, −1.32, −1.70	114–118
P3.Ni	423		540	584		209000		18000	14000		1.23, 1.10, 0.48, −1.27, −1.65	114–118
P3.Zn	425		560	598		282000		20000	12000		1.20, 0.98, 0.48, −1.34, −1.72	114–118
P4	424	524	568	601	655	263000	24000	15000	12000	3000		114–118
P4.Cu	421		549	587		234000		21000	15000			114–118
P4.Ni	424		540	580		178000		17000	12000			114–118
P4.Zn	425		557	595		148000		11000	6000			114–118
P5	425	521	570	604	654	521000	20000	11000	13000	5000		114–118

[a] Measured in DCM.

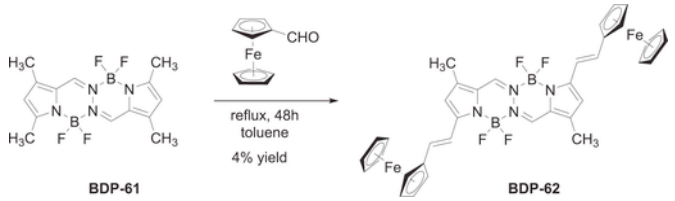

Fig. 24. Synthetic route to BOPHY-ferrocene conjugate **BDP-62**.

using a procedure similar to that developed for **BDP-43**. However, the cyclization step with ammonium acetate could be realized in higher yield than that obtained for **BDP-43**, reaching 19% (See Fig. 16).

With aim at developing a greener synthesis of BODIPYs, interestingly, the two chalcones used as precursors of **BDP-45** and **BDP-46** prepared in first step were obtained by mechanosynthesis, by grinding ferrocene-carbaldehyde with the appropriate acetyl derivative and sodium hydroxide. Using this unusual approach, the two chalcones were obtained in 51 and 55% yield respectively after 20 min of grinding. Here again, the limiting step was determined as being again the cyclization step, this latter being realized in 31% yield for the phenyl derivative and 13% for the thiophene derivative (See Fig. 17).

The combination of aza-BODIPYs and ferrocene is more and more examined in the literature due to the ability of aza-BODIPYs to be reduced at less negative potentials than their BODIPY analogues [75–81]. Aza-BODIPYs can also be reduced selectively in a one-electron process, providing new products displaying an absorption band beyond 800 nm. For these reasons, conjugates such as **BDP-47**, **BDP-48**, **BDP-49** and **BDP-50** based on ester linkages have been regarded as suitable candidates for light-harvesting applications (see Fig. 18) [82].

Indeed, the broad absorption band extending from 600 to 800 nm make these compounds potential candidates for energy conversion. A proof of concept was realized by combining within a single molecule the light harvester aza-BODIPY-ferrocene diad **BDP-48** with a fullerene acceptor, furnishing **BDP-51** [83]. Interaction between C_{60} with the aza-BODIPY-ferrocene diad resulted in a blue-shift of the ICT band of approximately 15 nm. This phenomenon was confirmed by the design of another structure i.e. **BDP-52** for which a similar blue-shift was observed relative to the absorption maximum of the parent aza-BODIPY-ferrocene diad which was not functionalized with C_{60} [84]. In these two structures, similarity of the blue-shift observed for **BDP-51** and **BDP-52** is representative of a through-space interaction resulting from the spatial proximity of both the ferrocene and BODIPY units and not from a direct interaction between ferrocene and C_{60}. Here again, bulkiness of the Buckminster fullerene required its linkage to be carried out sequentially, by first generating the dioxyboron derivatives further functionalized with C_{60} using the standard 1,3-dipolar cycloaddition reaction of *N*-methyl-2-aminoethanoic acid (sarcosine) with the corresponding aldehyde derivative to yield the fulleropyrrolidine (See Fig. 19) [85].

An efficient electronic interaction can also be issued from the spatial proximity between the electron donor and the electron acceptor. This point was notably examined with **BDP-54** in which the Buckminster fullerene is attached to the BODIPY core by mean of a flexible linkage [86]. From a synthetic point of view, the synthesis of **BDP-54** is less straightforward than that of **BDP-51** and **BDP-52** as it first requires to synthesize an asymmetrically substituted BODIPY (see Fig. 20). This goal is achieved by first condensing the aromatic aldehyde in 26% yield, followed by the introduction of the ferrocene unit by mean of a Knoevenagel reaction, achieved in 32% yield. Following this initial step, **BDP-54** could be obtained in three steps, by first alkylating the previous BODIPY with 1,3-dibromopropane, providing **BDP-53** in 94% yield. Finally, reaction of **BDP-53** with 4-hydroxybenzaldehyde in basic conditions followed by the 1,3-dipolar cycloaddition of C_{60} with sarcosine and the previous aldehyde provided the *N*-substituted *fulleropyrrolidine* compound **BDP-54** in 51% yield for the last step.

While examining the photophysical properties of **BDP-53** and **BDP-54**, unexpected results were obtained. Indeed, the UV–visible absorption spectrum of the fullerene adduct **BDP-54** was found to resemble that of the unsubstituted **BDP-53**, simply differing from that of **BDP-53** by the presence of two additional absorption bands issued from C_{60}. This absence of interaction between the ferrocene-BODIPY conjugates and the electron acceptor C_{60} was confirmed by electrochemistry, the oxidation of ferrocene in **BDP-53** and **BDP-54** being detected at the same potentials. However, upon photoexcitation of the BODIPY moiety, analyses by transient absorption spectroscopy and laser flash photolysis revealed **BDP-53** and **BDP-54** to undergo an extremely fast electron transfer, in the picosecond timescale, resulting in the formation of charge separated species. Transient absorption spectra revealed the electron transfer to occur first between ferrocene and BODIPY, forming the intermediate specie $Fc^{+\cdot}$-BODIPY$^{-\cdot}$-C_{60} further evolving towards the stabilized charge separated state $Fc^{+\cdot}$-BODIPY-$C_{60}^{-\cdot}$ with a lifetime of 500 ps. As positive point, **BDP-54** proved also to be an almost panchromatic chromophore with an absorption spectrum resulting from the sum of the different contributions (ferrocene, BODIPY, C_{60}) so that a broad absorption band extending from 470 nm until 850 nm could be evidenced, making this triad a potential light-harvester for photovoltaic applications (See Table 6). Concerning **BDP-53**, it has to be noticed that a derivative of this structure has been used as a molecular fluorescent imaging agent and a cell-selective fluorescent probe [87].

The possibility to photoinduce an electron-transfer in closely-spaced ferrocene-BODIPY-C_{60} conjugates and to obtain a stabilized charge separation state is not unusual and it was notably reported by the same authors for another triad i.e. **BDP-55** for which a lifetime of 416 ps was determined for the charge separated state $Fc^{+\cdot}$-BDP-$C_{60}^{-\cdot}$ (see Fig. 20). [88]. Due to the specific positioning of the ferrocene and C_{60} on both sides of the BODIPY core, and the distance between the two electroactive centers, an efficient charge separation between the radical cation and the radical anion could be obtained. Here again, examina-

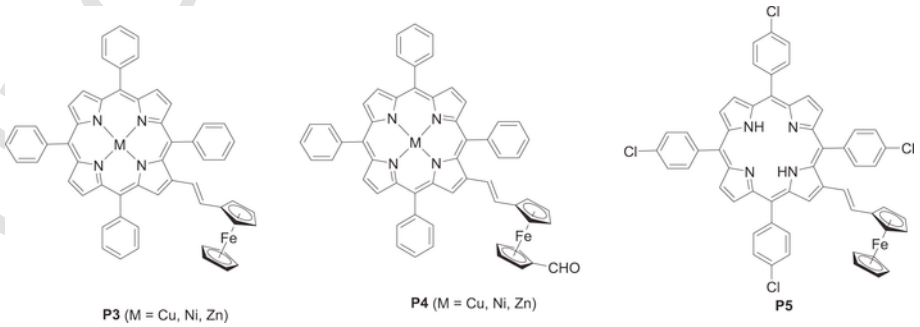

Fig. 25. Chemical structures of **P3**, **P4** and **P5** porphyrins.

Table 9
Photophysical characteristics of **P6, P7, P9 and P10.**

	λ_{abs1} (nm)	λ_{abs2} (nm)	ε_1 (M^{-1} cm^{-1})[b]	ε_2 (M^{-1} cm^{-1})[b]	E_{ox} (V)/E_{red}(V)	Ref
P6	572[a]	620[a]			0.70, 0.45, 0.02, −1.93, −2.30[c]	116,119
P7	577[a]	626[a]			0.68, 0.47, 0.04, −1.75, −2.11[c]	116,119
P9	577[b]	725[b]	14300	19000	0.1, −0.02, −0.16, −1.71, 2.19[d]	120
P10	623[b]	930[b]	30000	16300	0.32, 0.23, 0.12, −1.339, −2.02[d]	120

[a] Measured in ethanol.
[b] Measured in DCM.
[c] Recorded in DCM with $TBABF_4$ as the support electrolyte, potentials determined vs. ferrocene/ferrocenium couple.
[d] Recorded in DCM with TBAF as the support electrolyte, potentials determined vs. ferrocene/ferrocenium couple.

tion of the UV–visible absorption spectrum of **BDP-55** revealed its absorption maximum to coincide with that of **BDP-56**, evidencing the weak interaction existing between the ferrocene-BODIPY conjugate and the appended C_{60} in the ground state.

In all the above-mentioned examples, density functional theory (DFT) calculations have been carried out and these calculations have evidenced the ferrocene-centered HOMO energy level to be almost insensitive to the substitution of the BODIPY core contrarily to the LUMO energy level which can be greatly affected by the substitution pattern [56,59,65,89–94]. Notably, the MLCT band can be red-shifted by stabilization of the LUMO energy level, what is achievable by introduction of electron-withdrawing groups at the *meso*-position. The chemical modification of BODIPY is well-documented due to the considerable interest raised by these structures and the functionalization of BODIPY at the *meso*-position is among the easiest ones. Based on these considerations, the chemical modification of **BDP-4** has been explored and primarily its cyanation (see Fig. 9) [95]. If the benefits of this substitution are obvious, the old, complicated and inefficient synthetic procedures reported in the literature such as the Treibs method [96–99] have dras-

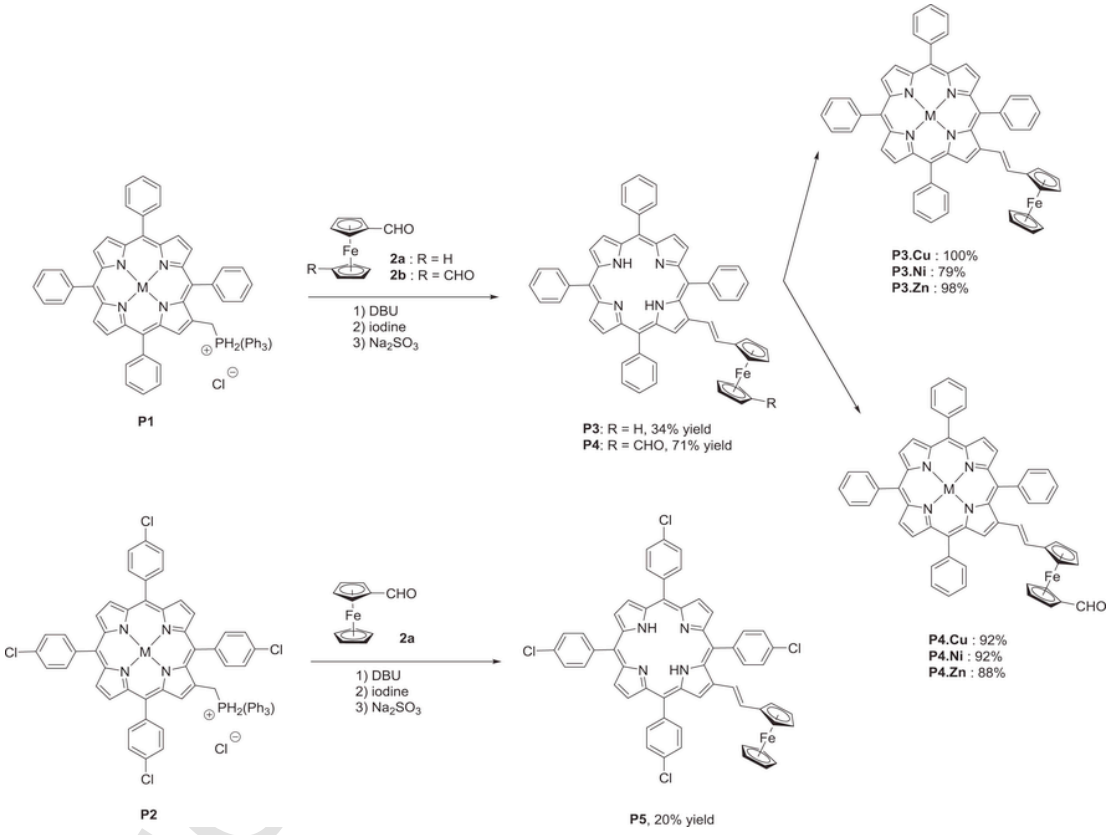

Fig. 26. Synthetic routes to **P3**, **P4** and **P5** porphyrins.

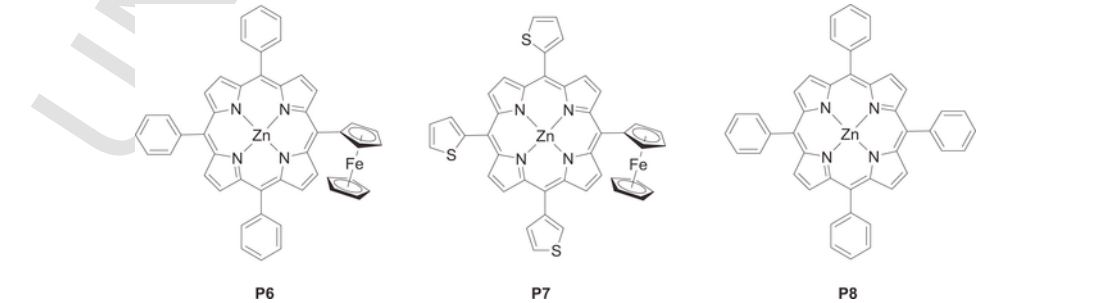

Fig. 27. Chemical structures of **P6–P8**.

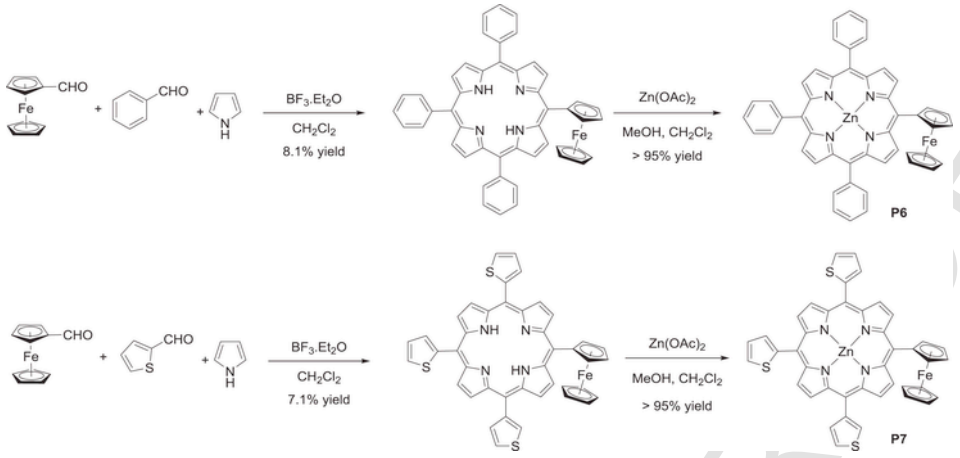

Fig. 28. Synthetic route to **P6**, **P7**.

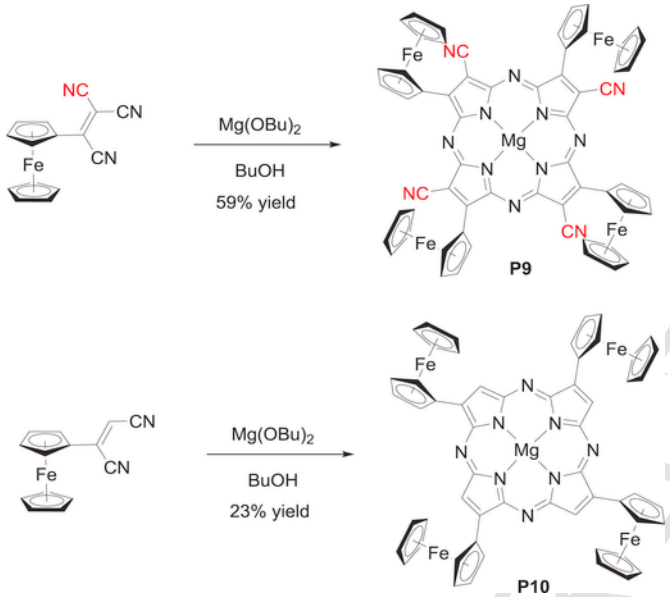

Fig. 29. Synthetic route to **P9** and **P10**.

tically limited the development of CN-substituted BODIPYs. Recently, the procedure to introduce cyano groups has been greatly improved, consisting in simply complexing the potassium cation of KCN with 18-crown-6 to increase the nucleophilicity of the cyanide anion. Subsequent treatment of the intermediate salt with lead tetraacetate in acidic conditions allowed to re-oxidize the BODIPY core (see Fig. 21) [100]. Finally, **BDP-57** could be obtained in 27% yield by reflux in a mixture acetic acid/piperidine.

From a photophysical point of view, the ability of the cyano group to modulate the electron density of the BODIPY core was evidenced by UV–visible absorption spectroscopy. Indeed, comparison of the MLCT bands of **BDP-57** and **BDP-6** (which is not substituted by the cyano group) revealed the position of the MLCT transition to be red-shifted by about 174 nm (926 nm for **BDP-57** vs. 752 nm for **BDP-6**). Parallel to this, the red-shift of the $S_0 \rightarrow S_1$ transition from 575 nm for **BDP-6** to 654 nm for **BDP-57** demonstrates the stabilization of the LUMO energy level upon introduction of the electron-accepting group.

Influence of the substitution pattern on the electronic distribution of BODIPY-ferrocene conjugates was also demonstrated with asymmetrically substituted BODIPYs. In the ferrocene-BODIDY-merocyanine triads **BDP-58** and **BDP-59**, elongation of the π-conjugated system on the merocyanine side was determined as destabilizing the π-centered molecular orbitals, what was confirmed by electrochemistry and by time-resolved photophysics. Due to the presence of the long-conjugated spacer between the BODIPY core and merocyanine end-group, protonation of this latter with a strong acid was examined for **BDP-58** and **BDP-59**, and a drastically modification of the photophysical properties was found [101]. In fact, modification of the optical properties of BODIPY-merocyanine conjugates by protonation was reported prior to this work [102–108], but the combination of the three partners within a single molecule is unprecedented. Elaboration of triads **BDP-58** and **BDP-59** required a multistep synthesis which is outlined in Fig. 22. **BDP-58** and **BDP-59** were obtained by a series of Knoevenagel reactions on the α-position of pyrrole, first by reaction of ferrocenecarboxaldehyde that provides the intermediate in 67% yield. Following an activation step consisting in converting the aldehyde function to the more reactive enol acetate, in a second step, the merocyanine moiety could be condensed efficiently, the reaction yield ranging from 65% for **BDP-59** to 75% for **BDP-58**. The spectroscopic signatures of these triads were unusual since the bands detected around 800 nm (810 nm for **BDP-58** and 818 nm for **BDP-59**) for the two structures were asymmetrical, with a shoulder at 650 nm, what is different from the NIR bands previously reported for ferrocene-BODIPY conjugates [56,59]. By electrochemistry, the transitions involved in this enlarged peak could be identified and the small energy separation between the oxidation of ferrocene and the merocyanine fragment revealed the closeness of the ferrocene-centered molecular orbitals and the BODIPY-merocyanine centered π-orbitals. While treating the solutions of **BDP-58** and **BDP-59** with a strong acid such as trifluoroacetic acid, the conjugated chain between the BODIPY core and the indole moieties could be protonated, converting the green solutions to red. By UV–visible spectroscopy, appearance of a new absorption band at 560 nm for the two compounds combined with the decrease of the NIR band confirmed the protonation. In fact, due to the interruption of the conjugation between the BODIPY core and the indole substituent, absorption spectra superimposing that of **BDP-5** could be obtained, demonstrating the protonation to occur on the indole side. Theoretical calculations confirmed the experimental results and revealed the protonation to occur specifically on the carbon atom close to the pyrrole (see Fig. 22). By transient absorption spectroscopy and contrarily to what is classically observed for ferrocene-BODIPY conjugates, a bimodal relaxation process was observed, the first component being extremely long (between 2 and 7.6 ns), indicative of a π-core centered deactivation process. The second component in the 200–250 ps timescale is typical from ferrocene-BODIPY diads with charge transfer states at low energy. In 2018, the design of aza-BODIPY bearing ferrocene substituents for the elaboration of π-complexes with carbon nanotubes was examined [109]. The peripheral functionalization of aza-BODIPY is less versatile than that of BOD-

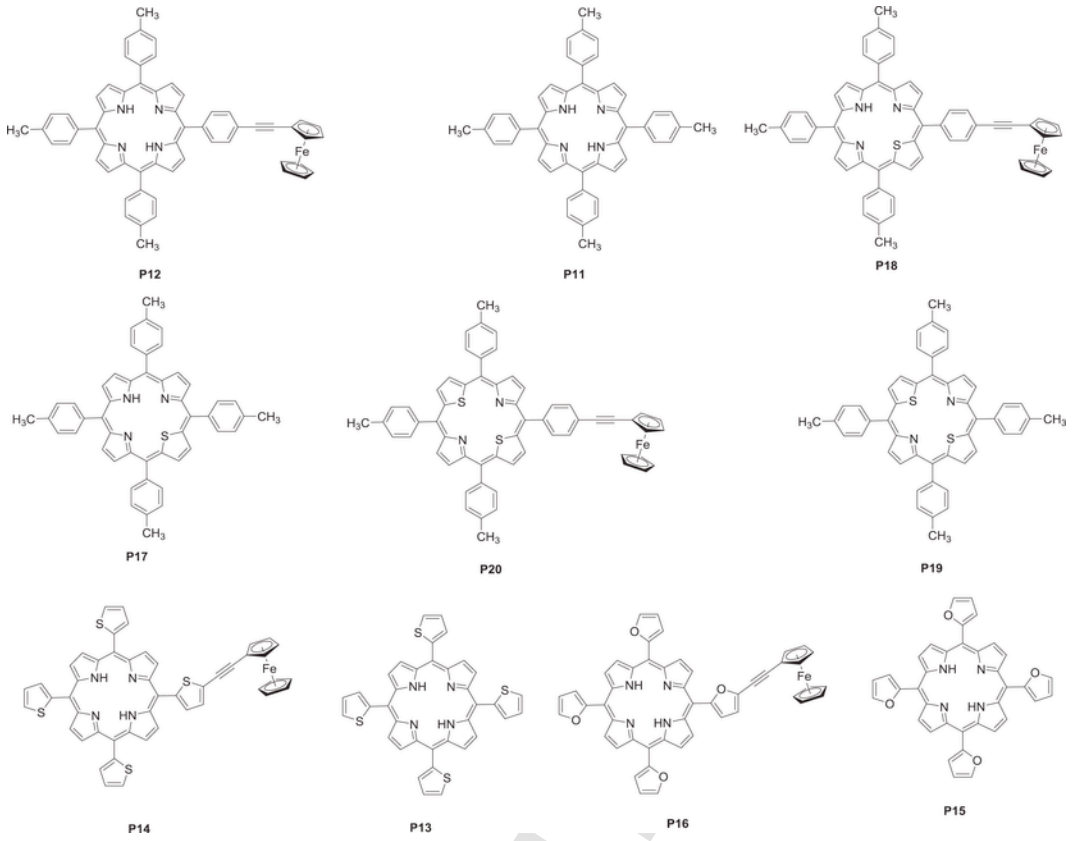

Fig. 30. Chemical structures of ferrocene-porphyrin conjugates with ferrocene and their corresponding references (without ferrocene substituents).

Table 10
Photophysical characteristics of porphyrin derivatives.

	λ_{abs1} (nm)[a]	λ_{abs2} (nm)[a]	λ_{abs3} (nm)[a]	λ_{abs4} (nm)[a]	λ_{abs5} (nm)[a]	E_{ox} (V)/E_{red}(V)[b]	Ref
P11	419	514	548	590	647	1.30, 1.03, −1.23, −1.55	122,123
P12	420	516	550	592	648	1.02, 0.61, −1.29, −1.67	122,123
P13	426	523	558	594	661	1.13, 0.89, −1.06, −1.41	122,123
P14	427	530	560	596	662	1.03, 0.62, −0.99, −1.37	122,123
P15	433	526	571	605	670	0.80, −0.98, −1.37	122,123
P16	434	527	573	605	672	0.99, 0.69, −0.90, −1.28	122,123
P17	428	514	550	618	680	1.51, 1.11, −1.03, −1.35	122,123
P18	432	516	552	620	680	1.07, 0.61, −1.07, −1.40	122,123
P19	435	514	547	633	696	1.18, −0.94, −1.23	122,123
P20	437	516	551	635	699	1.41, 1.16, 0.61, −0.95, −1.27	122,123

[a] Measured in toluene.
[b] Recorded in DCM, using tetrabutylammonium phosphate 0.1 M as the supporting electrolyte.

IPYs as the group that will further become the substituent of the pyrrole groups at the α-position is introduced in the first step of the four-step synthesis and not at the end, as classically done for the functionalization of BODIPYs (see Fig. 23). After formation of the chalcone in first step, this latter was nitromethylated with nitromethane and subsequently cyclized with ammonium acetate, providing the corresponding aza-dipyrromethane in only 15% yield. Finally, complexation with BF_3.etherate in the presence of diisopropylamine furnished **BDP-60** in 67% yield. Clearly, the synthesis of this family of aza-BODIPYs deserves to be improved with regards to the promising absorption of these structures. Indeed, the ICT was detected at 869 nm with a long tail extending until 1100 nm, making these compounds of crucial interest for numerous infrared applications (See Table 7) (see Table 8).

As the last family of derivatives associated with BODIPYs are BOPHY whose acronym stands for *bis*(difluoroboron)-1,2-*bis*{(pyrrol-2-yl)methylene}hydrazine. The first BOPHY-ferrocene conjugate **BDP-62** was reported in 2015 [110] but the chemistry of BOPHYs is recent since the first synthesis of these derivatives was reported in 2014 [111]. Photophysical properties of the BOPHY-ferrocene conjugates are drastically different from those of their BODIPY-ferrocene counterparts and these structures are now extensively studied due to the panchromatic character of their absorptions. Indeed, a broad absorption covering the visible range could be evidenced for **BDP-62**. Parallel to this, the separation of 200 mV between the two oxidation waves of ferrocene is greater than that determined in ferrocene-BODIPY conjugates (~100 mV), indicating an improved electronic interaction in these structures between the redox-responsive peripheral groups. However, if the photophysical properties are appealing, the access to these structures remains difficult, the last step being realized in only 4% yield (See Fig. 24).

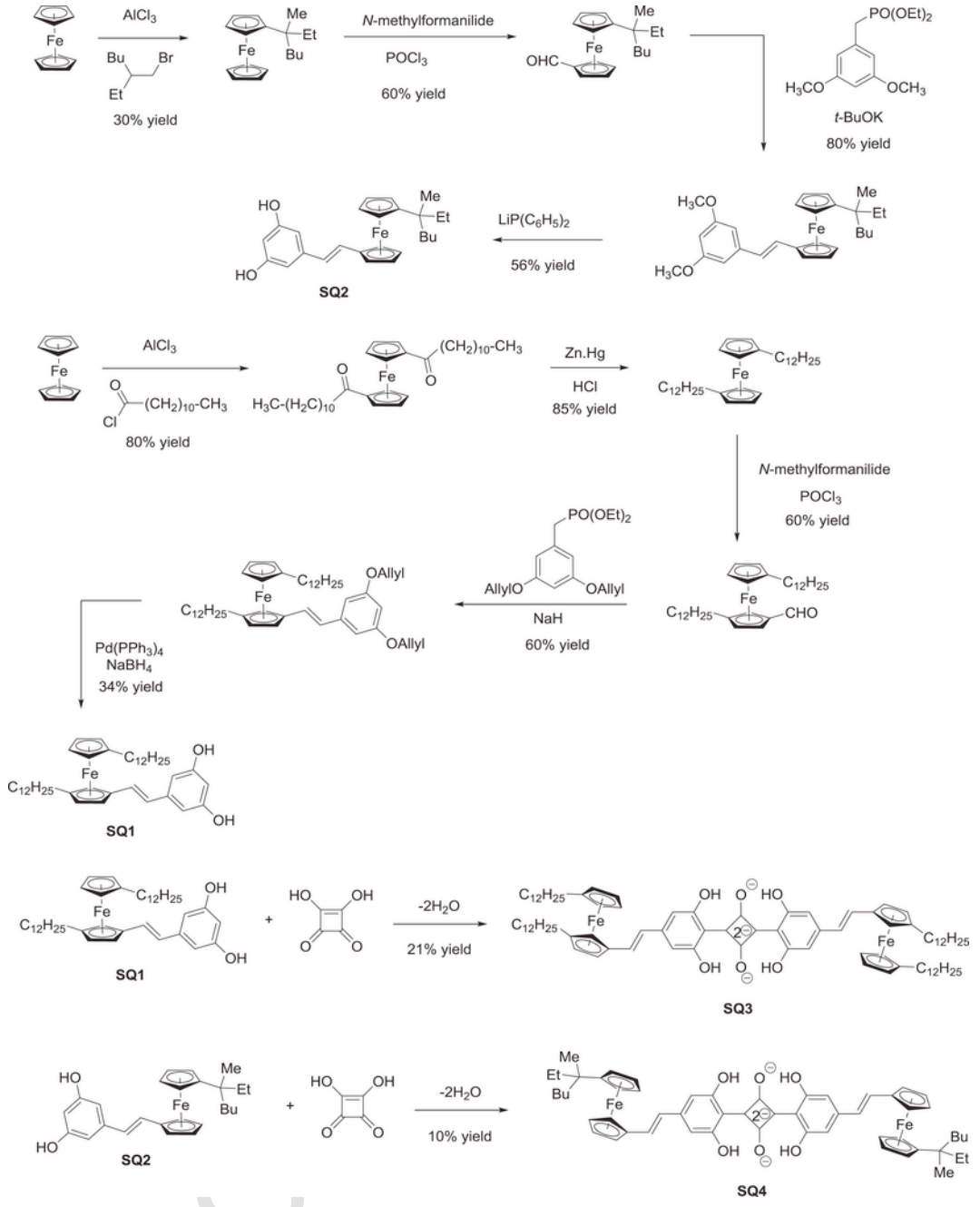

Fig. 31. Synthetic route to squaraines **SQ3** and **SQ4**.

2.3. Ferrocene with porphyrins

The combination of electroactive groups with porphyrins has been extensively studied in the literature due to the possibility to electrochemically evidence the complexation of metal cations inside the cavities [112,113]. Parallel to the modification of the electrochemical properties, the covalent linkage of highly luminescent structures (such as porphyrins) to electroactive groups provide new systems in which the oxidation state of the peripheral groups can allow to finely modulate the photoluminescence properties. Due to the extension of the π-conjugation by attachment of peripheral groups, a modification of the absorption properties of porphyrins can also be anticipated. Considering that the absorption, emission and electrochemical properties of porphyrins can be drastically modified by the substitution with ferrocene units [114–117], numerous derivatives have been developed, even if all of them don't exhibit an absorption extending until the NIR region. Only these latter will be discussed in this review. As soon as 1999, the electrochemical properties of ferrocene-metalloporphyrin conjugates with a NIR absorption were investigated [118]. In this work, only a weak mutual influence was observed by use of a vinyl spacer between the two partners, the oxidation potentials of ferrocene in **P3**, **P3.Cu**, **P3.Ni**, **P3.Zn** being identical to that of the unsubstituted ferrocene (0.48V vs. SCE) (see Fig. 25 and Table 5). The opposite situation was also true, the redox potentials of porphyrin **P3**, and metalloporphyrins **P3.Cu**, **P3.Ni** and **P3.Zn** being identical to that of the unsubstituted metalloporphyrins.

This fact was not only evidenced for **P3** derivatives but also for the **P4**-series. These observations could be transposed for their UV–visible

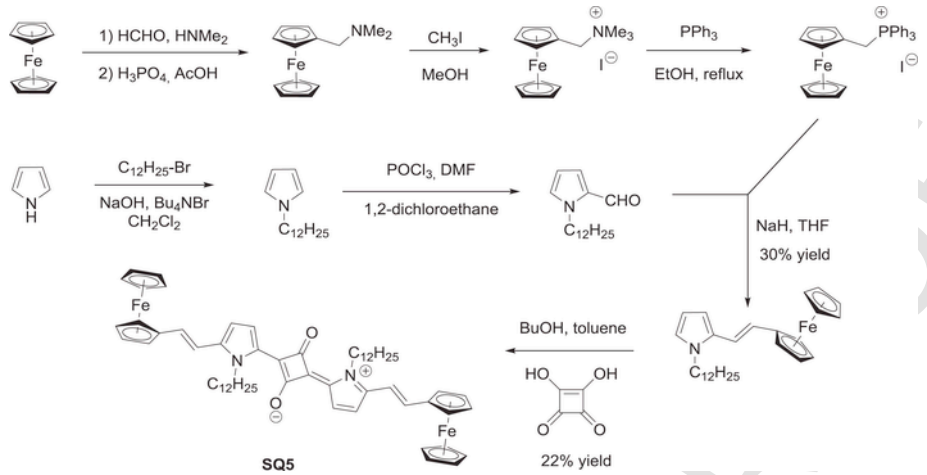

Fig. 32. Synthetic route to squaraine **SQ5**.

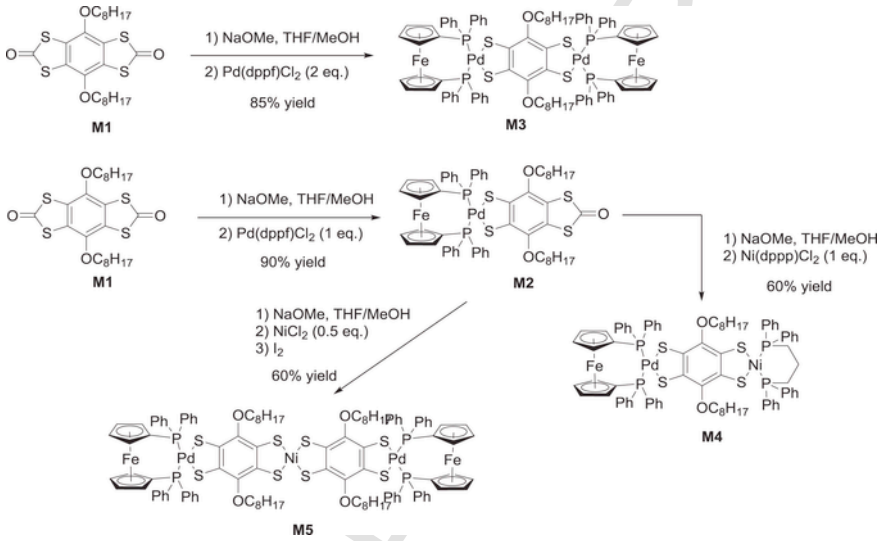

Fig. 33. Synthetic route to dithiolene-containing metal complexes **M2**, **M3**, **M4** and **M5**.

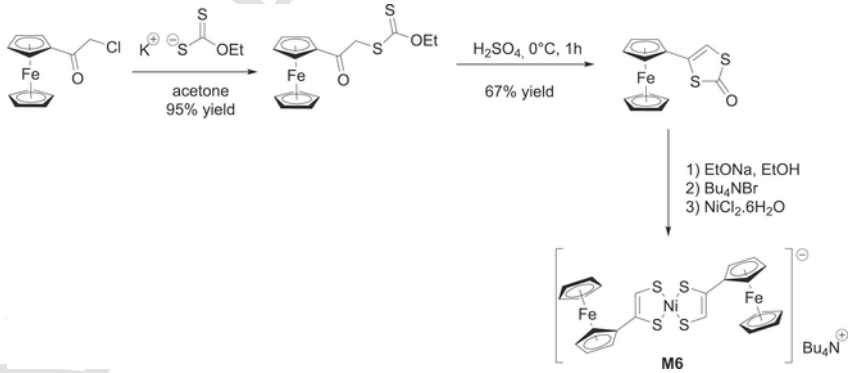

Fig. 34. Synthetic route to dithiolene-containing metal complex **M6**.

absorption spectra resulting simply from the contribution of both ferrocene and metalloporphyrin without reciprocal interactions. While comparing porphyrins **P3**, **P4** and **P5**, the four absorption bands were found at the same wavelengths for all porphyrins, demonstrating the complete isolation of the macrocycles from the ferrocene substituents. Despites the absence of electronic communication and due to the NIR contribution of metalloporphyrins, the resulting ferrocene-metalloporphyrin conjugates could exhibit an absorption extending until the NIR region (See Table 9). With regards to their syntheses, **P3**, **P4** and **P5** could be obtained in acceptable yields, the Horner-Wadworth-Emmons reaction realized between the ferrocene-aldehyde derivatives and the corresponding metal-free porphyrins being performed in 34, 71 and 20% yield (see Fig. 26).

However, due to the synthetic procedure used to introduce the ferrocene units, an inseparable mixture of cis/trans isomers was first obtained for all intermediates and the conversion of the cis/trans mixture

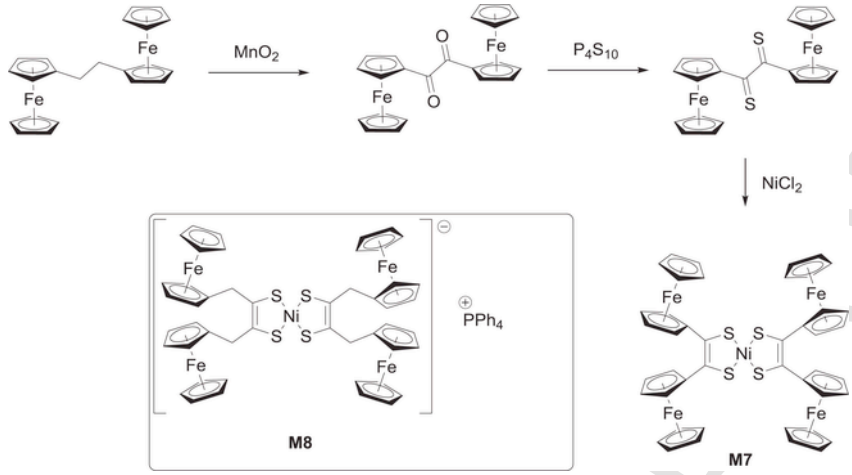

Fig. 35. Synthetic route to dithiolene-containing metal complex **M7**.

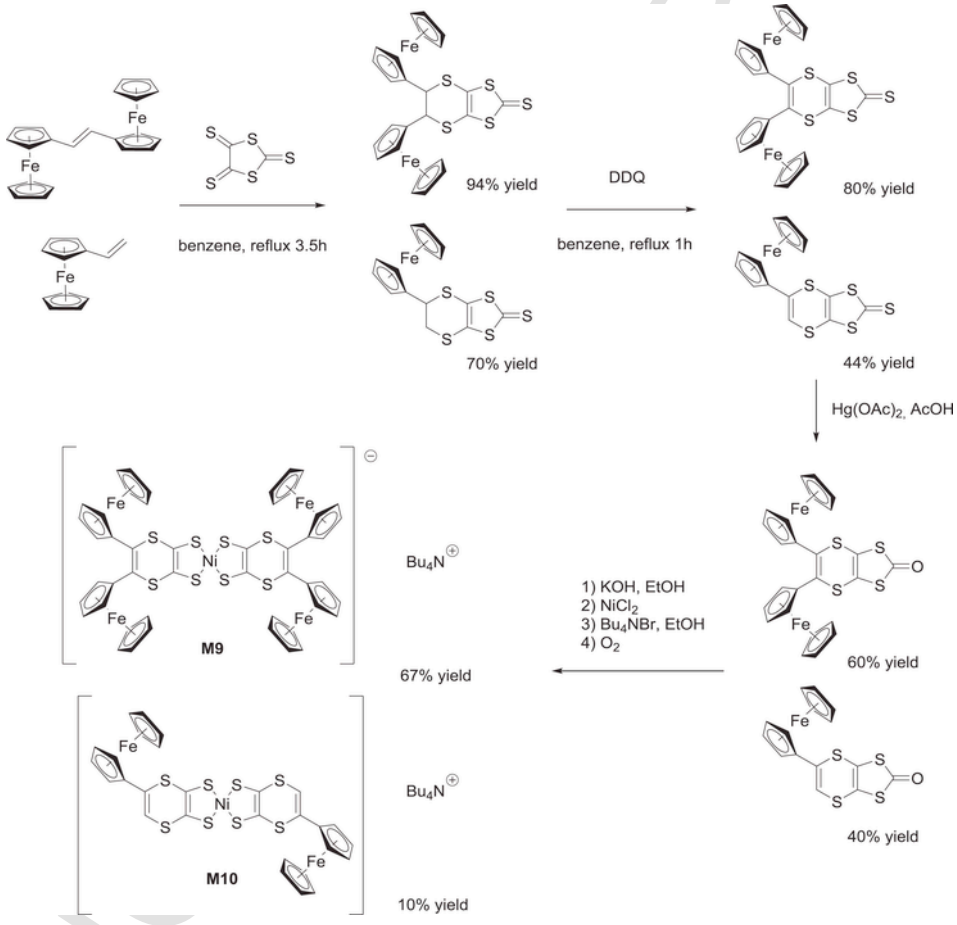

Fig. 36. Synthetic route to dithiolene-containing metal complexes **M9** and **M10**.

to the trans isomer was obtained by treatment the crude product with iodine. Finally, metalation of metal-free porphyrins could be obtained in almost quantitative yields, excepted for **P3.Ni** that was only obtained in 79% yield. Face to the detrimental contribution of the vinylic spacer to the electronic conjugation, numerous ferrocene-porphyrins conjugates differing by the spacer introduced between the two partners were designed and synthesized. Thus, by approaching the ferrocene unit from the porphyrin core, a restauration of the electronic communication could be established in **P6** and **P7** and as the first manifestation of this, a complete quenching of luminescence was observed for these two compounds [116]. Indeed, upon excitation, an electronic transfer occurs from ferrocene to the porphyrin, quenching the luminescence. Electronic coupling of porphyrin with ferrocene was also confirmed by UV–visible absorption, the Soret bands being enlarged and red-shifted compared to that of the reference **P8** (See Fig. 27). An absorption band extending until 900 nm could be detected for **P6** and **P7** and only a weak influence of the substitution pattern of the porphyrin core on the optical properties was again demonstrated (λ_{max} = 556 and 595 nm for **P6**, 562 and 604 nm for **P7** respectively) (See Table 9). Interestingly, oxidation of ferrocene to ferrocenium could restore the porphyrin fluo-

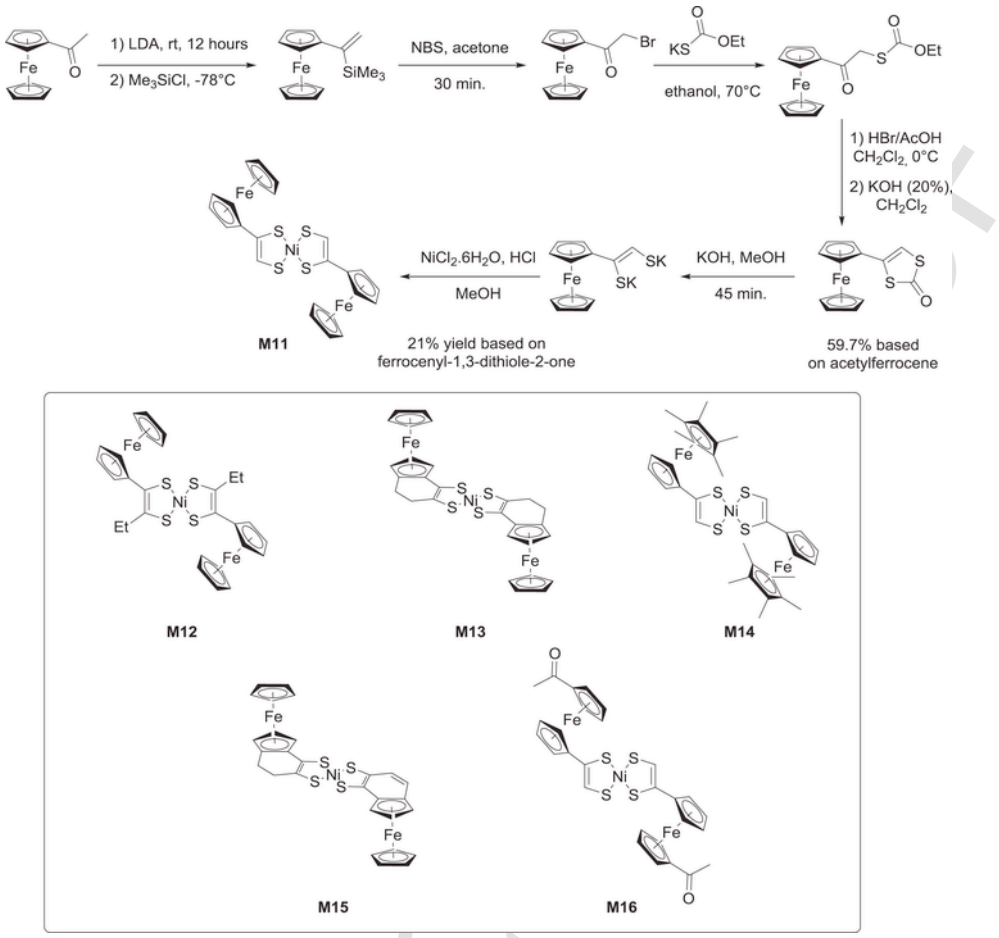

Fig. 37. Synthetic route to dithiolene-containing metal complexes **M11** and chemical structures of **M12-M16**.

Table 11
Photophysical characteristics of dithiolene-containing metal complexes **M1-M16**.

	M2	M3	M4	M5	M6	M7	M8	M9	M10
λ_{abs1} (nm)[a]	–	–	–	–	–	–	–	–	–
λ_{abs2} (nm)[a]	–	1258	1289	1278	–	1310	1250	1178	1155
Reference	138	138	138	138	138	141	142	142	142
	M11	M12	M13	M14	M15	M16	M17	M18	
λ_{abs1} (nm)[a]	746	762	772	765	779	736	340	–	
λ_{abs2} (nm)[a]	1235	1141	1235	1594	1721	1114	–	630	
Reference	144	144	144	144	144	144	148	148	

[a] Measured in dichloromethane in DCM, using tetrabutylammonium phosphate 0.1 M as the supporting electrolyte.

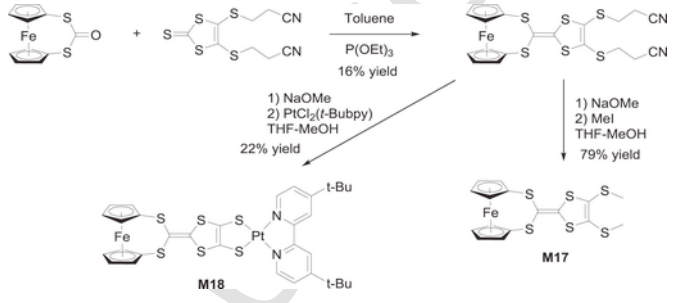

Fig. 38. Synthetic route to dithiolene-containing metal complexes **M17** and **M18.**

rescence, enabling to design redox-controlled fluorescence switches. From a synthetic point of view, access to these structures is extremely difficult. Indeed, the synthesis of monosubstituted porphyrins such as **P6** and **P7** is a hard work since it requires as reagents two aldehydes to be mixed with pyrroles. As a result of this, a complex mixture of porphyrins with various substitution patterns is obtained, required a careful chromatography to be separated (see Fig. 28). Thus, precursors of **P6** and **P7** were respectively obtained in 8.1 and 7.1% yields.

Still based on the direct linkage of ferrocene with porphyrins, the possibility to lower the LUMO level centered on BODIPY by introducing electron-withdrawing groups onto the porphyrin macrocycle was examined [119]. At present, only few structures exhibiting such a functionalization have been reported in the literature, due to the difficulty of synthesis of the reagents. In this field, 1,2,2-tricyano-1-ferrocenylethylene is one of those.

This synthetic challenge has only recently been overcome with the development of a mercury-free procedure for the synthesis of 1,2,2-tricyano-1-ferrocenylethylene enabling to get this compound in 26% yield [120,121]. Based on this optimization, sufficient quantities of 1,2,2-tri-

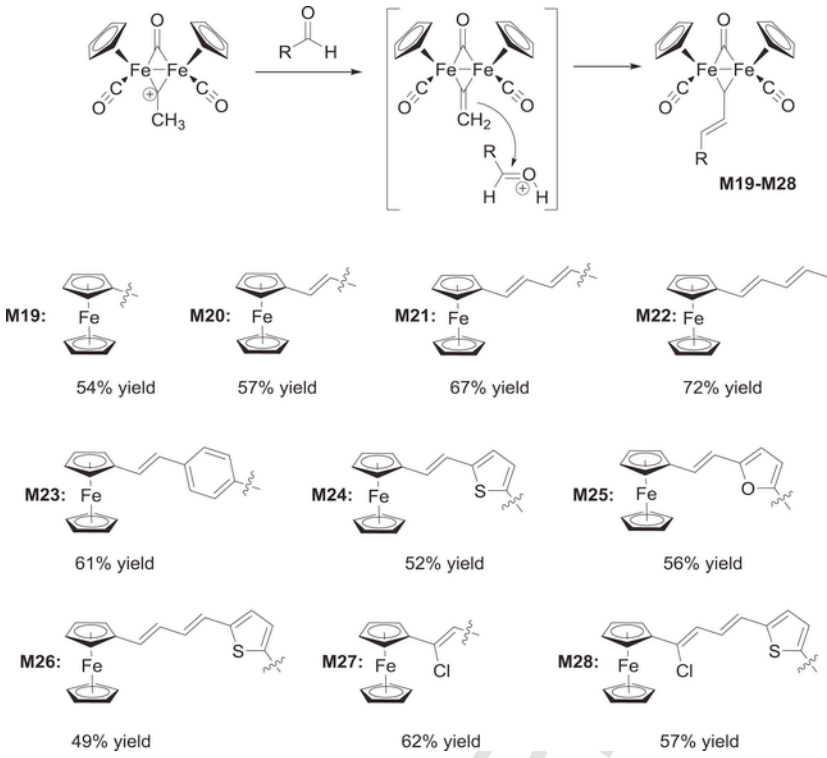

Fig. 39. Synthetic route to metallocenes **M19-M28**.

cyano-1-ferrocenylethylene could be obtained and the synthesis of tetraazaporphyrin **P10** in 59% yield was rendered possible (See Fig. 29). To evidence the benefits of the presence of cyano groups onto **P10**, tetraazaporphyrin **P9** was prepared from 1,2-dicyano-1-ferrocenylethylene in 23% yield. By absorption spectroscopy, presence of the cyano groups red-shifted the MLCT band from 725 nm for **P9** to 930 nm for **P10**. Especially, the NIR band was extremely broad, extending from 700 until 1300 nm. On the opposite, the NIR band of **P9** was less extended, ranging from 700 to 900 nm. Theoretical calculations revealed the major involvement of the porphyrin core to the LUMO and LUMO + 1 energy levels with a delocalization of the electronic density over the cyano groups. Conversely, ferrocene clearly dominates by its contribution to the HOMO level accompanied by a contribution of the macrocycle. Due to the delocalization of the LUMO orbital onto the cyano groups, a decrease of its energy level was observed for **P10** relative to that of **P9** whereas no modification of the HOMO level was detected, resulting in a red-shift of the MLCT band. By electrochemistry and due to the presence of four ferrocene units, mixed valence compounds could be formed upon oxidation or reduction and the presence of positional isomers drastically complexified the cyclic voltammograms so that no clear attribution of the electrochemical process could not be realized. However, upon oxidation of **P10**, appearance of a broad band extending until 1500 nm confirmed the oxidation process occurring on the ferrocene units.

Finally, further investigations on ferrocene-porphyrin conjugates revealed, once again, the phenyl spacer to interrupt the electronic coupling by its orthogonal arrangement relative to the porphyrin plane (**P12**, **P18**, **P20**) contrarily to the five-membered rings such as furan or pyrrole that facilitate the electronic delocalization by mean of a reduced dihedral angle (see **P14** and **P16** in Fig. 30) [122]. While comparing the optical properties of the tetrafuryl and tetrathienyl-porphyrins **P13** and **P15** with their corresponding ferrocene-substituted porphyrin conjugates **P14** and **P16**, the negligible shifts detected in the absorption bands of **P14** and **P16** confirmed nonetheless the electronic interactions between porphyrin and ferrocene (See Table 10).

Notably, a reduction of the extinction coefficients for the ferrocene-substituted porphyrin conjugates **P14** and **P16** relative to their unsubstituted analogues **P13** and **P15** was detected. In this work, special porphyrins (**P12**, **P18**, **P20)** were also studied since heteroporphyrins comprising thiophene groups instead of pyrroles inside the chelating cavity were designed and synthesized. By increasing the number of thiophene units inside the cavities, a red-shift of the absorption bands was regularly observed from **P12** to **P18** and **P20**, demonstrating the contribution of the thiophene unit in the electronic delocalization. Electrochemical experiments confirmed the electronic communication existing for the ferrocene-porphyrin dyads comprising furans or thiophene as spacers i.e. **P14** and **P16**. On the opposite, the complete isolation of the two redox active groups (ferrocene/porphyrin) was demonstrated in **P12**, **P18** and **P20**. However, inspection of the electrochemical data revealed that no clear trend could be deduced from the substitution pattern, the oxidation and reduction potentials of porphyrins in the ferrocene-porphyrins conjugates depending both of the *meso*-substituents but also of the nature of the porphyrin core. In turn, oxidation and reduction potentials of porphyrins varied arbitrarily due to this dual contribution so that no trends could be established (See Table 6).

As already mentioned for the different systems previously discussed in this paragraph, decrease of the photoluminescence quantum yield (PLQY) by substitution of porphyrins with ferrocene confirms the trend established for ferrocene-porphyrin conjugates. A reduction of the excited state lifetime was also evidenced for all porphyrins, irrespective to the *meso*-substituents and the nature of the porphyrin core. It has to be noticed that the synthetic access to this series of porphyrins was extremely difficult since the mixed condensation only furnished the asymmetric porphyrins in 5–7% yields [123–125].

2.4. Ferrocene with squaraines

Since their discovery in 1965 [126], squaraines have been extensively studied in the literature for applications ranging from photovoltaics, non-linear optical applications, organic light-emitting diodes

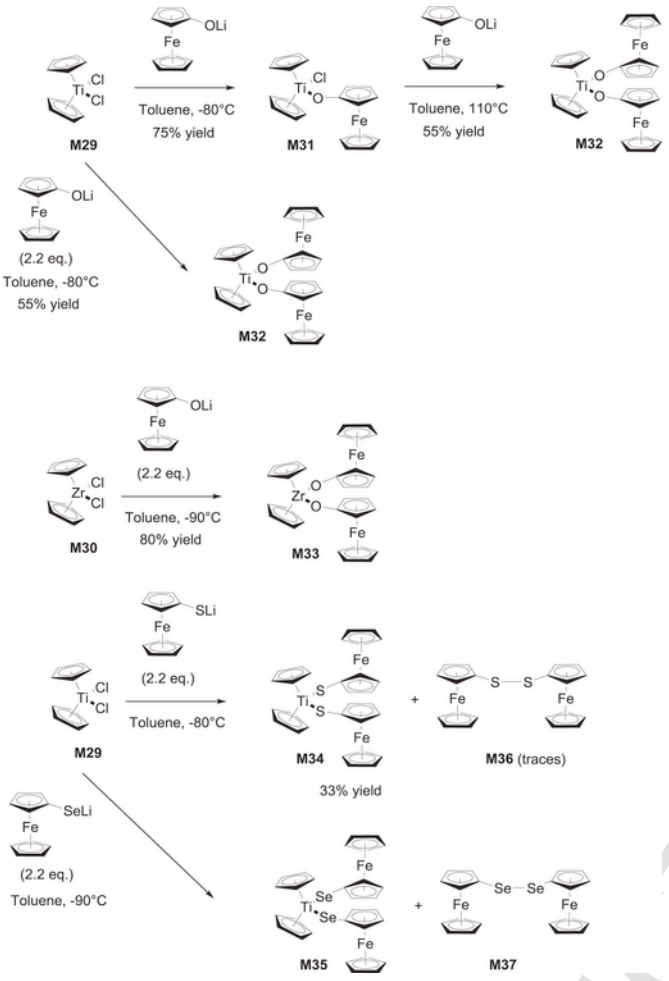

Fig. 40. Synthetic route to metallocenes **M32-M35**.

or fluorescent probes due to their NIR absorption properties [127]. To provide interesting electrochemical properties, the combination of squaraines and ferrocene has been examined. The first report mentioning the combination of ferrocene and squaraines were published twenty years ago, in 2000 [128]. The design of such NIR absorbing dyes in quite complicated since **SQ4** and **SQ3** could be obtained in five and six steps respectively, starting from ferrocene (See Fig. 31).

As limiting step, the reaction of the resorcinol derivatives **SQ2** and **SQ1** with squaric acid only yielded the two squaraine derivatives in moderate yields, namely 10% for **SQ4** and 21% for **SQ3**. If the examination of the photophysical properties of the two compounds was limited to only the acquisition of their UV–visible absorption spectra in chloroform, presence of two broad and intense absorption bands at 641 and 921 nm, 650 and 961 nm for **SQ4** and **SQ3** could be respectively determined.

In 2011, a slightly different structure was examined since pyrroles were used to form the squaraine core [129]. Overall, seven steps were required to synthesize the squaraine **SQ5** and the final step consisting in the condensation of the ferrocene-substituted pyrrole with squaric acid could only be realized in 22% yield (See Fig. 32). As interesting feature, **SQ5** was soluble in all solvents due to the presence of multiple alkyl chains so that the solvatochromism could be examined in solvents going from the apolar pentane until the highly polar ethanol. In this range of polarity, a positive solvatochromism accompanied with a variation of 26 nm for the position of the absorption maximum was determined, evidencing the polarity of the excited state to be larger than that of the ground state. In all solvents, **SQ5** displayed an intense absorption band in the NIR region, peaking at 708 nm in pentane and 734 nm in ethanol. By electrochemistry, three reversible oxidation one-electron processes at low potentials i.e. +0.35, +0.50 and + 0.79V were observed, making this compound an ideal candidate for photovoltaics applications.

2.5. Ferrocene with metallodithiolene complexes

Dithiolene-containing metal complexes have been extensively studied in the literature due to their remarkable molar extinction coefficients in the NIR region which can reach values of 10^5 L mol^{-1} cm^{-1} [130]. Absorption bands can be significantly altered by modifying both the metal cation (Ni^{2+}, Pt^{2+}, Pd^{2+}, …) but also the redox states or the ligand that have a major contribution on the electronic distribution of the molecular orbitals [131–137]. This tunability can be even accentuated when polynuclear assemblies are prepared, as exemplified with the binuclear complexes **M3** and **M4** and the trinuclear complex **M5** (see Fig. 33) [138]. Synthesis of these complexes (**M2**, **M3** and **M5**) was reported prior to this study and one of the most interesting features of these metallodithiolene complexes is the absence of absorption in the visible range for complexes **M4** and **M5**, rendering these dyes absolutely colorless [139].

Indeed, complexes **M3, M4** and **M5** displayed a typical metal-to-ligand transition characteristic between 1000 and 1600 nm, peaking at 1258, 1289 and 1278 nm for complexes **M3, M4** and **M5** respectively. If a contribution in the visible range was found at 553 nm for complex **M3**, complexes **M4** and **M5** were transparent in the visible range. A red-shift of the absorption was found for complex **M4** relative to complex **M3**, attributable to improved charge transfer ability of Pd compared to Ni. The broader and the most red-shifted absorption was found for complex **M5**, resulting from the simultaneous presence of three metal centers and the occurrence of multiple charge transfer

Table 12
Photophysical characteristics of **M19-M28.**

	λ_{abs1} (nm)[a]	λ_{abs2} (nm)[a]	ε_1 (mol^{-1}.cm^{-1})[a]	ε_2(mol^{-1}.cm^{-1})[a]	β (10^{30} esu)[b]	Ref
M19	428	655	17736	10953	113	139–143
M20	484	734	17094	13881	156	139–143
M21	541	775	22488	18277	227	139–143
M22	582	813	24670	23106	562	139–143
M23	512	705	28692	12162	1106	139–143
M24	569	757	32538	19966	679	139–143
M25	577	747	33211	22325	352	139–143
M26	606	764	29169	22363	1195	139–143
M27	495	746	27589	17162	459	139–143
M28	606	731	34798	24000	1424	139–143

[a] Measured in dichloromethane.
[b] Measured in dichloromethane while using *p*-nitroaniline as a reference (21.6×10^{30} esu).

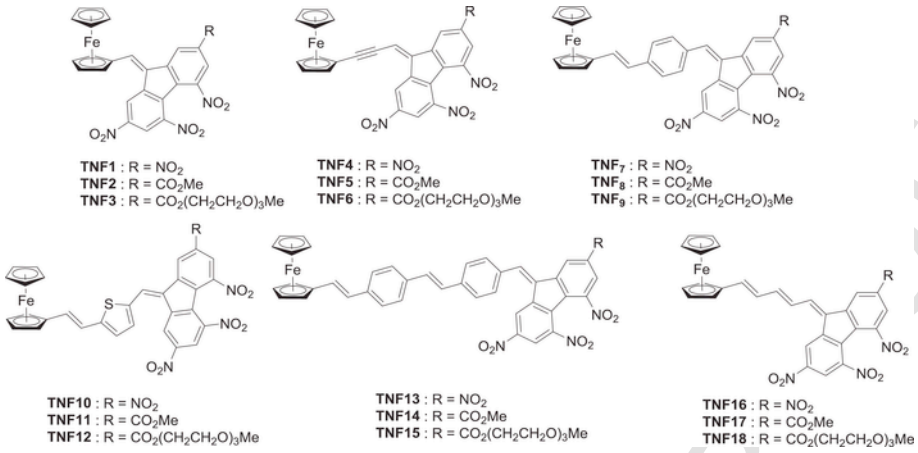

Fig. 41. Push-pull chromophores **TNF1-TNF18** based on poly(nitro)fluorenes as electron acceptors.

Table 13
Summary of the optical properties of the different dyes recorded in 1,2-dichloroethane.

Compounds	TNF1	TNF2	TNF4	TNF6	TNF7	TNF9
λ_{ICT1} (nm)	430	410	451	431	430	430
λ_{ICT2} (nm)	620	609	658	616	600	600
Compounds	TNF12	TNF15	TNF16	TNF17	TNF18	
λ_{ICT1} (nm)	502	450	464, 514	450, 485	455, 490	
λ_{ICT2} (nm)	640	–	706	660	660	

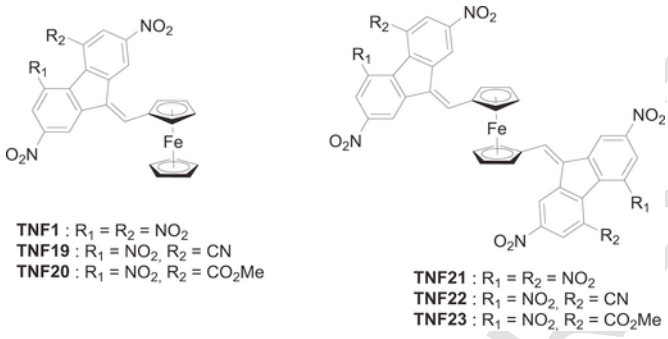

Fig. 42. Push-pull diads and triads based on ferrocene.

Table 14
Position of the second ICT bands of different dyes recorded in 1,2-dichloroethane.

Compounds	TNF1	TNF19	TNF20	TNF21	TNF22	TNF23
λ_{ICT2} (nm)	622	617	609	622	610	604

processes. The complexity of transitions resulting from the presence of multiple metal centers was confirmed by electrochemistry. While examining the redox properties of complexes **M4** and **M5**, presence of multiple mixed-valence states (Pd(III)/Ni(II), Pd(III)/Ni(III), Pd(IV)/Ni(III), Pd(IV)/Ni(IV)) and dianionic states furnished a complicated electrochemical signature to the two complexes. Examination of the electrochromic properties of complex **M4** upon oxidation of the complex at 0.6 V revealed the appearance of two new bands at 954 and 1064 nm respectively in addition to the metal-to-ligand transition detected at 1289 nm. Oxidation at +1.0 V resulted in the disappearance of the MLCT band at 1289 nm. Finally, oxidation at a higher potential resulted in the disappearance of all peaks in the NIR region. Conversely, due to the symmetrical substitution of complex **M5**, a simpler electrochromic behaviour was found with the gradual decrease of the absorption peak at 1278 nm upon oxidation at 1.4 V.

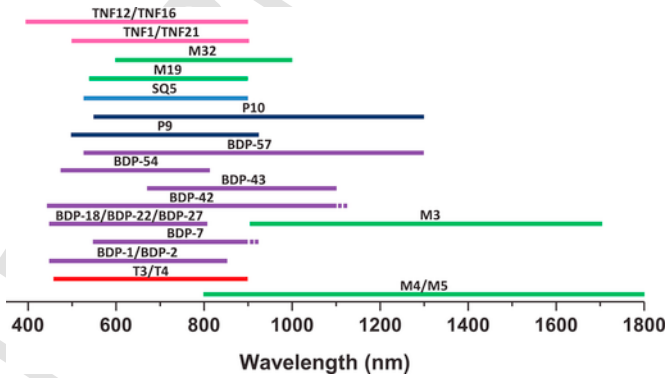

Fig. 43. Representative absorption properties of ferrocene derivatives mentioned in this review.

Nickel *bis*(dithiolene) complexes have been at the basis of numerous hybrid structures with ferrocene and a wide range of near-absorbing dyes have been reported using this promising combination. One of the pioneering works in this field has been published in 1994, but the lack of electronic communication between the central nickel *bis*(dithiolene) complex and the peripheral ferrocene units has been clearly evidenced in complex **M6** by electrochemistry (See Fig. 34) [140]. Interestingly, **M6** could be easily synthesized in three steps, by reaction of chloroacetylferrocene with potassium *o*-ethylxanthate in 95% yield, followed by an intramolecular cyclization in concentrated sulfuric acid, providing the 1,3-dithiole-2-one derivative in 67% yield. In a final step, treatment of the 1,3-dithiole-2-one derivative with a base followed by addition of $NiCl_2.6H_2O$ and tetrabutyl-ammonium bromide furnished **M6** as a solid exhibiting a low solubility in solvent such as dichloromethane (See Fig. 34).

Concerning the electrochemical properties, an opposite situation was found with **M7** [141]. In this last case, and despites the presence of four ferrocene units that introduce a severe steric hindrance around the central Ni complex, a modification of the oxidation potential of ferrocene was evidenced, demonstrating that an overlap between the molecular orbitals of the metal complex could exist with those of ferrocene. Here again, **M7** could be prepared in three steps, the first one consisting in the oxidation of the methylene bridge of 1,2-diferrocenylethane with manganese oxide, followed by treatment with P_4S_{10} in dioxane, and the reaction with nickel chloride in methanol furnished **M7** as a grey-green solid (see Fig. 35).

If not so must details were provided concerning the synthesis, **M7** proved to be an interesting candidate for NIR applications, its absorption maximum peaking at 1310 nm. As interesting feature, a broad ab-

sorption extending from 1000 to 1600 nm could be determined for **M7**. Theses photophysical properties are comparable to those determined for **M8** that differs from **M7** by the presence of a thiomethylene ((–CH_2S–) bridge between the Ni complex and the ferrocene units (λ_{max} = 1250 nm) (See Fig. 35) [142]. In 2000, two nickel *bis*(dithiolene) complexes **M9** and **M10** decorated with two or four ferrocenyl units and exhibiting a more extended central core than that of **M6-M8** were designed and examined for their spatial arrangement in the solid state [143]. **M9** and **M10** could be prepared following parallel synthetic routes, in four steps as depicted in Fig. 36. Cycloaddition of 1,3-dithiol-2,4,5-trithione with the corresponding alkene provided the intermediate cycloadducts that were oxidized with 2,3-dichloro-5,6-dicyanobenzo-1.4-quinone (DDQ) with reaction yields ranging from 44 to 80%. Finally, transchalcogenation with mercury (II) acetate followed the generation of the dithiolate ligands in basic conditions and addition of $NiCl_2$ provided **M9** and **M10** as anionic complexes after air oxidation in 10 and 67% yield respectively.

In the solid state, two different arrangements could be found for the terminal ferrocenyl groups in **M9** and **M10**. Thus, by crystal structure analysis, the two ferrocene groups in **M9** were determined to adopt a chair-like conformation contrarily to **M10** where all ferrocenes were found to be on the same side relative to the Ni-complex plane, exhibiting in turn a boat-like conformation. Analysis of the crystal structures also revealed the distance between complexes to be longer than 6 Å, impeding intermolecular interactions between complexes. These findings were confirmed by electrical measurements and the determination of a low conductivity at room temperature, in the order of 10^{-6} S cm^{-1}. Concerning their absorption properties, no major differences could be found between the absorption spectra of **M9** and **M10** since the two complexes exhibited absorption maxima at 1178 and 1175 nm respectively. By oxidizing **M10** with iodine and generating a neutral complex, a comparison could be established with **M7**, displaying a less extended aromaticity. The comparison revealed the oxidized form of **M10** to absorb at 1342 nm i.e. at lower energy than **M7** (λ_{max} = 1310 nm). Therefore, extension of the aromaticity of the ligands in Ni *bis*(dithiolene) complexes provides an efficient tool to red-shift the absorption maxima of Ni complexes. Examination of the absorption properties of ferrocenyl-substituted dithiolenes can be more difficult than anticipated as the oxidation state can be modified over the time, depending of the reducing ability of the solvent. This point was notably demonstrated with **M11**, for which contradictory results were reported in the literature concerning its absorption characteristics [144]. Indeed, an unexpected absorption peak at 746 nm was detected in addition of the usual absorption maxima in the NIR region (λ_{max} = 1235 nm), with an equal intensity for the two peaks in dichloromethane [145,146]. Compared to the previously mentioned **M6** complex, the dithiolate ligand used for the synthesis of **M11** was prepared according to a slightly different procedure compared to that used for **M6** and the synthetic route is depicted in Fig. 37. The ligand was obtained in a higher yield (59.7% starting from acetylferrocene) than previously reported. Starting from acetylferrocene, **M11** could be obtained in 11% yield and isolated as a black solid. While comparing the positions of the NIR peak of **M11** (1235 nm in dichloromethane) with that previously reported in the literature (1030 nm) [145,146], the difference of the absorption position was assigned to a modification of the oxidation degree of **M11** and the formation of the corresponding anion **M11**$^-$ [147]. Reduction of **M11** was demonstrated by using DMF as the solvent. Due to its mild reducing ability, a complete modification of the absorption spectrum could be observed after 4 h, with the disappearance of the NIR peak at 1257 nm in favour of a new peak at 1032 nm, close to the value reported in dichloromethane (1030 nm). Conversely, only a decrease of the peak intensity at 746 nm was observed and this absorption band was assigned to d-d transitions centrered on dithiolenes.

While aiming at determining the possible orientation of the peripheral ferrocenes relative to that of the central Ni complex, introduction of ethyl groups onto **M12** resulted in a blue-shift of the NIR peak by 116 nm, at 1141 nm, indicating the coplanarity of the ferrocene units with the central core in **M11**. These results were confirmed with the design of a second complex, **M13,** where the orientation of the peripheral ferrocene was maintained and parallel to the central core. In these conditions, the two absorption peaks were detected at 772 and 1235 nm in dichloromethane, close to the values determined for **M11** (746 and 1235 nm in the same solvent respectively). Finally, influence of the substitution pattern of **M11** was also examined. In this aim, **M14** that possesses ferrocenes bearing pentamethylcyclopentadienyl rings clearly evidenced the contribution of the electron-donating methyl groups (see Fig. 37). Thus, a drastic shift of the NIR peak was observed, this latter shifting from 1235 nm for the parent complex **M11** to 1594 nm for **M14** i.e. by 359 nm. This effect was notably reinforced by the presence of the unsubstituted cyclopentadienyl ligand on the ferrocene units, enabling the peripheral complexes to remain coplanar with the central core. A similar result was obtained by introducing an improved conjugation between the peripheral ferrocene and the Ni complex. Thus, the NIR transition of **M15** could be detected at 1721 nm, thus shifted from 486 nm relative to that of the parent complex **M11**. On the opposite, introduction of electron-withdrawing groups onto **M16** resulted in a blue-shift of the NIR peak to 1114 nm (See Table 11). In 2012, a novel class of ferrocene-dithiolene hybrids based on a planar structure derived from the well-known tetrathiafulvalene structure was reported [148]. Design of these structures was notably motivated by the desire to improve the electronic communication between the ferrocene and dithiolene units. To evidence this, two complexes **M17** and **M18** were prepared, using standard procedures developed for tetrathiafulvalene (See Fig. 38). Thus, the first step consisting in the generation of the dithiolene core by cross-coupling reaction in the presence of triethylphosphite could only be realized in low yield (16% yield). **M17** could be obtained by deprotection of the thiol groups in basic conditions followed by alkylation with iodomethane, providing the ferrocene derivative in 79% yield. Similarly, after deprotection in basic conditions of the thiol groups followed by reaction with $PtCl_2$(*t*-Bu_2bpy), **M18** was obtained in 22% yield. As specificity, the two compounds **M17** and **M18** have been designed so that the ferrocene unit was perpendicular to the plane of the dithiolene skeleton, enabling to determine the efficiency of the electronic coupling via the bridging sulfur atoms. By absorption spectroscopy, a broad absorption band extending from 500 to 800 nm could be determined for **M18** comprising two metal centers, the maximum absorption peaking at 630 nm. Contribution of the Pt complex in the absorption spectrum could be clearly evidenced, the absorption of **M17** ranging from 300 to 450 nm. The most interesting result was obtained by electrochemistry. Indeed, if the first oxidation process was determined as being centered on ferrocene in **M17**, a completely different behaviour was observed for **M18**, the oxidation process occurring first at the dithiolene moiety. Finally, electronic communication between the ferrocene unit and the dithiolene moiety was evidenced by EPR, upon oxidation of the two compounds. Thus, two NIR transitions would be detected at 834 nm and 1640 nm for the radical cation of **M17** whereas a broad band extending over 2500 nm could be detected for the radical cation of **M18**.

2.6. Ferrocene with metallocenes

Ferrocene has been extensively studied in the literature for the design of NLO-active chromophores due to its low oxidation potential and its remarkable electron-donating ability [149–154]. Its combination with the electron-deficient metallocene $[Fe_2(\eta–C_5H_5)_2–(CO)_2(\mu\text{-}CO)(\mu\text{-}C^-)]^+$ was especially attractive since this cationic group is characterized by an excellent electronic conjugation between the vinyl substituent

and the diiron-bridged unit [155–160]. With aim at examining the influence of the π-conjugated spacer, a series of 10 merocyanine salts were designed and obtained with yields ranging from 49% for **M26** until 72% for **M22** (See Fig. 39) [161] (see Fig. 40).

The UV–visible spectra of metallocenes **M19-M28** were characterized by two absorption bands, the first band at high energy corresponding to the ligand-ligand charge transfer and the second one at low energy corresponding to the intramolecular charge transfer band. By elongating the π-conjugated spacer in **M19-M22**, a red-shift from 655 to 813 nm could be observed for the ICT bands, combined with an increase of the molar extinction coefficients (See Table 12). In the **M19-M22** series, the most blue-shifted ICT band was found for **M6**, at 655 nm in dichloromethane. Besides, **M19** is clearly a NIR dye, onset of its ICT band being detected at 900 nm. Conversely, for the most red-shifted ICT band of the series (813 nm for **M22**), onset of the NIR band was found around 1200 nm, making **M22** a dye strongly absorbing in the NIR region. Solvatochromism of all chromophores was examined as it constitutes the first manifestation of the modification of the dipole moment upon excitation [162]. To get NLO-active chromophores, a significant modification of the dipole moment between the ground state and the excited state ensures high non-linearities. In fact, a negative solvatochromism was found for all dyes, indicating that the dipole moment in the excited state is lower than that of the ground state. As notable feature, introduction of a chlorine atom in the spacer reduced the electron-donating ability of ferrocene and this fact was evidenced by comparing the position of the ICT bands of **M26** (764 nm) vs. **M28** (731 nm), a blue-shift of 33 nm being detected in dichloromethane. By measuring the second harmonic generation by hyper Rayleigh scattering (HRS), at 1064 nm, high hyperpolarisabilities (β) were determined for the whole series. An enhancement of the β values with the length of the π-conjugated spacer was observed, increasing from 113×10^{30} esu for **M19** until 562×10^{30} esu for **M22** comprising four consecutive double bonds. By plotting β vs. the number of double bonds (n), a linear variation of the hyperpolarisabilities vs. n could be determined and no saturation effect was detected, even after elongating the spacer until four double bonds. Contrarily to most of the studies evidencing that heterocyclic units such as furans and thiophenes are better spacers than aromatic rings in terms of electronic conjugation for NLO applications [163–165], the opposite situation was found in this study, the higher hyperpolarisability being found for **M23** (1106×10^{30} esu) whereas the worse result was found for the furan-containing chromophore **M25** (352×10^{30} esu). These counter-intuitive results were assigned the increased aromaticities of furan and thiophene impeding the delocalization of the positive charge towards the ferrocene donor.

While examining other metals than iron, the direct linkage of ferrocene units to metallocenes can generate instable structures so that, for some of them, their characterizations are limited to NMR investigations, these structures being extremely sensitive to air and moisture [166,167]. This instability is notably the result of their facile reduction, notably for titanocenes. To improve their stability, an effective strategy consists in introducing heteroatoms such as oxygen, selenium or sulfur [168–174]. On this basis, a series of Zr and Ti-based metallocenes bearing ferrocene substitutes were examined for the spectroelectrochemical properties [175]. Metallocenes **M32** and **M33** could be prepared using the same methodology, by first generating the ferrocenyloxy lithium salt and by carrying out the nucleophilic substitution at low temperature with 2.2 equivalents of ferrocenyloxy lithium. Concerning **M32**, a two-step procedure was also developed, enabling to intermediately generate the monosubstituted titanocene **M31** (See Fig. 36). Examination of their chemical stability revealed **M31** and **M32** to be stable under inert atmosphere but to decompose under air and in solution. On the opposite, **M33** was unstable, even in the solid state. Synthesis of **M34** and **M35** was more challenging since only **M33** could be isolated in pure form (33% yield), **M35** being contaminated by 37% of the dimer **M37**. Despites their instability, their optical properties could be however determined in dichloromethane and metallocenes **M32-M35** revealed their absorption spectra to be characterized by a strong band centered in the NIR region, the ICT band extending from 600 until 1200 nm.

2.7. Ferrocene with poly(nitro)fluorenes

Among all organic electron acceptors reported to date, a family is absolutely remarkable by its ability to exhibit a NIR absorption even when these electron acceptors are not connected to electron donors. These electron acceptors belong to poly(nitro)fluorenes and the most interesting one is undoubtedly tetranitrofluorene (TNF) [176]. Interestingly, an absorption band ranging from 650 to 950 nm could be found in the UV–visible absorption spectrum of TNF recorded in DMF. Numerous organic electron donors have been connected to poly(nitro)fluorenes by mean of a Knoevenagel reaction. However, for a wide range of applications, the reversibility of the electrochemical process is of crucial importance, justifying the covalent linkage of poly(nitro)fluorenes with ferrocene. Here again, influence of the π-conjugated spacer on the electronic delocalization was examined and a series of poly(nitro)fluorene-ferrocene conjugates **TNF1-TNF18** were prepared in this aim (See Fig. 41) [177]. One major drawback of the simultaneous presence of multiple nitro groups on polyaromatic structures is the resulting low solubility of the final chromophores, often impeding further characterizations and drastically limiting their applications. In this aim, soluble versions were prepared, as exemplified with **TNF3, TNF6, TNF9, TNF12, TNF15** and **TNF18** for which a triethylene glycol chain has been introduced onto the electron-accepting moiety.

Only few details concerning the synthesis of the different conjugates were provided in this work. However, irrespective of the spacer and the substitution pattern of the electron acceptors, all structures displayed an intense and broad absorption band peaking between 600 and 706 nm, the absorption extending beyond 900 nm for all compounds (See Table 13). Influence of the π-conjugated spacer on the electronic communication between the donor and the acceptors could be evidenced, the absorption maxima for the ICT band shifting from 600 nm for **TNF7** and **TNF9** to 706 nm for **TNF16** exhibiting the longest spacer without heterocycles and/or aromatic rings. Due to the exceptional electron-withdrawing ability of nitrofluorene derivatives, the non-linear optical properties of **TNF1-TNF18** was examined.

Due to the permanent dipole moment existing in these structures, nonlinear optical properties of this series were examined by electric field induced second harmonic (EFISH) generation. The classical trends could be determined from this work. Notably, elongation of the conjugated spacer between the donor and the acceptor drastically contributed to enhance the quadratic hyperpolarisability, increasing from 100×10^{-48} esu for **TNF3** to 2400×10^{-48} esu for **TNF18.** Lower hyperpolarisabilities were obtained with other spacers such as divinylbenzene ($\mu\beta$ value $= 800 \times 10^{-48}$ esu for **TNF9**) or the combination of double and triple bonds in **TNF6** ($\mu\beta$ value $= 200 \times 10^{-48}$ esu). Parallel to D-A diads, A-D-A triads were also designed, as exemplified in Fig. 42 and a comparison with their D-A counterparts were also established [178]. Here again, solubility of the different dyes was a major issue so that several derivatives were synthesized. Interestingly, comparison of the UV–visible absorption spectra of the diads **TNF1**, **TNF19**, **TNF20** and the triads **TNF21**, **TNF22** and **TNF23** revealed their absorption spectra to be almost the same (See Table 14). Considering the challenge that constitutes the double functionalization of ferrocene and the subsequent difficulty of purification, the diads are easier to synthesize than the triads.

3. Conclusions

Since its discovery in 1951, ferrocene by its remarkable reversible electrochemical properties has driven an ever-increasing interest nonetheless for chemists by also for physicists. Interest for ferrocene is notably supported for chemists by the excellent thermal, chemical and photochemical stability of this metal complex making this structure an appealing candidate for the design of dyes. By the presence of numerous molecular orbitals, ferrocene can be advantageously used as an electron donor in push-pull chromophore and initiate low-lying transitions. For physicists, interest for ferrocene is notably sustained by its potential applications in telecommunication and defence by the possibility of designing NIR dyes. The convergence of interest of both communities has resulted in the design of more than 150 dyes with absorption extending from the visible to the infrared region. The diversity of structures (BODIPYs, squaraines, porphyrins, metallocenes and metallodithiolene complexes) attests of the on-going efforts to design dyes with an absorption centrered in the NIR and infrared region. If porphyrins and BODIPYs can absorb between 500 and 1300 nm, the most red-shifted absorption are found for metallodithiolene complexes (**M3-M5**), with absorptions extending from 800 to 1800 nm (see Fig. 43). Dithiolene-containing metal complexes based on palladium and nickel are clearly the most promising candidates and future prospects will certainly focus on the design of new dyes based on these scaffolds.

Acknowledgments

This research was funded by Aix-Marseille University and the Centre National de la Recherche Scientifique. The DGA is acknowledged for its financial support through the PhD grant of Damien Brunel.

References

[1] G.B. Kauffman, The discovery of ferrocene, the first sandwich compound, J Chem Educ 60 (1983) 185–186 https://doi.org/10.1021/ed060p185.
[2] T.J. Kealy, P.L. Pauson, A new type of organo-iron compound, Nature 168 (1951) 1039–1040 https://doi.org/10.1038/1681039b0.
[3] S.A. Miller, J.A. Tebboth, J.F. Tremaine, Dicyclopentadienyliron. J Chem Soc 0 (1952) 632–635 https://doi.org/10.1039/JR9520000632.
[4] H. Werner, At least 60 years of ferrocene: the discovery and rediscovery of the sandwich complexes, Angew Chem Int Ed 51 (2012) 6052–6058 https://doi.org/10.1002/anie.201201598.
[5] D. Astruc, Why is ferrocene so exceptional?, Eur J Inorg Chem 1 (2017) 6–29 https://doi.org/10.1002/ejic.201600983.
[6] R.R. Gagne, C.A. Koval, G.C. Lisensky, Ferrocene as an internal standard for electrochemical measurements, Inorg Chem 19 (1980) 2854–2855 https://doi.org/10.1021/ic50211a080.
[7] F. Bures, Fundamental aspects of property tuning in push-pull molecules, RSC Adv 4 (2014) 58826–58851 https://doi.org/10.1039/C4RA11264D.
[8] X. Xia, H. Yu, L. Wang, Z.U. Abdin, Recent progress in ferrocene- and azobenzene based photoelectric responsive materials, RSC Adv 6 (2016) 105296–105316 https://doi.org/10.1039/C6RA16201K.
[9] A.M. El-Zohry, J. Cong, M. Karlsson, L. Kloo, B. Zietz, Ferrocene as a rapid charge regenerator in dye-sensitized solar cells, Dyes Pigments 132 (2016) 360–368 https://doi.org/10.1016/j.dyepig.2016.05.021.
[10] T. Daeneke, T.-H. Kwon, A.B. Holmes, N.W. Duffy, U. Bach, L. Spiccia, High-efficiency dye-sensitized solar cells with ferrocene-based electrolytes, Nat Chem 3 (2011) 211–215 https://doi.org/10.1038/nchem.966.
[11] Y. Patil, R. Misra, R. Singhal, G.D. Sharma, Ferrocene-diketopyrrolopyrrole based non-fullerene acceptors for bulk heterojunction polymer solar cells, J Mater Chem 5 (2017) 13625–13633 https://doi.org/10.1039/C7TA03322B.
[12] Y.-W. Chang, M.-J. Huang, C.-C. Lai, C.-C. Chang, M.-P. Huang, C.-Y. Liao, C.-H. Cheng, A versatile ferrocene-containing material as a p-type charge generation layer for high-performance full color tandem OLEDs, Chem Commun 52 (2016) 14294–14297 https://doi.org/10.1039/C6CC07999G.
[13] N.Y. Shim, D.A. Bernards, D.J. Macaya, J.A. DeFranco, M. Nikolou, R.M. Owens, G.G. Malliaras, All-plastic electrochemical transistor for glucose sensing using a ferrocene mediator, Sensors 9 (2009) 9896–9902 https://doi.org/10.3390/s91209896.
[14] R. Teimuri-Mofrad, K. Rahimpour, R. Ghadari, S. Ahmadi-Kandjani, Ferrocene based nonlinear optical chromophores: synthesis, characterization and study of optical properties, J Mol Liq 244 (2017) 322–329 https://doi.org/10.1016/j.molliq.2017.09.002.
[15] R. Sun, L. Wang, H. Yu, Z.-U. Abdin, Y. Chen, J. Huang, R. Tong, Molecular recognition and sensing based on ferrocene derivatives and ferrocene-based polymers, Organometallics 33 (2014) 4560–4573 https://doi.org/10.1021/om5000453.
[16] M.S. Morad, A.A.O. Sarhan, Application of some ferrocene derivatives in the field of corrosion inhibition, Corros Sci 50 (2008) 744–753 https://doi.org/10.1016/j.corsci.2007.09.002.
[17] O. Karagollu, M. Gorur, F. Gode, B. Sennik, F. Yilmaz, Phosphate ion sensors based on triazole connected ferrocene moieties, Sens Actuators, B 193 (2014) 788–798 https://doi.org/10.1016/j.snb.2013.12.046.
[18] J. Lalevée, P. Garra, F. Dumur, D. Gigmes, J.-P. Fouassier, F. Morlet-Savary, D. Duche, D. Brunel, B. Graff, G. Noirbent, V.F. Sidorkin, C. Dietlin, Ferrocene-based (photo)redox polymerization under long wavelengths, Polym Chem (2019) https://doi.org/10.1039/C9PY00059C.
[19] C. Ornelas, Application of ferrocene and its derivatives in cancer research, New J Chem 35 (2011) 1973–1985 https://doi.org/10.1039/C1NJ20172G.
[20] A. Guerlin, F. Dumur, E. Dumas, F. Miomandre, G. Wantz, C.R. Mayer, Tunable optical properties of chromophores derived from oligo(p-phenylene vinylene), Org Lett 12 (2010) 2382–2385 https://doi.org/10.1021/ol1007263.
[21] M.-A. Tehfe, F. Dumur, B. Graff, F. Morlet-Savary, J.-P. Fouassier, D. Gigmes, J. Lalevée, New push-pull dyes derived from Michler's ketone for polymerization reactions upon visible lights, Macromolecules 46 (2013) 3761–3770 https://doi.org/10.1021/ma400766z.
[22] K.S. Egorova, V.P. Ananikov, Toxicity of metal compounds: knowledge and myths, Organometallics 36 (2017) 4071–4090 https://doi.org/10.1021/acs.organomet.7b00605.
[23] K.Y. Law, Organic photoconductive materials: recent trends and developments, Chem Rev 93 (1993) 449–486 https://doi.org/10.1021/cr00017a020.
[24] L.E. Wilson, C. Hassenrgck, R.F. Winter, A.J.P. White, T. Albrecht, N.J. Long, Ferrocene- and biferrocene-containing macrocycles towards single-molecule electronics, Angew Chem Int Ed 56 (2017) 6838–6842 https://doi.org/10.1002/anie.201702006.
[25] Y. Lin, H. Fan, Y. Li, X. Zhan, Thiazole-based organic semiconductors for organic electronics, Adv Mater 24 (2012) 3087–3106 https://doi.org/10.1002/adma.201200721.
[26] S. Chen, Y. Li, W. Yang, N. Chen, H. Liu, Y. Li, Synthesis and tuning optical nonlinear properties of molecular crystals of benzothiadiazole, J Phys Chem C 114 (2010) 15109–15115 https://doi.org/10.1021/jp103159b.
[27] H. Zhang, X. Wan, X. Xue, Y. Li, A. Yu, Y. Chen, Selective tuning of the HOMO–LUMO gap of carbazole-based donor–acceptor–donor compounds toward different emission colors, Eur J Org Chem 9 (2010) 1681–1687 https://doi.org/10.1002/ejoc.200901167.
[28] X. Liu, S. Li, J. Li, J. Wang, Z. Tan, F. Yan, H. Li, Y.H. Lo, C.-H. Chui, W.-Y. Wong, Synthesis, characterization and photovoltaic properties of benzo[1,2-b:4,5-b′]dithiophene-bridged molecules, RSC Adv 4 (2014) 63260–63267 https://doi.org/10.1039/C4RA10081F.
[29] S. Chen, Y. Li, C. Liu, W. Yang, Y. Li, Strong charge-transfer chromophores from [2 + 2] cycloadditions of TCNE and TCNQ to peripheral donor-substituted alkynes, Eur J Org Chem (2011) 6445–6451 https://doi.org/10.1002/ejoc.201101009.
[30] W. Li, C. Du, F. Li, Y. Zhou, M. Fahlman, Z. Bo, F. Zhang, Benzothiadiazole-based linear and star molecules: design, synthesis, and their application in bulk heterojunction organic solar cells, Chem Mater 21 (2009) 5327–5334 https://doi.org/10.1021/cm902611b.
[31] C. He, Q. He, Y. Yi, G. Wu, F. Bai, Z. Shuaia, Y. Li, Improving the efficiency of solution processable organic photovoltaic devices by a star-shaped molecular geometry, J Mater Chem 18 (2008) 4085–4090 https://doi.org/10.1039/B807456A.
[32] H. Shang, H. Fan, Y. Liu, W. Hu, Y. Li, X. Zhan, A solution-processable star-shaped molecule for high-performance organic solar cells, Adv Mater 23 (2011) 1554–1557 https://doi.org/10.1002/adma.201004445.
[33] S. Ellinger, K.R. Graham, P. Shi, R.T. Farley, T.T. Steckler, R.N. Brookins, P. Taranekar, J. Mei, L.A. Padilha, T.R. Ensley, H. Hu, S. Webster, D.J. Hagan, E.W.V. Stryland, K.S. Schanze, J.R. Reynolds, Donor-acceptor-donor-based π-conjugated oligomers for nonlinear optics and near-IR emission, Chem Mater 23 (2011) 3805–3817 https://doi.org/10.1021/cm201424a.
[34] R. Misra, P. Gautam, R. Maragani, Ferrocenyl thiazoles: synthesis and properties, Tetrahedron Lett 56 (2015) 1664–1666 https://doi.org/10.1016/j.tetlet.2015.02.031.
[35] S. Erten-Ela, M.D. Ylimaz, B. Icil, Y. Dede, S. Icli, E.U. Akkaya, A panchromatic boradiazaindacene (BODIPY) sensitizer for dye-sensitized solar cells, Org Lett 10 (2008) 3299–3302 https://doi.org/10.1021/ol8010612.
[36] D. Kumaresan, R.P. Thummel, T. Bura, G. Ulrich, R. Ziessel, Color tuning in new metal-free organic sensitizers (Bodipys) for dye-sensitized solar cells, Chem Eur J 15 (2009) 6335–6339 https://doi.org/10.1002/chem.200900518.
[37] S. Kolemen, Y. Cakmak, S. Erten-Ela, Y. Altay, J. Brendel, M. Thelakkat, E.U. Akkaya, Solid-state dye-sensitized solar cells using red and near-IR absorbing Bodipy sensitizers, Org Lett 12 (2010) 3812–3815 https://doi.org/10.1021/ol1014762.
[38] M.T. Whited, P.I. Djurovich, S.T. Roberts, A.C. Durrell, C.W. Schlenker, S.E. Bradforth, M.E. Thompson, Singlet and triplet excitation management in a bichromophoric near-infrared-phosphorescent BODIPY-benzoporphyrin platinum complex, J Am Chem Soc 133 (2011) 88–96 https://doi.org/10.1021/ja108493b.
[39] J. Lehl, J.-F. Nierengarten, A. Harriman, T. Bura, R. Ziessel, Artificial light-harvesting arrays: electronic energy migration and trapping on a sphere and between

spheres, J Am Chem Soc 134 (2012) 988–998 https://doi.org/10.1021/ja206894z.
[40] K. Flavin, K. Lawrence, J. Bartelmess, M. Tasior, C. Navio, C. Bittencourt, D.F. O'Shea, D.M. Guldi, S. Giordani, Synthesis and characterization of boron azadipyrromethene single-wall carbon nanotube electron donor-acceptor conjugates, ACS Nano 5 (2011) 1198–1206 https://doi.org/10.1021/nn102831x.
[41] A. Florian, M.J. Mayoral, V. Stepanenko, G. Fernandez, Alternated stacks of nonpolar oligo(p-phenyleneethynylene)-BODIPY systems, Chem Eur J 18 (2012) 14957–14961 https://doi.org/10.1002/chem.201203279.
[42] Q. Zheng, G. Xu, P. Prasad, Conformationally restricted dipyrromethene boron difluoride (BODIPY) dyes: highly fluorescent, multicolored probes for cellular imaging, Chem Eur J 14 (2008) 5812–5819 https://doi.org/10.1002/chem.200800309.
[43] P. Didier, G. Ulrich, Y. Mely, R. Ziessel, Improved push-pull-push E-Bodipy fluorophores for two-photon cell-imaging, Org Biomol Chem 7 (2009) 3639–3642 https://doi.org/10.1039/B911587K.
[44] P.A. Bouit, K. Kamada, P. Feneyrou, G. Berginc, L. Toupet, O. Maury, C. Andraud, Two-photon absorption-related properties of functionalized BODIPY dyes in the infrared range up to telecommunication wavelengths, Adv Mater 21 (2009) 1151–1154 https://doi.org/10.1002/adma.200801778.
[45] J. Murtagh, D.O. Frimannsson, D.F. O'Shea, Azide conjugatable and pH responsive near-infrared fluorescent imaging probes, Org Lett 11 (2009) 5386–5389 https://doi.org/10.1021/ol902140v.
[46] A. Coskun, M. Yilmaz, E.U. Akkaya, Bis(2-pyridyl)-substituted boratriazaindacene as an NIR-emitting chemosensor for Hg(II), Org Lett 9 (2007) 607–609 https://doi.org/10.1021/ol062867t.
[47] J. Han, A. Loudet, R. Barhoumi, R.C. Burghardt, K. Burgess, A ratiometric pH reporter for imaging protein-dye conjugates in living cells, J Am Chem Soc 131 (2009) 1642–1643 https://doi.org/10.1021/ja8073374.
[48] W.J. Shi, J.Y. Liu, D.K.P. Ng, A highly selective colorimetric and fluorescent probe for Cu2 + and Hg2 + ions based on a distyryl BODIPY with two bis(1,2,3-triazole)amino receptors, Chem Asian J 7 (2012) 196–200 https://doi.org/10.1002/asia.201100598.
[49] S. Madhu, R. Gonnade, M. Ravikanth, Synthesis of 3,5-bis(acrylaldehyde) boron-dipyrromethene and application in detection of cysteine and homocysteine in living cells, J Org Chem 78 (2013) 5056–5060 https://doi.org/10.1021/jo4004597.
[50] P.G. Van Patten, A.P. Shreve, J.S. Lindsey, R.J. Donohoe, Energy-transfer modeling for the rational design of multiporphyrin light-harvesting arrays, J Phys Chem B 102 (1998) 4209–4216 https://doi.org/10.1021/jp972304m.
[51] R.W. Wagner, J.S. Lindsey, J. Seth, V. Palaniappan, D.F. Bocian, Molecular optoelectronic gates, J Am Chem Soc 118 (1996) 3996–3997 https://doi.org/10.1021/ja9602657.
[52] R.K. Lammi, R.W. Wagber, A. Ambroise, J.R. Diers, D.F. Bocian, D. Holten, J.S. Lindsey, Mechanisms of excited-state energy-transfer gating in linear versus branched multiporphyrin arrays, J Phys Chem B 105 (2001) 5341–5352 https://doi.org/10.1021/jp010857y.
[53] T. Yogo, Y. Urano, Y. Ishitsuka, F. Maniwa, T. Nagano, Highly efficient and photostable photosensitizer based on BODIPY chromophore, J Am Chem Soc 127 (2005) 12162–12163 https://doi.org/10.1021/ja0528533.
[54] S. Ozlem, E.U. Akkaya, Thinking outside the silicon box: molecular and logic as an additional layer of selectivity in singlet oxygen generation for photodynamic therapy, J Am Chem Soc 131 (2009) 48–49 https://doi.org/10.1021/ja808389t.
[55] S. Kolemen, E.U. Akkaya, Reaction-based BODIPY probes for selective bio-imaging, Coord Chem Rev 354 (2018) 121–134 https://doi.org/10.1016/j.ccr.2017.06.021.
[56] Y.V. Zatsikha, E. Maligaspe, A.A. Purchel, N.O. Didukh, Y. Wang, Y.P. Kovtun, D.A. Blank, V.N. Nemykin, Tuning electronic structure, redox, and photophysical properties in asymmetric NIR-absorbing organometallic BODIPYs, Inorg Chem 54 (2015) 7915–7928 https://doi.org/10.1021/acs.inorgchem.5b00992.
[57] X. Yin, Y. Li, Y. Li, Y. Zhu, X. Tang, H. Zheng, D. Zhu, Electrochromism based on the charge transfer process in a ferrocene–BODIPY molecule, Tetrahedron 65 (2009) 8373–8377 https://doi.org/10.1016/j.tet.2009.08.008.
[58] R. Ziessel, P. Retailleau, K.J. Elliott, A. Harriman, Boron dipyrrin dyes exhibiting "push–pull–pull" electronic signatures, Chem Eur J 15 (2009) 10369–10374 https://doi.org/10.1002/chem.200901725.
[59] O. Galangau, I. Fabre-Francke, S. Munteanu, C. Dumas-Verdes, G. Clavier, R. Méallet-Renault, R.B. Pansu, F. Hartl, F. Miomandre, Electrochromic and electrofluorochromic properties of a new boron dipyrromethene-ferrocene conjugate, Electrochim Acta 87 (2013) 809–815 https://doi.org/10.1016/j.electacta.2012.09.048.
[60] Y.V. Zatsikha, N.O. Didukh, T. Blesener, M.P. Kayser, Y.P. Kovtun, D.A. Blank, V.N. Nemykin, Preparation, characterization, redox, and photoinduced electron-transfer properties of the NIR-absorbing N-ferrocenyl-2-pyridone BODIPYs, Eur J Inorg Chem (2017) 318–324 https://doi.org/10.1002/ejic.201600855.
[61] M.P. Shandura, V.P. Yakubovskyi, Y.P. Kovtun, (4,4-Difluoro-4-bora-3a,4a,-diaza-s-indacen-3-yl)acetaldehyde: synthesis and chemical properties, J Heterocycl Chem 46 (2009) 1386–1391 https://doi.org/10.1002/jhet.263.
[62] M.R. Rao, K.V. Pavan Kumar, M. Ravikanth, Synthesis of boron-dipyrromethene–ferrocene conjugates, J Organomet Chem 695 (2010) 863–869 https://doi.org/10.1016/j.jorganchem.2010.01.009.
[63] X. Yin, Y. Li, Y. Zhu, X. Jing, Y. Li, D. Zhu, A highly sensitive viscosity probe based on ferrocene-BODIPY dyads, Dalton Trans 39 (2010) 9929–9935 https://doi.org/10.1039/c0dt00309c.
[64] B. Dhokale, P. Gautam, S.M. Mobin, R. Misra, Donor-acceptor, ferrocenyl substituted BODIPYs with marvelous supramolecular interactions, Dalton Trans 42 (2013) 1512–1518 https://doi.org/10.1039/C2DT31632C.
[65] R. Misra, B. Dhokale, T. Jadhav, S.M. Mobin, Donor-acceptor meso-alkynylated ferrocenyl BODIPYs: synthesis, structure, and properties, Dalton Trans 42 (2013) 13658–13666 https://doi.org/10.1039/C3DT51374B.
[66] B. Dhokale, T. Jadhav, S.M. Mobin, R. Misra, Tetracyanobutadiene functionalized ferrocenyl BODIPY dyes, Dalton Trans 45 (2016) 1476 https://doi.org/10.1039/C5DT04037J.
[67] T.K. Khan, R.R.S. Pissurlenkar, M.S. Shaikh, M. Ravikanth, Synthesis and studies of covalently linked meso-furyl boron-dipyrromethene ferrocene conjugates, J Organomet Chem 697 (2012) 65–73 https://doi.org/10.1016/j.jorganchem.2011.10.016.
[68] E. Maligaspe, T.J. Pundsack, L.M. Albert, Y.V. Zatsikha, P.V. Solntsev, D.A. Blank, V.N. Nemykin, Synthesis and charge-transfer dynamics in a ferrocene-containing organoboryl aza-BODIPY donor-acceptor triad with boron as the hub, Inorg Chem 54 (2015) 4167–4174 https://doi.org/10.1021/acs.inorgchem.5b00494.
[69] C.J. Ziegler, K. Chanawanno, A. Hasheminsasab, Y.V. Zatsikha, E. Maligaspe, V.N. Nemykin, Synthesis, redox properties, and electronic coupling in the diferrocene aza-dipyrromethene and azaBODIPY donor–acceptor dyad with direct ferrocene–α-pyrrole bond, Inorg Chem 53 (2014) 4751–4755 https://doi.org/10.1021/ic500526k.
[70] J.L. Jin, S.X. Wu, Y. Geng, S.Y. Yang, G.C. Yang, J. Wu, S. Muhammad, Y. Liao, Z.M. Su, L.Z. Hao, Theoretical study on photophysical properties of novel bis(BF2)-2,2′-bidipyrrins dyes: effect of variation in monomer structure, Int J Quantum Chem 112 (2012) 440–452 https://doi.org/10.1002/qua.22893.
[71] R. Sharma, R. Maragani, R. Misra, Ferrocenyl aza-dipyrromethene and aza-BODIPY: synthesis and properties, J Organomet Chem 825–826 (2016) 8–14 https://doi.org/10.1016/j.jorganchem.2016.10.019.
[72] L. Gao, W. Senevirathna, G. Sauvé, Azadipyrromethene-based conjugated oligomers with Near-IR absorption and high electron affinity, Org Lett 13 (2011) 5354–5357 https://doi.org/10.1021/ol202211t.
[73] Y.V. Zatsikha, C.D. Holstrom, K. Chanawanno, A.J. Osinski, C.J. Ziegler, V.N. Nemykin, Observation of the strong electronic coupling in Near-infrared-absorbing tetraferrocene aza-dipyrromethene and aza-BODIPY with direct ferrocene-α- and ferrocene–β-pyrrole bonds: toward molecular machinery with four-bit information storage capacity, Inorg Chem 56 (2017) 991–1000 https://doi.org/10.1021/acs.inorgchem.6b02806.
[74] N. Balsukuri, S. Mori, I. Gupta, Donor acceptor type ferrocene substituted aza-BODIPYs: synthesis, optical and electrochemical studies, J Porphyr Phthalocyanines 20 (2016) 719–729 https://doi.org/10.1142/S1088424616500693.
[75] A. Gorman, J. Killoran, C. O'Shea, T. Kenna, W.M. Gallagher, D.F. O'Shea, In vitro demonstration of the heavy-atom effect for photodynamic therapy, J Am Chem Soc 126 (2004) 10619–10631 https://doi.org/10.1021/ja047649e.
[76] M.J. Hall, S.O. McDonnell, J. Killoran, D.F. O'Shea, A modular synthesis of unsymmetrical tetraarylazadipyrromethenes, J Org Chem 70 (2005) 5571–5578 https://doi.org/10.1021/jo050696k.
[77] A. Loudet, K. Burgess, BODIPY dyes and their derivatives: Syntheses and spectroscopic properties, Chem Rev 107 (2007) 4891–4932 https://doi.org/10.1021/cr078381n.
[78] F. Li, S.I. Yang, T. Ciringh, J. Seth, C.H. Martin, D.L. Singh, D. Kim, R.R. Birge, D.F. Bocian, D. Holten, J.S. Lindsey, Design, synthesis, and photodynamics of light-harvesting arrays comprised of a porphyrin and one, two, or eight boron-dipyrrin accessory pigments, J Am Chem Soc 120 (1998) 10001–10017 https://doi.org/10.1021/ja9812047.
[79] M. Tasior, D.F. O'Shea, BF2-chelated tetraarylazadipyrromethenes as NIR fluorochromes, Bioconjug Chem 21 (2010) 1130–1133 https://doi.org/10.1021/bc100051p.
[80] M.E. El-Khouly, S. Fukuzumi, F. D'Souza, Photosynthetic antenna–reaction center mimicry by using boron dipyrromethene sensitizers, ChemPhysChem 15 (2014) 30–47 https://doi.org/10.1002/cphc.201300715.
[81] V.N. Nemykin, T.S. Blesener, C.J. Ziegler, Photophysics, redox processes, and electronic structures of ferrocenyl-containing BODIPYs, aza-BODIPYs, BOPHYs, transition-metal dipyrromethenes and aza-dipyrromethenes, Macroheterocycles 10 (2017) 9–26 https://doi.org/10.6060/mhc170188n.
[82] A.N. Amin, M.E. El-Khouly, N.K. Subbaiyan, M.E. Zandler, M. Supur, S. Fukuzumi, F. D'Souza, Syntheses, electrochemistry, and photodynamics of ferrocene-azadipyrromethane donor-acceptor dyads and triads, J Phys Chem A 115 (2011) 9810–9819 https://doi.org/10.1021/jp205236n.
[83] V. Bandi, M.E. El-Khouly, K. Ohkubo, V.N. Nesterov, M.E. Zandler, S. Fukuzumi, F. D'Souza, Bisdonor-azaBODIPY-fullerene supramolecules: syntheses, characterization, and light-induced electron-transfer studies, J Phys Chem C 118 (2014) 2321–2332 https://doi.org/10.1021/jp4112469.
[84] V. Bandi, M.E. El-Khouly, K. Ohkubo, V.N. Nesterov, M.E. Zandler, S. Fukuzumi, F. D'Souza, Excitation-wavelength-dependent, ultrafast photoinduced electron transfer in bisferrocene/BF2-chelated-azadipyrromethene/fullerene tetrads, Chem Eur J 19 (2013) 7221–7230 https://doi.org/10.1002/chem.201204317.
[85] J. Lenoble, N. Maringa, S. Campidelli, B. Donnio, D. Guillon, R. Deschenaux, Liquid-crystalline fullerodendrimers which display columnar phases, Org Lett 8 (2006) 1851–1854 https://doi.org/10.1021/ol0603920.
[86] J.-Y. Liu, M.E. El-Khouly, S. Fukuzumi, D.K.P. Ng, Photoinduced electron transfer in a ferrocene-distyryl BODIPY dyad and a ferrocene-distyryl BODIPY-C60 triad, ChemPhysChem 13 (2012) 2030–2036 https://doi.org/10.1002/cphc.201200167.

[87] W.-J. Shi, P.-C. Lo, S. Zhao, R.C.H. Wong, Q. Wang, W.-P. Fong, D.K.P. Ng, A biotin-conjugated glutathione-responsive FRET based fluorescent probe with a ferrocenyl BODIPY as the dark quencher, Dalton Trans 45 (2016) 17798–17806 https://doi.org/10.1039/C6DT03141B.
[88] C.A. Wijesinghe, M.E. El-Khouly, J.D. Blakemore, M.E. Zandler, S. Fukuumi, F. D'Souza, Charge stabilization in a closely spaced ferrocene–boron dipyrrin–fullerene triad, Chem Commun 46 (2010) 3301–3303 https://doi.org/10.1039/C000565G.
[89] A. Vecchi, P. Galloni, B. Floris, V.N. Nemykin, New developments in chemistry of organometallic porphyrins and their analogs, J Porphyr Phthalocyanines 17 (2013) 165–196 https://doi.org/10.1142/S1088424613300012.
[90] A. Vecchi, P. Galloni, B. Floris, S.V. Dudkin, V.N. Nemykin, Metallocenes meet porphyrinoids: consequences of a "fusion", Coord Chem Rev 291 (2015) 95–171 https://doi.org/10.1016/j.ccr.2015.02.005.
[91] E. Pena-Cabrera, A. Aguilar-Aguilar, M. Gonzalez-Domingues, E. Lager, R. Zamudio-Vazquez, J. Godoy-Vargas, F. Villanueva-Garcia, Simple, general, and efficient synthesis of meso-substituted borondipyrromethenes from a single platform, Org Lett 9 (2007) 3985–3988 https://doi.org/10.1021/ol7016615.
[92] P. Gautam, B. Dhokale, S.M. Mobin, R. Misra, Ferrocenyl BODIPYs: synthesis, structure and properties, RSC Adv 2 (2012) 12105–12107 https://doi.org/10.1039/C2RA21964F.
[93] R. Ziessel, P. Retailleau, K.J. Elliott, A. Harriman, Boron dipyrrin dyes exhibiting "push-pull-pull" electronic signatures, Chem Eur J 15 (2009) 10369–10374 https://doi.org/10.1002/chem.200901725.
[94] R. Misra, B. Dhokale, T. Jadhav, S.M. Mobin, Heteroatom-connected ferrocenyl BODIPYs: synthesis, structure, and properties, Organometallics 33 (2014) 1867–1877 https://doi.org/10.1021/om5002292.
[95] N.O. Didukh, Y.V. Zatsikha, G.T. Rohde, T.S. Blesener, V.P. Yakubovskyi, Y.P. Kovtun, V.N. Nemykin, NIR absorbing diferrocene-containing meso-cyano-BODIPY with a UV-Vis-NIR spectrum remarkably close to that of magnesium tetracyanotetraferrocenyltetraazaporphyrin, Chem Commun 52 (2016) 11563–11566 https://doi.org/10.1039/C6CC06344F.
[96] A. Treibs, F.-H. Kreuzer, Difluorboryl-Komplexe von Di- und Tripyrrylmethenen, Liebigs Ann Chem 718 (1968) 208–223 https://doi.org/10.1002/jlac.19687180119.
[97] J.H. Boyer, A.M. Haag, G. Sathyamoorthi, M. Soong, K. Thangaraj, T.G. Pavlopoulos, Pyrromethene–BF_2 complexes as laser dyes: 2, Heteroat Chem 1 (1993) 39–49 https://doi.org/10.1002/hc.520040107.
[98] G. Sathyamoorthi, J.H. Boyer, T.H. Allik, S. Chandra, Laser active cyanopyrromethene-BF2 complexes, Heteroat Chem 5 (1994) 403–407 https://doi.org/10.1002/hc.520050413.
[99] S. Kim, J. Bouffard, Y. Kim, Tailoring the solid-state fluorescence emission of BODIPY dyes by meso substitution, Chem Eur J 21 (2015) 17459–17465 https://doi.org/10.1002/chem.201503040.
[100] V.P. Yakubovskyi, N.O. Didukh, Y.V. Zatsikha, Y.P. Kovtun, A new approach to the synthesis of meso-CN-substituted BODIPYs, Chemistry 1 (2016) 1462–1466 https://doi.org/10.1002/slct.201600246.
[101] Y.V. Zatsikha, N.O. Didukh, D. Nemez, A.C. Schlachter, P.-L. Karsenti, Y.P. Kovtun, P.D. Harvey, V.N. Nemykin, Ferrocene–BODIPY merocyanine dyads: new NIR absorbing platforms with optical properties susceptible to protonation, Chem Commun 53 (2017) 7612–7615 https://doi.org/10.1039/C7CC03332J.
[102] V.P. Yakubovskyi, M.P. Shandura, Y.P. Kovtun, Boradipyrromethenecyanines. Eur J Org Chem (2009) 3237–3243 https://doi.org/10.1002/ejoc.200900192.
[103] V.P. Yakubovskyi, M.P. Shandura, Y.P. Kovtun, Boradipyrromethenecyanines derived from conformationally restricted nuclei, Dyes Pigments 87 (2010) 17–21 https://doi.org/10.1016/j.dyepig.2010.01.017.
[104] M.P. Shandura, V.P. Yakubovskyi, A.O. Gerasov, O.D. Kachkovsky, Y.M. Poronik, Y.P. Kovtun, α-Polymethine-substituted boron dipyrromethenes-BODIPY-based NIR cyanine-like dyes, Eur J Org Chem (2012) 1825–1834 https://doi.org/10.1002/ejoc.201101674.
[105] M.P. Shandura, V.P. Yakubovskyi, Y.P. Kovtun, 3,5-Bis(acetaldehyde) substituted BODIPY, Org Biomol Chem 11 (2011) 835–841 https://doi.org/10.1039/C2OB27004H.
[106] M.P. Shandura, V.P. Yakubovskyi, Y.V. Zatsikha, O.D. Kachkovsky, Y.M. Poronik, Y.P. Kovtun, Anionic, cationic and merocyanine polymethine dyes based on dipyrromethene core, Dyes Pigments 98 (2013) 113–118 https://doi.org/10.1016/j.dyepig.2013.02.004.
[107] Y.V. Zatsikha, V.P. Yakubovskyi, M.P. Shandura, Y.P. Kovtun, Boradipyrromethenecyanines on the base of a BODIPY nucleus annelated with a pyridone ring: a new approach to long-wavelength dual fluorescent probe design, RSC Adv 3 (2013) 24193–24201 https://doi.org/10.1039/C3RA42633E.
[108] V.P. Yakubovskyi, Y.V. Zatsikha, M.P. Shandura, Y.P. Kovtun, Boradipyrromethenecyanines of different electronic symmetry: a demonstration of the potential of BODIPY nucleus as end group in polymethine chromophoric system, Dyes Pigments 106 (2014) 161–167 https://doi.org/10.1016/j.dyepig.2014.03.013.
[109] Y.V. Zatsikha, T.S. Blesener, P.C. Goff, A.T. Healy, R.K. Swedin, D.E. Herbert, G.T. Rohde, K. Chanawanno, C.J. Ziegler, R.V. Belosludov, D.A. Blank, V.N. Nemykin, 1,7-Dipyrene-containing aza-BODIPYs: are pyrene groups effective as ligands to promote and direct complex formation with common nanocarbon materials?, J Phys Chem C 122 (2018) 27893–27916 https://doi.org/10.1021/acs.jpcc.8b09504.
[110] H.M. Rhoda, K. Chanawanno, A.J. King, Y.V. Zatsikha, C.J. Ziegler, V.N. Nemykin, Unusually strong long-distance metal-metal coupling in bis(ferrocene)-containing BOPHY: an introduction to organometallic BOPHYs, Chem Eur J 21 (2015) 18043–18046 https://doi.org/10.1002/chem.201504004.
[111] I.-S. Tamgho, A. Hasheminasab, J.T. Engle, V.N. Nemykin, C.J. Ziegler, A new highly fluorescent and symmetric pyrrole–BF2 chromophore: BOPHY, J Am Chem Soc 136 (2014) 5623–5626 https://doi.org/10.1021/ja502477a.
[112] D. Delmarre, R. Méallet, C. Bied-Charreton, R.B. Pansu, Heavy metal ions detection in solution, in sol-gel and with grafted porphyrin monolayers, J Photochem Photobiol A Chem 124 (1999) 23–28 https://doi.org/10.1016/S1010-6030(99)00046-5.
[113] Y. Ding, W.-H. Zhu, Y. Xie, Development of ion chemosensors based on porphyrin analogues, Chem Rev 117 (2017) 2203–2256 https://doi.org/10.1021/acs.chemrev.6b00021.
[114] A.K. Burrell, W.M. Campbell, G.B. Jameson, D.L. Officer, P.D.W. Boyd, Z. Zhao, P.A. Cocks, K.C. Gordon, Bis(ferrocenyl)porphyrins. Compounds with strong long-range metal–metal coupling, Chem Commun (1999) 637–638 https://doi.org/10.1039/A900691E.
[115] S.J. Narayanan, S. Venkatraman, S.R. Dey, B. Sridevi, V.G. Anand, T.K. Chandrashekar, Synthesis of meso ferrocenyl porphyrins, Synlett (2000) 1834–1836 https://doi.org/10.1055/s-2000-8700.
[116] J. Rochford, A.D. Rooney, M.T. Pryce, Redox control of meso-zinc(II) ferrocenylporphyrin based fluorescence switches, Inorg Chem 46 (2007) 7247–7249 https://doi.org/10.1021/ic0703326.
[117] D.T. Gryko, F. Zhao, A.A. Yasseri, K.M. Roth, D.F. Bocian, W.G. Kuhr, J.S. Lindsey, Synthesis of thiol-derivatized ferrocene-porphyrins for studies of multibit information storage, J Org Chem 65 (2000) 7356–7362 https://doi.org/10.1021/jo0004862.
[118] A.K. Burrell, W.M. Campbell, D.L. Officer, S.M. Scott, K.C. Gordon, M.R. McDonald, Synthesis, reactivity and spectroscopy of ferrocene-functionalized porphyrins, with a conjugated connection between the ferrocene and the porphyrin core, J Chem Soc Dalton Trans (1999) 3349–3354 https://doi.org/10.1039/A902931A.
[119] V.N. Nemykin, E.A. Makarova, J.O. Grosland, S.V. Dudkin, R. Dennison, A.A. Purchel, Tuning the near-IR band energy and redox potentials of magnesium tetra(ferrocenyl)tetraazaporphyrins, J Porphyr Phthalocyanines 18 (2014) 792–803 https://doi.org/10.1142/S1088424614500588.
[120] V.N. Nemykin, A.Y. Maximov, A.Y. Koposov, Mercury-free preparation, characterization, and molecular structure of tricyanovinylferrocene using an unusual reaction between ferrocene and tetracyanoethylene, Organometallics 26 (2007) 3138–3148 https://doi.org/10.1021/om070160k.
[121] V.N. Nemykin, E.A. Makarova, J.O. Grosland, R.G. Hadt, A.Y. Koposov, Preparation, characterization, molecular and electronic structures, TDDFT, and TDDFT/PCM study of the solvatochromism in cyanovinylferrocenes, Inorg Chem 46 (2007) 9591–9601 https://doi.org/10.1021/ic700558v.
[122] S. Rai, G. Gayatri, G. Narahari Sastry, M. Ravikanth, Effects of meso-substituents and core-modification on photophysical and electrochemical properties of porphyrin–ferrocene conjugates, Chem Phys Lett 467 (2008) 179–185 https://doi.org/10.1016/j.cplett.2008.10.076.
[123] I. Gupta, M. Ravikanth, Synthesis of meso-furyl porphyrins with N4, N3S, N2S2 and N3O porphyrin cores, Tetrahedron 59 (2003) 6131–6139 https://doi.org/10.1016/S0040-4020(03)00950-5.
[124] L.L. Grazynski, J. Lisowski, M.M. Olmstead, A.L. Balch, 21-Thiatetra-p-tolylporphyrin and its copper(II) bicarbonate complex. Structural effects of copper-thiophene binding, J Am Chem Soc 109 (1987) 4428–4429 https://doi.org/10.1021/ja00248a067.
[125] A. Ulman, J. Manassen, Synthesis of new tetraphenylporphyrin molecules containing heteroatoms other than nitrogen. I. Tetraphenyl-21,23-dithiaporphyrin, J Am Chem Soc 97 (1975) 6540–6544 https://doi.org/10.1021/ja00855a042.
[126] A. Treibs, K. Jacob, Cyclotrimethine dyes derived from squaric acid, Angew Chem, Int Ed Engl 4 (1965), 694-694 https://doi.org/10.1002/anie.196506941.
[127] L. Hu, Z. Yan, H. Xu, Advances in synthesis and application of near-infrared absorbing squaraine dyes, RSC Adv 3 (2013) 7667–7676 https://doi.org/10.1039/C3RA23048A.
[128] H. Meier, R. Petermann, Near infrared dyes by combination of squaraine and ferrocene chromophores, Tetrahedron Lett 41 (2000) 5475–5478 https://doi.org/10.1016/S0040-4039(00)00892-3.
[129] Y.W. Huang, N.Y. Fu, Synthesis and properties of a novel squaraine dye modified by ferrocene, Chin Chem Lett 22 (2011) 1301–1304 https://doi.org/10.1016/j.cclet.2011.05.039.
[130] M.C. Aragoni, M. Arca, F. Demartin, New [M(R,R'timdt)2] metal-dithiolenes and related compounds (M = Ni, Pd, Pt; R,R'timdt = monoanion of disubstituted imidazolidine-2,4,5-trithiones): an experimental and theoretical investigation, J Am Chem Soc 121 (1999) 7098–7107 https://doi.org/10.1021/ja990827x.
[131] P. Chandrasekaran, A.F. Greene, K. Lillich, S. Capone, J.T. Mague, S. Debeer, J.P. Donahue, A structural and spectroscopic investigation of octahedral platinum bis(dithiolene)phosphine complexes: platinum dithiolene internal redox chemistry induced by phosphine association, Inorg Chem 53 (2014) 9192–9205 https://doi.org/10.1021/ic501273b.
[132] S. Dalgleish, M.M. Matsushita, L.G. Hu, B. Li, H. Yoshikawa, K. Awaga, Utilizing photocurrent transients for dithiolene-based photodetection: stepwise improvements at communications relevant wavelengths, J Am Chem Soc 134 (2012) 12742–12750 https://doi.org/10.1021/ja304228c.
[133] G. Bruno, M. Almeida, F. Artizzu, J.C. Dias, M.L. Mercuri, L. Pilia, C. Rovira, X. Ribas, A. Serpe, P. Deplano, Innocence and noninnocence of the ligands in bis(pyrazine-2,3-dithiolate and -diselonate) d8-metal complexes. A theoretical

and experimental study for the Cu(III), Au(III) and Ni(II) cases, Dalton Trans 39 (2010) 4566–4574 https://doi.org/10.1039/B922626E.
[134] R. Perochon, P. Davidson, S. Rouzière, F. Camerel, L. Piekara-Sady, T. Guizouarn, M. Fourmigué, Probing magnetic interactions in columnar phases of a paramagnetic gold dithiolene complex, J Mater Chem 21 (2011) 1416–1422 https://doi.org/10.1039/C0JM02171G.
[135] S. Dalgleish, N. Robertson, A stable near IR switchable electrochromic polymer based on an indole-substituted nickel dithiolene, Chem Commun 39 (2009) 5826–5828 https://doi.org/10.1039/B913174D.
[136] S. Oliveira, M.L. Afonso, S.I.G. Dias, I.C. Santos, R.T. Henriques, S. Rabaça, M. Almeida, An electropolymerisable pyridine-functionalised gold bis(dithiolene) complex, Eur J Inorg Chem 18 (2013) 3133–3136 https://doi.org/10.1002/ejic.201300222.
[137] D. Espa, L. Marchiò, L. Pilia, M.L. Mercuri, F. Artizzu, A. Serpe, D. Simão, M. Almeida, M. Pizzotti, P. Deplano, Mixed-ligand Pt(II) dithione-dithiolato complexes: influence of the dicyanobenzodithiolato ligand on the second-order NLO properties, Dalton Trans 41 (2012) 3485–3493 https://doi.org/10.1039/C2DT11956K.
[138] X. Chen, W. Qiao, B. Liu, J. Ren, Z. Wang, Synthesis and near infrared electrochromic properties of metallodithiolene complexes, Sci China Chem 60 (2017) 1–7 https://doi.org/10.1007/s11426-016-0252-x.
[139] B. Liu, W. Qiao, Z.Y. Wang, Colorless metallodithiolene oligomers and polymers with intense near- and mid-infrared absorption, RSC Adv 5 (2015) 6815–6822 https://doi.org/10.1039/C4RA13039A.
[140] S.B. Wilkes, I.R. Butler, A.E. Underhill, A. Kobayashi, H. Kobayashi, Synthesis of the first diferrocenyl-dithiolene metal complex: bis(ferrocenylethy1ene-12-dithiolato)nickelate(ii), J Chem Soc, Chem Commun (1994) 53–54 https://doi.org/10.1039/C39940000053.
[141] U.T. Mueller-Westerhoff, D.I. Yoon, K. Plourde, Near-ir dyes for the 1.3 to 1.5 micron region: the use of substituted dithiolene complexes, Mol Cryst Liq Cryst 183 (1990) 291–302 https://doi.org/10.1080/15421409008047466.
[142] S.B. Wilkes, I.R. Butler, A.E. Underhill, M.B. Hursthouse, D.E. Hibbs, K.M.A. Malik, Synthesis, crystal structure and properties of novel ferrocenyl multisulfur compounds, J Chem Soc Dalton Trans (1995) 897–903 https://doi.org/10.1039/DT9950000897.
[143] H.-J. Lee, D.-Y. Noh, Syntheses, X-ray crystal structures and properties of di- and tetraferrocenyl nickel-bis(1,4-dithiin-5,6-dithiolate) complexes, J Mater Chem 10 (2000) 2167–2172 https://doi.org/10.1039/b001829p.
[144] U.T. Mueller-Westerhoff, R.W. Sanders, Electronic spectra of ferrocenyl-dithiolene nickel complexes: steric and electron donor/acceptor effects, Organometallics 22 (2003) 4778–4782 https://doi.org/10.1021/om0210053.
[145] S.B. Wilkes, I.R. Butler, A.E. Underhill, A. Kobayashi, H. Kobayashi, Synthesis of the first diferrocenyl–dithiolene metal complex: bis(ferrocenylethylene-1,2-dithiolato) nickelate(II), J Chem Soc, Chem Commun (1994) 53–54 https://doi.org/10.1039/C39940000053.
[146] A.E. Underhill, A. Charlton, S.B. Wilkes, I.R. Butler, A. Kobayashi, H. Kobayashi, Developments in the chemistry of sulphur-donor ligands, Synth Met 70 (1995) 1101–1104 https://doi.org/10.1016/0379-6779(94)02774-S.
[147] H.J. Lee, Dong-Youn N. Syntheses, X-ray crystal structures and properties of di-and tetra-ferrocenyl nickel-bis(1,4-dithiin-5,6-dithiolate)complexes, J Mater Chem 10 (2000) 2167–2172 https://doi.org/10.1039/B001829P.
[148] T. Kusamoto, K. Takada, R. Sakamoto, S. Kume, H. Nishihara, Ferrocene-dithiolene hybrids: control of strong donor−acceptor electronic communication to reverse the charge transfer direction, Inorg Chem 51 (2012) 12102–12113 https://doi.org/10.1021/ic300581a.
[149] S.R. Marder, J.W. Perry, B.G. Tiemann, Organometallic salts with large second-harmonic-generation powder efficiencies: (E)-1-ferrocenyl-2-(1-methyl-4-pyridiniumyl)ethylene salts, Organometallics 10 (1991) 1896–1901 https://doi.org/10.1021/om00052a039.
[150] V. Alain, M. Blanchard-Desce, C.-T. Chen, S.R. Marder, A. Fort, M. Barzoukas, Large optical nonlinearities with conjugated ferrocene and ruthenocene derivatives, Synth Met 81 (1996) 133–136 https://doi.org/10.1016/S0379-6779(96)03743-5.
[151] C. Lambert, W. Gaschler, M. Zabel, R. Matschiner, R. Wortmann, Linear and non-linear optical properties of arene-Fe-Cp complexes, J Organomet Chem 592 (1999) 109–114 https://doi.org/10.1016/S0022-328X(99)00497-0.
[152] Müller TJJ, A. Netz, M. Ansorge, Syntheses and NLO properties of chromium carbonyl arene complexes with conjugated side chains: the amphoteric nature of chromium carbonyl complexation in push-pull chromophores, Organometallics 18 (1999) 5066–5074 https://doi.org/10.1021/om9904551.
[153] H. Wong, T. Meyer-Friedrichsen, T. Farrell, C. Mecker, J. Heck, Second harmonic generation and two-photon fluorescence as nonlinear optical properties of dipolar mononuclear sesquifulvalene complexes, Eur J Inorg Chem (2000) 631–646 https://doi.org/10.1002/(SICI)1099-0682(200004)2000:4<631::AID-EJIC631>3.0.CO;2-E.
[154] I.R. Whitall, A.M. McDonagh, M.G. Humphrey, Organometallic complexes in nonlinear optics I: second-order nonlinearities, Adv Organomet Chem 42 (1998) 291–362 https://doi.org/10.1016/S0065-3055(08)60545-6.
[155] M.B. Hall, R.F. Fenske, Electronic structure and bonding in methyl- and perfluoromethyl (pentacarbonyl)manganese, Inorg Chem 11 (1972) 768–775 https://doi.org/10.1021/ic50110a022.
[156] C.P. Casey, M.S. Konings, S.R. Marder, Y. Takezawa, Diiron μ-vinylcarbyne complexes have unusually low barriers to vinyl rotation because conjugation is maintained throughout rotation, J Organomet Chem 358 (1988) 347–361 https://doi.org/10.1016/0022-328X(88)87089-X.
[157] C.P. Casey, M.S. Konings, S.R. Marder, Synthesis of cationic diiron μ-vinylcarbyne complexes, Polyhedron 7 (1988) 881–902 https://doi.org/10.1016/S0277-5387(00)86310-X.
[158] C.P. Casey, M.S. Konings, S.R. Marder, Addition of nucleophiles to cationic diiron μ-vinylcarbyne complexes; synthesis of functionalized diiron μ-alkenylidene complexes, J Organomet Chem 345 (1988) 125–134 https://doi.org/10.1016/0022-328X(88)80241-9.
[159] J.A. Bandy, H.E. Bunting, M.-H. Garcia, M.L.H. Green, S.R. Marder, M.E. Thompson, Second-order non-linear optical properties of diironalkenylidyne complexes; crystal structure of {(η-C5H5)2Fe2(CO)2(μ-CO)(μ-(E)C-CH=CH-C6H4-(p)-NMe2)}+BF4−, Polyhedron 12 (1992) 1429–1435 https://doi.org/10.1016/S0277-5387(00)83135-6.
[160] T. Farrell, T. Meyer-Friedrichsen, J. Heck, A.R. Manning, Linear and nonlinear optical properties of diiron μ-vinylcarbyne acceptor and stilbenyl donor based chromophores, Organometallics 19 (2000) 3410–3419 https://doi.org/10.1021/om000112z.
[161] T. Farrell, A.R. Manning, T.C. Murphy, T. Meyer-Friedrichsen, J. Heck, I. Asselberghs, A. Persoons, Structure-property dependence of the first hyperpolarisabilities of organometallic merocyanines based on the ì-vinylcarbynediiron acceptor and ferrocene donor, Eur J Inorg Chem (2001) 2365–2375 https://doi.org/10.1002/1099-0682(200109)2001:9<2365::AID-EJIC2365>3.0.CO;2-H.
[162] C. Reichardt, Solvents and solvent effects in organic chemistry, second ed., VCH, Weinheim, 1988.
[163] A.K.-Y. Jen, V. Pushkara Rao, K.Y. Wong, K.J. Drost, Functionalized thiophenes: second-order nonlinear optical materials, J Chem Soc, Chem Commun (1993) 90–92 https://doi.org/10.1039/C39930000090.
[164] V. Pushkara Rao, A.K.-Y. Jen, K.Y. Wong, K.J. Drost, Dramatically enhanced second-order nonlinear optical susceptibilities in tricyanovinylthiophene derivatives, J Chem Soc, Chem Commun (1993) 1118–1120 https://doi.org/10.1039/C39930001118.
[165] A.K.-Y. Jen, Y. Cai, P.V. Bedworth, S.R. Marder, Synthesis and characterization of highly efficient and thermally stable diphenylamino-substituted thiophene stilbene chromophores for nonlinear optical applications, Adv Mater 9 (1997) 132–135 https://doi.org/10.1002/adma.19970090207.
[166] G.A. Razuvaev, G.A. Domrachev, V.V. Sharutin, O.N. Suvorova, Ferrocenyl derivatives of dicyclopentadienyl-titanium, -zirconium and -hafnium, J Organomet Chem 141 (1977) 313–317 https://doi.org/10.1016/S0022-328X(00)90854-4.
[167] M. Wedler, H.W. Roesky, F.T. Edelmann, Behrens UT-ferrocenyl-komplexe der frühen ubergangsmetalle-synthese und struktur, Z Naturforsch B Chem Sci 43 (1988) 1461–1467 http://www.znaturforsch.com/ab/v43b/c43b.htm.
[168] H. Gornitzka, F.T. Edelmann, K. Jacob, Ferrocenhaltige liganden in der lanthanid-chemie: alkoxide und thiolate, J Organomet Chem 436 (1992) 325–332 https://doi.org/10.1016/0022-328X(92)85064-4.
[169] S. Köcher, B. Walfort, G. Rheinwald, T. Rüffer, H. Lang, Alkyloxy- and aryloxy-titanocenes: synthesis, solid-state structure and cyclic voltammetric studies, J Organomet Chem 693 (2008) 3213–3222 https://doi.org/10.1016/j.jorganchem.2008.07.016.
[170] P.-C. Song L-C Liu, C. Han, Q.-M. Hu, Synthesis and characterization of Cp2Ti-containing organometallics via in situ oxidative-addition of ‘Cp2Ti’ intermediate.: crystal structures of (1-C10H7S)2TiCp2, [(η5-C5H5)Fe(η5-C5H4CH2S)]2TiCp2 and [η2-OC(Ph)-C(ph)O]TiCp2, J Organomet Chem 648 (2002) 119–125 https://doi.org/10.1016/S0022-328X(01)01413-9.
[171] H. Muraoka, S. Ogawa, N. Nagahora, Y. Kawai, R. Sato, Synthesis of new pentathiepin and dithiatriselenepin fused to ferrocene via dithiametallacycles, Bull Chem Soc Jpn 78 (2005) 2026–2036 https://doi.org/10.1246/bcsj.78.2026.
[172] R. Steudel, K. Hassenberg, J. Pickardt, E. Grigiotti, P. Zanello, Synthetic and electrochemical studies on 1,1‘-dithia-substituted derivatives of ferrocene and structure of 1,3-dithia[3]ferrocenophane [Fe(C5H4S)2CH2], Organometallics 21 (2002) 2604–2608 https://doi.org/10.1021/om020041z.
[173] B. Gautheron, G. Tainturier, Conformation de metalladiselenaferocenophanes Fe(η5-C5H4Se)2M(η5-C5H4R)2 (M = Zr, Hf), J Organomet Chem 262 (1984) C30–C34 https://doi.org/10.1016/S0022-328X(00)99169-1.
[174] R. Broussier, Y. Gobet, R. Amardeil, A. Da Rold, M.M. Kubicki, B. Gautheron, Un nouveau type de ferrocénophane, premier exemple de structure dimère, J Organomet Chem 445 (1993) C4–C5 https://doi.org/10.1016/0022-328X(93)80221-V.
[175] P. Frenzel, M. Korb, A. Hildebrandt, H. Lang, Synthesis and electrochemical behavior of ferrocenyl-functionalized metallocenes M(η5-C5H5)2(EFc)2 (M = Ti, Zr; E = O, S, Se), Eur J Inorg Chem 27 (2018), 3143-3143 https://doi.org/10.1002/ejic.201800759.
[176] G. Noirbent, F. Dumur, Recent advances on nitrofluorene derivatives: versatile electron acceptors to create dyes absorbing from the visible to the near and far infrared region, Materials 11 (2018) 2425 https://doi.org/10.3390/ma11122425.
[177] I.F. Perepichka, D.F. Perepichka, M.R. Bryce, A. Chesne, A.F. Popov, V. Khodorkovsky, G. Meshulamd, Z. Kotler, Push-pull fluorene acceptors with ferrocene donor moiety, Synth Met 102 (1999) 1558–1559 https://doi.org/10.1016/S0379-6779(98)00563-3.
[178] D.F. Perepichka, I.F. Perepichka, A.F. Popov, M.R. Bryce, A.S. Batsanov, A. Chesney, J.A.K. Howard, N.I. Sokolov, Electron acceptors of the fluorene series. Part 12. 9-(Metalloceneylidene)nitrofluorene derivatives of Fc–NF, NF–Fc–NF, and NF–Rc–NF types, and the vinylogues Fc—NF: synthesis, characterisation, intramolecular charge transfer, redox properties and X-ray structures for three fluo-

rene–ferrocene derivatives, J Organomet Chem 637–639 (2001) 445–462, https://doi.org/10.1016/S0022-328X(01)00948-2.